# Chemoreceptor Co-Expression in *Drosophila* Olfactory Neurons

Darya Task[1,10], Chun-Chieh Lin[1,2,7], Alina Vulpe[3], Ali Afify[1], Sydney Ballou[3], Maria Brbić[4], Philipp Schlegel[5,8], Gregory S. X. E. Jefferis[5,8], Hongjie Li[6,9], Karen Menuz[3] and Christopher J. Potter[1]*

[1]The Solomon H. Snyder Department of Neuroscience, Center for Sensory Biology, Johns Hopkins University School of Medicine, Baltimore, MD 21205, USA.

[2]Mortimer B. Zuckermann Mind Brain Behavior Institute, Columbia University, New York, NY 10027, USA.

[3]Physiology & Neurobiology Department, University of Connecticut, Mansfield, CT 06269, USA.

[4]Department of Computer Science, Stanford University, Stanford, CA 94305, USA.

[5]Drosophila Connectomics Group, Department of Zoology, University of Cambridge, Cambridge, CB2 3EJ, UK.

[6]Department of Biology, Howard Hughes Medical Institute, Stanford University, Stanford, CA 94305, USA.

[7]Present Address: The Department of Pathology and Laboratory Medicine, Giesel School of Medicine, Dartmouth-Hitchcock Medical Center, Lebanon, NH 03756, USA.

[8]Neurobiology Division, MRC Laboratory of Molecular Biology, Cambridge, CB2 OQH, UK.

[9]Present Address: Huffington Center on Aging, Department of Molecular and Human Genetics, Baylor College of Medicine, Houston, TX 77030, USA.

[10]Present Address: Department of Biology, Johns Hopkins University, Baltimore, MD 21218, USA.

***Correspondence**: cpotter@jhmi.edu

## Abstract

*Drosophila melanogaster* olfactory neurons have long been thought to express only one chemosensory receptor gene family. There are two main olfactory receptor gene families in *Drosophila*, the Odorant Receptors (ORs) and the Ionotropic Receptors (IRs). The dozens of odorant binding receptors in each family require at least one co-receptor gene in order to function: *Orco* for ORs, and *Ir25a*, *Ir8a*, and *Ir76b* for IRs. Using a new genetic knock-in strategy, we targeted the four co-receptors representing the main chemosensory families in *Drosophila* (*Orco, Ir8a, Ir76b, Ir25a*). Co-receptor knock-in expression patterns were verified as accurate representations of endogenous expression. We find extensive overlap in expression among the different co-receptors. As defined by innervation into antennal lobe glomeruli, *Ir25a* is broadly expressed in 88% of all olfactory sensory neuron classes and is co-expressed in 82% of Orco+ neuron classes, including all neuron classes in the maxillary palp. *Orco*, *Ir8a*, and *Ir76b* expression patterns are also more expansive than previously assumed. Single sensillum recordings from Orco-expressing *Ir25a* mutant antennal and palpal neurons identify changes in olfactory responses. These results suggest co-expression of chemosensory receptors is common in olfactory neurons. Together, our data present the first comprehensive map of chemosensory co-receptor expression and reveal their unexpected widespread co-expression in the fly olfactory system.

## Keywords:

Insect, olfaction, Odorant Receptor, Ionotropic Receptor, sensory neuron, CRISPR, *QF2*, antennal lobe, HACK, knock-in.

# Introduction

The sense of smell is crucial for many animal behaviors, from conspecific recognition and mate choice (Dweck et al., 2015; Stengl, 2010), to location of a food source (Auer et al., 2020;

Hansson and Stensmyr, 2011), to avoidance of predators (Kondoh et al., 2016; Papes et al., 2010) and environmental dangers (Mansourian et al., 2016; Stensmyr et al., 2012). Peripheral sensory organs detect odors in the environment using a variety of chemosensory receptors (Carey and Carlson, 2011; Su et al., 2009). The molecular repertoire of chemosensory receptors expressed by the animal, and the particular receptor expressed by any individual olfactory neuron, define the rules by which an animal interfaces with its odor environment. Investigating this initial step in odor detection is critical to understanding how odor signals first enter the brain to guide behaviors.

The olfactory system of the vinegar fly, *Drosophila melanogaster*, is one of the most extensively studied and well understood (Depetris-Chauvin et al., 2015). *Drosophila* is an attractive model for studying olfaction due to its genetic tractability, numerically simpler nervous system (compared to mammals), complex olfactory-driven behaviors, and similar organizational principles to vertebrate olfactory systems (Ache and Young, 2005; Wilson, 2013). Over sixty years of research have elucidated many of the anatomical, molecular, and genetic principles underpinning fly olfactory behaviors (Gomez-Diaz et al., 2018; Harris, 1972; Pask and Ray, 2016; Siddiqi, 1987; Stocker, 2001; Venkatesh and Singh, 1984; Vosshall and Stocker, 2007; Yan et al., 2020). Recent advances in electron microscopy and connectomics are revealing higher brain circuits involved in processing of olfactory information (Bates et al., 2020; Berck et al., 2016; Frechter et al., 2019; Horne et al., 2018; Marin et al., 2020; Zheng et al., 2018); such endeavors will aid the full mapping of neuronal circuits from sensory inputs to behavioral outputs.

The fly uses two olfactory appendages to detect odorants: the antennae and maxillary palps (Figure 1A) (Stocker, 1994). Each of these is covered by sensory hairs called sensilla, and each sensillum houses between one and four olfactory sensory neurons or OSNs (Figure 1B) (de Bruyne et al., 2001; Venkatesh and Singh, 1984). The dendrites of these neurons are found within the sensillar lymph, and they express chemosensory receptors from three gene

73 families: *Odorant Receptors* (*ORs*), *Ionotropic Receptors* (*IRs*), and *Gustatory Receptors* (*GRs*)
74 (Figure 1C, left) (Benton et al., 2009; Clyne et al., 1999; Gao and Chess, 1999; Jones et al.,
75 2007; Kwon et al., 2007; Vosshall et al., 1999; Vosshall et al., 2000). These receptors bind
76 odorant molecules that enter the sensilla from the environment, leading to the activation of the
77 OSNs, which then send this olfactory information to the fly brain (Figure 1D), to the first olfactory
78 processing center – the antennal lobes (ALs) (Figure 1E) (reviewed in: Depetris-Chauvin et al.,
79 2015; Gomez-Diaz et al., 2018; Pask and Ray, 2016). The standard view regarding the
80 organization of the olfactory system in *Drosophila* is that olfactory neurons express receptors
81 from only one of the chemosensory gene families (either *ORs*, *IRs*, or *GRs*), and all neurons
82 expressing the same receptor (which can be considered an OSN class) project their axons to
83 one specific region in the AL called a glomerulus (Figure 1C, right) (Couto et al., 2005;
84 Fishilevich and Vosshall, 2005; Gao et al., 2000; Laissue et al., 1999; Pinto et al., 1988;
85 Vosshall et al., 2000). This pattern of projections creates a map in which the OR+ (Figure 1E,
86 teal), IR+ (Figure 1E, purple), and GR+ (Figure 1E, dark blue) domains are segregated from
87 each other in the AL. The OR+ domains innervate 38 anterior glomeruli, while the IR+ (19
88 glomeruli) and GR+ (1 glomerulus) domains occupy more posterior portions of the AL. One
89 exception is the Or35a+ OSN class, which expresses an *IR* (*Ir76b*) in addition to the *OR* and
90 *Orco*, and innervates the VC3 glomerulus (Figure 1E, striped glomerulus) (Benton et al., 2009;
91 Couto et al., 2005; Fishilevich and Vosshall, 2005). Different OSN classes send their information
92 to different glomeruli, and the specific combination of OSN classes and glomeruli that are
93 activated by a given smell (usually a blend of different odorants) constitutes an olfactory 'code'
94 which the fly brain translates into an appropriate behavior (Grabe and Sachse, 2018;
95 Haverkamp et al., 2018; Seki et al., 2017).
96 The receptors within each chemosensory gene family form heteromeric ion channels
97 (receptor complexes) (Abuin et al., 2011; Butterwick et al., 2018; Sato et al., 2008). The *ORs*
98 require a single co-receptor, *Orco*, to function (Figure 1C, middle row) (Benton et al., 2006;

99 Larsson et al., 2004; Vosshall and Hansson, 2011). The ligand-binding *OrX* confers odorant
100 specificity upon the receptor complex, while the co-receptor *Orco* is necessary for trafficking of
101 the *OrX* to the dendritic membrane and formation of a functional ion channel (Benton et al.,
102 2006; Larsson et al., 2004). Likewise, the ligand-binding *IrXs* require one or more *IR* co-
103 receptors: *Ir8a*, *Ir25a*, and/or *Ir76b* (Figure 1C, top row). The *IR* co-receptors are similarly
104 required for trafficking and ion channel function (Abuin et al., 2011; Abuin et al., 2019; Ai et al.,
105 2013; Vulpe et al., 2021b). The *GR* gene family generally encodes receptors involved in taste,
106 which are typically expressed outside the olfactory system (such as in the labella or the legs)
107 (Dunipace et al., 2001; Park and Kwon, 2011; Scott, 2018; Scott et al., 2001); however, *Gr21a*
108 and *Gr63a* are expressed in one antennal OSN neuron class, and form a complex sensitive to
109 carbon dioxide (Figure 1C, bottom row) (Jones et al., 2007; Kwon et al., 2007).
110 The majority of receptors have been mapped to their corresponding OSNs, sensilla, and
111 glomeruli in the fly brain (Bhalerao et al., 2003; Couto et al., 2005; Fishilevich and Vosshall,
112 2005; Frank et al., 2017; Grabe et al., 2016; Hallem and Carlson, 2006; Hallem et al., 2004;
113 Knecht et al., 2017; Marin et al., 2020; Ray et al., 2008; Silbering et al., 2011). This detailed
114 map has allowed for exquisite investigations into the developmental, molecular,
115 electrophysiological, and circuit/computational bases of olfactory neurobiology. This work has
116 relied on transgenic lines to identify and manipulate OSN classes (Ai et al., 2013; Brand and
117 Perrimon, 1993; Couto et al., 2005; Fishilevich and Vosshall, 2005; Kwon et al., 2007; Lai and
118 Lee, 2006; Larsson et al., 2004; Menuz et al., 2014; Potter et al., 2010; Silbering et al., 2011).
119 These transgenic lines use segments of DNA upstream of the chemosensory genes that are
120 assumed to reflect the enhancers and promoters driving expression of these genes. While a
121 powerful tool, transgenic lines may not contain all of the necessary regulatory elements to
122 faithfully recapitulate the expression patterns of the endogenous genes. Some transgenic lines
123 label a subset of the cells of a given olfactory class, while others label additional cells: for
124 example, the transgenic *Ir25a-Gal4* line is known to label only a portion of cells expressing Ir25a

125 protein (as revealed by antibody staining) (Abuin et al., 2011); conversely, *Or67d-Gal4*
126 transgenes incorrectly label two glomeruli, whereas a *Gal4* knock-in at the *Or67d* genetic locus
127 labels a single glomerulus (Couto et al., 2005; Fishilevich and Vosshall, 2005; Kurtovic et al.,
128 2007). While knock-ins provide a faithful method to capture a gene's expression pattern,
129 generating these lines has traditionally been cumbersome.

130 In this paper, we implement an efficient knock-in strategy to target the four main
131 chemosensory co-receptor genes in *Drosophila melanogaster (Orco, Ir8a, Ir76b, Ir25a)*. We find
132 broad co-expression of these co-receptor genes in various combinations in olfactory neurons,
133 challenging the current view of segregated olfactory families in the fly. In particular, *Ir25a* is
134 expressed in the majority of olfactory neurons, including most Orco+ OSNs. In addition, the *Ir8a*
135 and *Ir25a* knock-in lines help to distinguish two new OSN classes in the sacculus that target
136 previously un-identified glomerular subdivisions in the posterior AL. Recordings in *Ir25a* mutant
137 sensilla in Orco+ neurons reveal subtle changes in odor responses, suggesting that multiple
138 chemoreceptor gene families could be involved in the signaling or development of a given OSN
139 class. These data invite a re-examination of odor coding in *Drosophila*. We present a
140 comprehensive model of co-receptor expression, which will inform future investigations of
141 combinatorial chemosensory processing.

# 142 Results

## 143 *Generation and Validation of Co-Receptor Knock-in Lines*

144 We previously developed the HACK technique for CRISPR/Cas9-mediated *in vivo* gene
145 conversion of binary expression system components, such as the conversion of transgenic *Gal4*
146 to *QF2* (Brand and Perrimon, 1993; Jinek et al., 2012; Lin and Potter, 2016a, b; Potter et al.,
147 2010; Riabinina et al., 2015; Xie et al., 2018). Here, we adapt this strategy for the efficient
148 generation of targeted knock-ins (see Table 1 and Table 1-Source Data 1 for details). We chose

149 to target the four chemosensory co-receptor genes to examine unmapped patterns of co-
150 receptor expression in *Drosophila melanogaster*. We inserted a *T2A-QF2* cassette and mCherry
151 selection marker before the stop codon of the four genes of interest (Figure 2A and Figure 2-
152 Figure Supplement 1). By introducing the T2A ribosomal skipping peptide, the knock-in will
153 produce the full-length protein of the gene being targeted as well as a functional QF2
154 transcription factor (Figure 2A, Protein Products). This approach should capture the
155 endogenous expression pattern of the gene under the control of the gene's native regulatory
156 elements, while retaining the gene's normal function (Baena-Lopez et al., 2013; Bosch et al.,
157 2020; Chen et al., 2020; Diao et al., 2015; Diao and White, 2012; Du et al., 2018; Gnerer et al.,
158 2015; Gratz et al., 2014; Kanca et al., 2019; Lee et al., 2018; Li-Kroeger et al., 2018; Lin and
159 Potter, 2016a; Vilain et al., 2014; Xue et al., 2014). We found that *T2A-QF2* knock-ins were
160 functional with some exceptions (See Figure 2-Figure Supplement 2 and Figure 2-Source Data
161 1). For example, *Orco-T2A-QF2* knock-in physiology was normal, while a homozygous *Ir25a-*
162 *T2A-QF2* knock-in exhibited a mutant phenotype. This suggests that the addition of the T2A
163 peptide onto the C-terminus of Ir25a might interfere with its co-receptor function.
164 We examined the expression of the co-receptor knock-in lines in the adult olfactory
165 organs by crossing each line to the same *10XQUAS-6XGFP* reporter (Figure 2B – I). *Orco-T2A-*
166 *QF2* driven GFP expression was detected in the adult antennae and maxillary palps (Figure
167 2B), as previously described (Larsson et al., 2004). We validated the *Orco-T2A-QF2* knock-in
168 line with whole-mount antibody staining of maxillary palps (Figure 2C) and found a high degree
169 of correspondence between anti-Orco antibody staining and knock-in driven GFP in palpal
170 olfactory neurons (quantified in Table 2; see also Figure 2-Figure Supplement 3A – D for PCR
171 and sequencing validation of all knock-in lines). We confirmed the specificity of the anti-Orco
172 antibody by staining *Orco*$^{2}$ mutant palps and found no labeling of olfactory neurons (Figure 2-
173 Figure Supplement 3E).

174 Unlike *Orco*, *Ir8a* expression has previously been localized only to the antenna, to
175 olfactory neurons found in coeloconic sensilla and in the sacculus (Abuin et al., 2011). As
176 expected, the knock-in line drove GFP expression only in the antenna (Figure 2D). To validate
177 the *Ir8a-T2A-QF2* knock-in line, we performed antibody staining on antennal cryosections and
178 found the majority of cells to be double-labeled (Figure 2E, Table 2). There was no anti-Ir8a
179 staining in control *Ir8a*$^{1}$ mutant antennae (Figure 2-Figure Supplement 3F).
180 The *Ir76b* gene has previously been implicated in both olfaction and gustation and has
181 been shown to be expressed in adult fly antennae, labella (mouthparts), legs, and wings (Abuin
182 et al., 2011; Chen and Amrein, 2017; Croset et al., 2010; Ganguly et al., 2017; Hussain et al.,
183 2016; Sanchez-Alcaniz et al., 2018; Zhang et al., 2013). We examined the *Ir76b-T2A-QF2*
184 knock-in line and found a similar pattern of expression in the periphery, with GFP expression in
185 the antennae and labella (Figure 2F). Because an anti-Ir76b antibody has not previously been
186 tested in fly antennae, we performed *in situs* on *Ir76b-T2A-QF2 > GFP* antennal cryosections to
187 validate knock-in expression (Figure 2G) and confirmed the specificity of the probe in *Ir76b*$^{1}$
188 mutant antennae (Figure 2-Figure Supplement 3G).
189 Of the four *Drosophila* co-receptor genes, *Ir25a* has been implicated in the broadest
190 array of cellular and sensory functions, from olfaction (Abuin et al., 2011; Benton et al., 2009;
191 Silbering et al., 2011) and gustation (Chen and Amrein, 2017; Chen and Dahanukar, 2017;
192 Jaeger et al., 2018), to thermo- and hygro-sensation (Budelli et al., 2019; Enjin et al., 2016;
193 Knecht et al., 2017; Knecht et al., 2016), to circadian rhythm modulation (Chen et al., 2015). In
194 the adult olfactory system, *Ir25a* expression has previously been reported in three types of
195 structures in the antenna: coeloconic sensilla, the arista, and the sacculus (Abuin et al., 2011;
196 Benton et al., 2009). We examined the *Ir25a-T2A-QF2* knock-in line and found GFP expression
197 in the adult antennae, labella, and maxillary palps (Figure 2H). This was surprising because no
198 Ionotropic Receptor expression has previously been reported in fly palps. To verify Ir25a protein
199 expression in the maxillary palps, we performed whole-mount anti-Ir25a antibody staining in

200 *Ir25a-T2A-QF2* > *GFP* flies. We found broad *Ir25a* expression in palpal olfactory neurons
201 (Figure 2I), and a high degree of overlap between knock-in driven GFP expression and antibody
202 staining (Table 2). As expected, there was no anti-Ir25a staining in *Ir25a*$^{2}$ mutant palps (Figure
203 2-Figure Supplement 3H).

204 We also examined co-receptor knock-in expression in *Drosophila* larvae. As in the adult
205 stage, larval GFP expression was broadest in the *Ir25a-T2A-QF2* and *Ir76b-T2A-QF2* knock-in
206 lines, with GFP labeling of neurons in the head and throughout the body wall (Figure 2-Figure
207 Supplement 4). The *Orco-T2A-QF2* knock-in line labeled only the olfactory dorsal organs in the
208 larva, while the *Ir8a-T2A-QF2* knock-in line did not have obvious expression in the larval stage
209 (Figure 2-Figure Supplement 4). All subsequent analyses focused on the adult olfactory system.

## 210 *Expanded Expression of Olfactory Co-Receptors*

211 We next examined the innervation patterns of the four co-receptor knock-in lines in the adult
212 central nervous system: the brain and ventral nerve cord (VNC) (Figure 3). Only two of the four
213 lines (*Ir25a* and *Ir76b*) showed innervation in the VNC, consistent with the role of these genes in
214 gustation in addition to olfaction (Figure 3-Figure Supplement 1A). In the brain, we compared
215 the expression of each knock-in line (Figure 3A – D, green) to the corresponding transgenic
216 *Gal4* line (Figure 3A – D, orange) to examine differences in expression to what has previously
217 been reported. Reporter alone controls for these experiments are shown in Figure 3-Figure
218 Supplement 1B. All four knock-in lines innervated the ALs, and the *Ir25a-T2A-QF2* and *Ir76b-*
219 *T2A-QF2* lines additionally labeled the suboesophageal zone (SEZ), corresponding to gustatory
220 axons from the labella (Figure 3C and D, arrowheads) (Hussain et al., 2016; Zhang et al., 2013).
221 The co-labeling experiments revealed that all four knock-ins label more glomeruli than
222 previously reported (see Figure 3-Source Data 1 for AL analyses, Figure 3-Source Data 2 for
223 traced examples of newly identified glomeruli in each knock-in line, and Table 3 for a summary
224 of glomerular expression across all knock-in lines). Some glomeruli were not labeled

225 consistently in all flies, which we define as variable expression (found in <50% of brains
226 examined).

227 *Orco-T2A-QF2* labels seven 'non-canonical' glomeruli consistently, and one sporadically.
228 These include VM4 and VL2a, which correspond to Ir76b+ and Ir8a+ OSN populations,
229 respectively (Figure 3A, outlines). We also found that the *Orco* knock-in sparsely but
230 consistently labels the V glomerulus, which is innervated by Gr21a+/Gr63a+ neurons (Figure
231 3A, box and zoom panel). *Orco-T2A-QF2* also labels one Ir25a+ glomerulus consistently (VL1),
232 three additional Ir8a+ glomeruli consistently (DL2d, DL2v, DP1l) and one variably (DC4).
233 Surprisingly, when we crossed the transgenic *Orco-Gal4* line (Larsson et al., 2004) to a stronger
234 reporter (Shearin et al., 2014), we found that several of these additional glomeruli were weakly
235 labeled by the transgenic line (Figure 3-Figure Supplement 2A). This suggests that there are
236 OSN populations in which *Orco* is expressed either at low levels or in few cells, which might be
237 why this expression was previously missed. We found this to be the case with the *IrCo* knock-
238 ins, as well (described below).

239 There has been some inconsistency in the literature as to which glomeruli are innervated
240 by Ir8a-expressing OSNs. For example, Silbering et al., 2011 note that their *Ir8a-Gal4* line labels
241 approximately ten glomeruli, six of which are identified (DL2, DP1l, VL2a, VL2p, DP1m, DC4).
242 An *Ir8a-Gal4* line generated by Ai et al., 2013 also labels about ten glomeruli, only two of which
243 are identified (DC4 and DP1m) and which correspond to two glomeruli in Silbering et al., 2011.
244 Finally, Min et al., 2013 identify three additional glomeruli innervated by an *Ir8a-Gal4* line (VM1,
245 VM4, and VC5) but not reported in the other two papers. DL2 was later subdivided into two
246 glomeruli (Prieto-Godino et al., 2017), bringing the total number of identified Ir8a+ glomeruli to
247 ten. However, we found that *Ir8a-T2A-QF2* consistently labels twice as many glomeruli as
248 previously reported. These additional glomeruli include an Ir25a+ glomerulus (VL1, Figure 3B),
249 numerous Orco+ glomeruli (such as VA3 and VA5), and an Orco+/Ir76b+ glomerulus (VC3)
250 (see Figure 3-Source Data 1 for a full list of new glomeruli and Figure 3-Source Data 2 for

251 outlined examples). Some of these additional glomeruli are weakly labeled by an *Ir8a-Gal4* line
252 (Figure 3-Figure Supplement 2B), but this innervation is only apparent when examined with a
253 strong reporter.

254 Of the four chemosensory co-receptor genes, the previously reported expression of
255 *Ir76b* is the narrowest, with only four identified glomeruli (VM1, VM4, VC3, VC5) (Silbering et al.,
256 2011). The *Ir76b-T2A-QF2* knock-in labels more than three times this number, including several
257 Orco+ glomeruli (such as DC3 and VC4), most Ir8a+ glomeruli (including DP1l), and one
258 additional Ir25a+ glomerulus (VL1) (Figure 3C). As with *Orco* and *Ir8a*, some but not all of these
259 glomeruli can be identified by crossing the transgenic *Ir76b-Gal4* line to a strong reporter
260 (Figure 3-Figure Supplement 2C). However, the *Ir76b-Gal4* line labels additional glomeruli not
261 seen in the knock-in (Figure 3-Figure Supplement 2C, Orco+ cluster). In total, the *Ir76b-T2A-*
262 *QF2* knock-in labels 15 glomeruli consistently and two variably (Figure 3-Source Data 1 and 2).

263 *Ir25a-T2A-QF2* innervation of the AL was the most expanded compared to what has
264 previously been reported. In addition to the novel expression we identified in the palps (Figure
265 2H), we found that the *Ir25a* knock-in innervates many Orco+ glomeruli receiving inputs from
266 the antennae (Figure 3D). The extensive, dense innervation of the AL by Ir25a+ processes
267 made identification of individual glomeruli difficult and necessitated further experiments to fully
268 characterize this expression pattern (described in greater detail below). While it was previously
269 reported that the transgenic *Ir25a-Gal4* line labels only a subset of Ir25a+ neurons (compared to
270 anti-Ir25a antibody staining), it was assumed that neurons not captured by the transgenic line
271 would reside in coeloconic sensilla, the arista or sacculus (the original locations for all IR+
272 OSNs) (Abuin et al., 2011). When we crossed *Ir25a-Gal4* to a strong reporter, we found labeling
273 of a few Orco+ glomeruli (Figure 3-Figure Supplement 2D), but this was a small fraction of those
274 labeled by the knock-in. To further examine *Ir25a* expression and the potential co-expression of
275 multiple co-receptors in greater detail, we employed a combination of approaches including
276 single nucleus RNAseq (snRNAseq), immunohistochemistry, and optogenetics.

277 ## *Confirmation of Co-Receptor Co-Expression*

278 The innervation of the same glomeruli by multiple co-receptor knock-in lines challenges the
279 previous view of segregated chemosensory receptor expression in *Drosophila* and suggests two
280 possible explanations: either the same olfactory neurons express multiple co-receptors (co-
281 expression), or different populations of olfactory neurons expressing different receptors
282 converge upon the same glomeruli (co-convergence). These scenarios are not necessarily
283 mutually exclusive. To examine these possibilities in a comprehensive, unbiased way, we
284 analyzed snRNAseq data from adult fly antennae (McLaughlin et al., 2021). Figure 4A shows
285 the expression levels of the four co-receptor genes in 20 transcriptomic clusters (tSNE plots
286 (Van der Maaten and Hinton, 2008), top row) which were mapped to 24 glomerular targets in
287 the brain (AL maps, bottom row). The proportion of cells in each cluster expressing the given
288 co-receptor gene is indicated by the opacity of the glomerular fill color, normalized to maximum
289 expression for that gene (see Methods and Figure 4-Source Data 1 for details on expression
290 normalization). The OSN classes to which these clusters map include Orco+ neurons (Figure
291 4A right column, teal), Ir25a+ neurons (Figure 4A right column, purple), Ir8a+ neurons (Figure
292 4A right column, pink), and GR+ neurons (Figure 4A right column, dark blue). They also include
293 example OSNs from all sensillar types (basiconic, intermediate, trichoid, coeloconic) as well as
294 from the arista and sacculus. The snRNAseq analyses confirmed expanded expression of all
295 four co-receptor genes into OSN classes not traditionally assigned to them. For example, *Orco*
296 and *Ir25a* are expressed in cluster 1, which maps to the V glomerulus (Gr21a+/Gr63a+).
297 Similarly, *Ir8a* and *Ir76b* are expressed in cluster 19 (VL1 glomerulus, Ir25a+), and *Ir25a* is
298 expressed in multiple Orco+ clusters (such as 15/VA2, 16/DL3, and 8/DC1).

299 The snRNAseq analyses confirm transcript co-expression in olfactory neurons in the
300 periphery. To demonstrate protein co-expression in OSNs, we performed anti-Orco antibody
301 staining on *Ir25a-T2A-QF2 > GFP* antennae and palps (Figure 4B). In the antennae, we found

302 examples of Orco+ GFP+ double-labeled cells, as well as many cells that were either GFP+ or
303 Orco+ (Figure 4B, top right panel). Interestingly, in the palps the vast majority of cells were
304 double-labeled. We found a small population of palpal neurons which were only Orco+, and no
305 neurons that were only GFP+ (Figure 4B, bottom right panel). These results are consistent with
306 our anti-Ir25a staining experiments in the palps (Figure 2I), which showed that most of the ~120
307 palpal OSNs express Ir25a protein.

308 The snRNAseq data from the antennae and peripheral immunohistochemical
309 experiments in the palps helped to identify some of the novel OSN populations expressing
310 *Ir25a*. We extended these analyses with co-labeling experiments in which we combined
311 transgenic *OrX*-, *IrX*-, or *GrX-Gal4* lines labeling individual glomeruli with the *Ir25a* knock-in to
312 verify the glomerular identity of Ir25a+ axonal targets in the AL. Two examples are shown in
313 Figure 4C (one antennal and one palpal OSN population), and the full list of OSN classes
314 checked can be found in Figure 4-Source Data 2.

315 For some OSN classes not included in the snRNAseq dataset for which co-labeling
316 experiments yielded ambiguous results, we employed an optogenetic approach. We used the
317 *Ir25a-T2A-QF2* knock-in to drive expression of *QUAS-CsChrimson*, a red-shifted
318 channelrhodopsin (Klapoetke et al., 2014), and performed single sensillum recordings (SSR)
319 from sensilla previously known to house only Orco+ neurons. If these neurons do express *Ir25a*,
320 then stimulation with red light should induce neuronal firing. We recorded from ab3 sensilla,
321 which have two olfactory neurons (A and B; indicated with blue and green dots, respectively, in
322 Figure 4D). Ab3A neurons innervate DM2 and ab3B neurons innervate VM5d. Both neurons
323 responded to pulses of 627 nm light at various intensities in a dose-dependent manner,
324 confirming *Ir25a* expression in these neurons. No light-induced responses were found in control
325 flies not fed all-trans retinal (-ATR), a necessary co-factor for channelrhodopsin function (see
326 Methods). We used similar optogenetic experiments to examine *Ir25a* expression in OSN
327 classes innervating DM4 (ab2A, Or59b+) and DM5 (ab2B, Or85a/Or33b+) (Figure 4-Figure

328 Supplement 1A-B), as well as D (ab9A, Or69aA/aB+) and VA3 (ab9B, Or67b+) (Figure 4-Figure
329 Supplement 1C-D). These experiments indicated that *Ir25a* is expressed in ab2A (DM4) and
330 ab9B (VA3) neurons, but not ab2B (DM5) or ab9A (D) neurons (see also Figure 4-Source Data
331 2 and 3). Results of these experiments are summarized in Table 3.

## 332 *Identification of New OSN Classes*

333 The co-receptor knock-ins allowed us to analyze the olfactory neuron innervation patterns for all
334 antennal lobe glomeruli. Interestingly, the *Ir8a-T2A-QF2* and *Ir25a-T2A-QF2* knock-ins strongly
335 labeled a previously uncharacterized posterior region of the AL. By performing a co-labeling
336 experiment with *Ir41a-Gal4*, which labels the VC5 glomerulus, we narrowed down the
337 anatomical location of this region and ruled out VC5 as the target of these axons (Figure 5A).
338 While both knock-ins clearly labeled VC5, they also labeled a region lateral and slightly posterior
339 to it (Figure 5A, outline). We performed additional co-labeling experiments with *Ir8a-T2A-QF2*
340 and various *Gal4* lines labeling all known posterior glomeruli to confirm that this AL region did
341 not match the innervation regions for other previously described OSN populations (Figure 5-
342 Figure Supplement 1). We recognized that this novel innervation pattern appeared similar to a
343 portion of the recently identified Rh50+ ammonia-sensing olfactory neurons (Vulpe et al.,
344 2021a). Co-labeling experiments with *Rh50-Gal4* and *Ir8a-T2A-QF2* confirmed that they indeed
345 partially overlapped (Figure 5B). We determined that these Rh50+ olfactory neurons mapped to
346 a portion of the VM6 glomerulus, with the strongly Ir8a+ region innervating the 'horn' of this
347 glomerulus. The difference in innervation patterns between Ir8a+ and Rh50+ neurons in this AL
348 region suggested at least two different subdivisions or OSN populations within this VM6
349 glomerulus. In fact, in between the main body of VM6 and the Ir8a+ horn there appeared to be a
350 third region (Figure 5B, horn outlined in white, other two regions outlined in blue). We
351 designated these subdivisions VM6l, VM6m, and VM6v (for lateral, medial, and ventral). We
352 coordinated the naming of this glomerulus with recent connectomics analyses of the entire fly

353 antennal lobe (Schlegel et al., 2021). In this connectomics study, dendrites of olfactory
354 projection neurons were found to innervate the entire region described here as VM6l, VM6m,
355 and VM6v. No projection neurons were identified to innervate only a subdomain. As such, the
356 new VM6 nomenclature reflects this unique subdivision of a glomerulus by olfactory sensory
357 neurons but not second order projection neurons.

358 We sought to determine the identity of the olfactory neurons that might be innervating
359 these three VM6 subdivisions. Rh50+ neurons can be found in two regions of the antenna: ac1
360 coeloconic sensilla and the sacculus (Figure 5C) (Vulpe et al., 2021a). The shape of the VM6v
361 subdomain most closely matches the glomerulus described as VM6 by previous groups (e.g.
362 Couto et al., 2005; Endo et al., 2007), which had been suggested to be innervated by
363 coeloconic sensilla (Chai et al., 2019; Li et al., 2016). In addition, antibody staining had
364 previously shown that Rh50+ ac1 neurons broadly co-express Ir25a but generally not Ir8a
365 (Vulpe et al., 2021a). This suggested that the other VM6 subdomains might be innervated by
366 the Rh50+ sacculus olfactory neurons. Antibody staining in *Rh50-Gal4>GFP* antennae
367 confirmed co-expression with both Ir25a protein (broad overlap) and Ir8a protein (narrow
368 overlap) in the third chamber of the sacculus (Figure 5D; quantified in Table 4). Most sacculus
369 neurons appear to be Ir25a+, and in contrast to the *Ir8a* knock-in, the three VM6 subdivisions
370 are all strongly innervated by the *Ir25a* knock-in (Figure 5A). Two previously described OSN
371 populations in the third chamber of the sacculus had been characterized to express *Ir8a* along
372 with *Ir64a* and innervate the DP1m and DC4 glomeruli (Ai et al., 2013; Ai et al., 2010). To
373 demonstrate that the Rh50+ Ir8a+ sacculus neurons represented a distinct olfactory neuron
374 population, we performed immunohistochemistry experiments in *Rh50-Gal4>GFP* antennae
375 with an anti-Ir64a antibody (Figure 5E, top), and in *Ir64a-Gal4>GFP* antennae with an anti-Ir8a
376 antibody (Figure 5E, bottom). These experiments confirmed a new, distinct population of Ir8a+
377 Ir64a- cells in the sacculus.

The VM6l olfactory projections are difficult to identify in the hemibrain connectome (Scheffer et al., 2020) due to the medial truncation of the AL in that dataset (see Schlegel et al., 2021 for additional details). Here, we used FlyWire (Dorkenwald et al., 2020), a recent segmentation of a full adult fly brain (FAFB) (Zheng et al., 2018), to reconstruct the VM6 OSN projections in both left and right AL. Synapse-based hierarchical clustering (syNBLAST) (Buhmann et al., 2021) of the VM6 OSNs demonstrated the anatomical segregation into three distinct subpopulations: VM6l, VM6m and VM6v (Figure 5F). This subdivision was subsequently confirmed in a re-analysis of the VM6 glomerulus in the hemibrain dataset (Schlegel et al., 2021). Olfactory neurons innervating VM6l were strongly Ir8a+, while olfactory neurons innervating VM6m and VM6v were weakly and sparsely Ir8a+ (see Figure 3-Source Data 2, page 3). This pattern may be due to *Ir8a* expression in only one or a few cells. Interestingly, this sparse Ir8a+ expression in olfactory neurons targeting VM6m and VM6v may be sexually dimorphic: we found that male brains had stronger and more frequent Ir8a+ innervation in these two glomeruli compared to female brains (see also Figure 3-Source Data 1).

Based on the EM reconstructions, genetic AL analyses, and peripheral staining experiments, we propose a model of the anatomical locations and molecular identities of the olfactory neurons innervating the VM6 subdivisions (Figure 5F). All VM6 subdivisions broadly express *Rh50* and *Ir25a*; the VM6v OSNs are housed in ac1 sensilla and express *Ir8a* either weakly or only in a small subset of neurons; both the VM6m and VM6l OSNs are found in the sacculus and can be distinguished by their levels or extent of *Ir8a* expression, with VM6l neurons being strongly Ir8a+. Because all three VM6 subdivisions share the same downstream projection neurons, this AL region has been classified as a single glomerulus (Schlegel et al., 2021). We maintain this convention here, for a total of 58 AL glomeruli. It is possible that this number may need to be re-evaluated in the future, and the three VM6 subdivisions reconsidered as *bona fide* separate glomeruli (bringing the OSN glomerular total to 60). Such a separation

403 might be warranted if it is found that these OSN populations express different tuning receptors,
404 and those receptors respond to different odorants.

405 Table 3 summarizes the chemosensory receptor expression patterns for all four co-
406 receptor knock-in lines across all OSNs, sensillar types, and glomeruli. For clarity, this summary
407 considers the newly identified OSN populations described here separately. We find that *Orco-*
408 *T2A-QF2* consistently labels 45 total glomeruli out of 58 (7 more than previously reported); *Ir8a-*
409 *T2A-QF2* consistently labels 18 glomeruli (8 more than previously identified); *Ir76b-T2A-QF2*
410 consistently labels 15 glomeruli (11 more than previously identified); and *Ir25a-T2A-QF2*
411 consistently labels 51 glomeruli (39 more than previously identified).

## 412 *Co-receptor Contributions to Olfactory Neuron Physiology*

413 How might the broad, combinatorial co-expression of various chemosensory families affect
414 olfactory neuron function? To begin to address this question we examined olfactory responses
415 in neuronal populations co-expressing just two of the four chemosensory receptor families (*Orco*
416 and *Ir25a*). We chose to test eight OSN classes previously assigned to the Orco+ domain that
417 we found to have strong or intermediate *Ir25a* expression – two in the antennae, and six in the
418 maxillary palps. The two antennal OSN classes are found in the same ab3 sensillum (ab3A,
419 Or22a/b+, DM2 glomerulus; and ab3B, Or85b+, VM5d glomerulus). The six palpal OSN classes
420 represent the entire olfactory neuron population of the maxillary palps (pb1A, Or42a+, VM7d;
421 pb1B, Or71a+, VC2; pb2A, Or33c/Or85e+, VC1; pb2B, Or46a+, VA7l; pb3A, Or59c+, VM7v;
422 pb3B, Or85d+, VA4). In both the antennae and the palps, we compared the olfactory responses
423 of OSNs to a panel of 13 odorants in three genotypes: *wildtype*, *Ir25a*$^{2}$ mutant, and *Orco*$^{2}$
424 mutant flies. This panel included odorants typically detected by *ORs*, such as esters and
425 aromatics, and odorants typically detected by *IRs*, such as acids and amines (Silbering et al.,
426 2011). In the previously accepted view of olfaction in *Drosophila*, Orco+ neurons express only
427 Orco/OrX receptors, and all olfactory responses in the neurons can be attributed to these

428 receptors. Thus, in an *Ir25a*$^2$ mutant background, there should be no difference in olfactory
429 responses from *wildtype* if either a) *Ir25a* is not expressed in these neurons, or b) *Ir25a* is
430 expressed, but is not playing a functional role in these neurons. In an *Orco*$^2$ mutant background,
431 there would be no trafficking of Orco/OrX receptors to the dendritic membrane, and no formation
432 of functional ion channels (Benton et al., 2006; Larsson et al., 2004). Thus, in the traditional
433 view of insect olfaction, *Orco*$^2$ mutant neurons should have no odor-evoked activity. However, in
434 the new co-receptor co-expression model of olfaction, if *Ir25a* is contributing to olfactory
435 responses in Orco+ neurons, then mutating this co-receptor might affect the response profiles of
436 these neurons. Similarly, *Orco*$^2$ mutant neurons that co-express *Ir25a* might retain some odor-
437 evoked activity.

438 We first examined olfactory responses in palp basiconic sensilla. In the palps, three
439 types of basiconic sensilla (pb1, pb2, and pb3) contain two neurons each (A and B) (Figure 6A),
440 for a total of six OSN classes (Couto et al., 2005; de Bruyne et al., 1999; Fishilevich and
441 Vosshall, 2005; Goldman et al., 2005; Ray et al., 2008; Ray et al., 2007). We found robust
442 responses to several odorants in our panel in both the *wildtype* and *Ir25a*$^2$ mutant flies, including
443 odorants like 1-octen-3-ol typically considered as an OR ligand (Figure 6B), and IR ligands like
444 pyrrolidine. Neither odor-evoked nor spontaneous activity was detected in the *Orco*$^2$ mutant
445 (Figure 6B, bottom row; see also Figure 6-Figure Supplement 1A). This was true of all sensilla
446 tested in the palps. The SSR experiments in Figure 6A-D were performed at 4 – 8 DPE. We
447 recently discovered that neurodegeneration of *Orco*$^2$ mutant olfactory neurons occurs in the
448 palps by ~6 DPE (Task and Potter, 2021), which could potentially confound our interpretation.
449 We repeated the experiments in young (1 – 3 DPE) flies but similarly detected neither odor-
450 evoked activity nor spontaneous activity in mutant palpal neurons (Figure 6-Figure Supplement
451 1B). There was also no spontaneous or odor-evoked activity in an *Ir25a*$^2$; *Orco*$^2$ double mutant
452 (Figure 6-Figure Supplement 1C). This suggests one of three possibilities: first, *Orco*$^2$ mutant
453 neurons in the palps could already be dysfunctional at this early stage, despite not yet showing

454 cell loss, and *Ir25a*-dependent activity is not sufficient to maintain either baseline or stimulus-
455 induced activity; second, *Ir25a* function may be *Orco*-dependent in these cells, or act
456 downstream of *Orco*, such that loss of *Orco* function affects *Ir25a* function; third, we did not
457 stimulate neurons with an *Ir25a*-dependent odorant. The latter possibility would not, however,
458 explain why there is no spontaneous activity in these cells. Future experiments will be needed to
459 address these possibilities. Given the lack of neuronal activity in the $Orco^2$ mutant, we focused
460 subsequent analyses in the palps on the two other genotypes: *wildtype* and $Ir25a^2$.

461 The response in the pb1A neuron to 1-octen-3-ol was significantly higher in the $Ir25a^2$
462 mutant compared to the *wildtype* (Mann-Whitney *U* test, $p = 0.0016$), as was the response to
463 methyl salicylate ($p = 0.0177$), while the response to ethyl acetate was higher in *wildtype* ($p =$
464 $0.008$) (Figure 6C; see Figure 6-Source Data 1 for results of all statistical analyses). The
465 differences in responses across all six OSN classes in the palps between *wildtype* and $Ir25a^2$
466 mutant flies are summarized in Figure 6D. In each neuron class, we found one to three odorants
467 whose response profiles differed between the two genotypes. However, the specific stimuli
468 eliciting different responses, and the directionality of those responses, varied. For example, 2,3-
469 butanedione elicited higher responses in the $Ir25a^2$ mutant in both pb2B and pb3A neurons, but
470 lower responses in the mutant (higher in the *wildtype*) in pb3B. Interestingly, when we examined
471 a list of candidate IrX tuning receptors (Li et al., 2021) in the palps using *in situs*, we did not find
472 expression (see Figure 6-Figure Supplement 2 and Figure 6-Source Data 2). This suggests that
473 *Ir25a* may not be functioning as a traditional co-receptor in Orco+ olfactory neurons in the palps
474 (an expanded role for *Ir25a* beyond co-reception has previously been suggested; see Budelli et
475 al., 2019; Chen et al., 2015).

476 We next examined olfactory responses in antennal basiconic ab3 sensilla in *wildtype*,
477 $Ir25a^2$ mutant, and $Orco^2$ mutant flies (Figure 6E – I). As in the palps, ab3 sensilla contain two
478 neurons, A and B (Figure 6E). In contrast to the palps, $Orco^2$ mutant ab3 sensilla did
479 occasionally show spontaneous activity (Figure 6F, bottom row; see Figure 6-Figure

480 Supplement 1D for additional example traces). Although there are two Orco+ neurons in this
481 sensillum, we consistently observed only a single spike amplitude in the *Orco*$^2$ mutant. Thus, we
482 cannot determine at this time whether this activity arises from the A or B neuron. We
483 occasionally observed small responses (≤ 10 Δ spikes/sec) in the *Orco*$^2$ mutant; however,
484 across all flies tested, these responses were not significantly different from the mineral oil
485 control (Figure 6I; statistical analyses can be found in Figure 6-Source Data 1). For these
486 reasons, *Orco*$^2$ mutant flies were excluded from the analyses in Figure 6G and Figure 6H.
487 As in the palps, we found significant differences in the responses of both ab3A and ab3B
488 neurons to some odorants between the two genotypes. Comparison of all ab3A responses
489 between *wildtype* and *Ir25a*$^2$ mutant are shown in Figure 6G, and results from both the A and B
490 neurons are summarized in Figure 6H (Mann-Whitney *U*, as in Figure 6A-C; see Figure 6-
491 Source Data 1 for all analyses). In the ab3A neuron, the *wildtype* showed higher responses to
492 propionic acid ($p$ = 0.0441), 1-octen-3-ol ($p$ = 0.0004), phenylacetaldehyde ($p$ = 0.015), and
493 pentyl acetate ($p$ = 0.0164). Interestingly, two of these four odorants are typically associated
494 with *IRs* (propionic acid and phenylacetaldehyde). In the ab3B neuron, only two odorants
495 elicited significantly different responses between the *wildtype* and *Ir25a*$^2$ mutant: propionic acid
496 (response higher in *wildtype*, as with ab3A; $p$ = 0.0388), and pentyl acetate (response higher in
497 mutant, in contrast to ab3A; $p$ = 0.0385). While responses to propionic acid are small in both
498 ab3 neurons, they are abolished in the *Ir25a*$^2$ mutant background (Kruskal-Wallis with
499 uncorrected Dunn's comparing odorant responses to mineral oil control; ab3A $p$ = 0.3957; ab3B
500 $p$ = 0.5184), suggesting that propionic acid detection in ab3 may be *Ir25a*-dependent.

## 501 *The Co-Receptor Co-Expression Map of Olfaction in Drosophila*

502 Co-receptor co-expression of insect chemosensory receptors suggests multiple receptors may
503 influence the response properties of an olfactory neuron, as we have shown in ab3 and palpal
504 sensilla. To aid future investigations of co-receptor co-expression signaling, we synthesized our

505 results (Table 3) into a comprehensive new map of the AL. Figure 7 summarizes the expression
506 patterns of all the co-receptor knock-in lines and presents a new model for chemosensory
507 receptor expression in *Drosophila melanogaster*. In Figure 7A, the expression pattern of each
508 knock-in line is presented separately (see also Figure 3-Source Data 1). The new AL map is
509 updated with the recent re-classification of VP1 into three glomeruli (Marin et al., 2020) and
510 indicates the new VM6 subdivisions. In Figure 7A, the original glomerular innervation pattern for
511 each co-receptor is shown in green, with new innervation revealed by the *T2A-QF2* knock-in
512 lines color coded by intensity: strongly labeled glomeruli are in orange, intermediate glomeruli in
513 yellow, and weakly labeled glomeruli are in pink. Glomeruli labeled in <50% of brains examined
514 are designated variable (grey), and glomeruli not labeled by the given knock-in are in white. The
515 new VM6v, VM6m, and VM6l subdivisions are labeled with grey stripes.

516 In the previous model of olfaction in *Drosophila*, the Orco/OR domain primarily occupied
517 the anterior AL, while the IR domains innervated more posterior glomeruli. While the former is
518 still, for the most part, accurate (Figure 7A, *Orco*), the latter is not: both *Ir8a-T2A-QF2* and
519 *Ir76b-T2A-QF2* label several more anterior glomeruli (such as VA3 or VA6), and *Ir25a-T2A-QF2*
520 labels the majority of glomeruli throughout the anterior to posterior axis (Figure 7A, *Ir25a*). The
521 expansion of the Ir25a+ domain is the most dramatic of the four co-receptors: previously, Ir25a+
522 glomeruli accounted for 21% of the AL (12/58 glomeruli) (Enjin et al., 2016; Frank et al., 2017;
523 Marin et al., 2020; Silbering et al., 2011); the *Ir25a-T2A-QF2* knock-in consistently labels 88% of
524 the AL (51/58 glomeruli, excluding variable). This represents a greater than fourfold expansion.
525 Similarly, the number of Ir76b+ glomeruli increased more than threefold, from 7% of the AL
526 (4/58 glomeruli) (Silbering et al., 2011), to 26% (15/58, excluding variable). The Ir8a+ domain
527 has nearly doubled, from 17% of the AL originally (10/58 glomeruli) (Silbering et al., 2011) to
528 31% (18/58 glomeruli, excluding variable). The most modest increase in reported expression is
529 in the Orco+ domain: from 66% of the AL (38/58 glomeruli) (Couto et al., 2005; Fishilevich and
530 Vosshall, 2005), to 78% (45/58, excluding variable).

531 The expression overlap in the AL of the four co-receptor families is summarized in the
532 Venn diagram shown in Figure 7B (excluding the variably labeled glomeruli from Figure 7A).
533 The table at the right lists the names of the glomeruli which correspond to the sections of the
534 Venn diagram. This analysis reveals 9 glomeruli labeled by all four knock-in lines; furthermore, it
535 shows that the Ir8a+ and Ir76b+ domains do not have glomeruli unique to them. Most of the AL
536 is innervated by Orco+ Ir25a+ neurons (25 glomeruli that are only Orco+ Ir25a+, plus an
537 additional 13 that have Orco, Ir25a, and one or both other co-receptors). The Orco+ and Ir25a+
538 domains reveal glomeruli unique to them (6 glomeruli that are only Orco+, 7 glomeruli that are
539 only Ir25a+). Expression analyses also reveal that Ir8a does not co-express with Orco alone or
540 Ir76b alone.

541 A unified AL map organized by chemosensory gene families (ORs, IRs, and GRs) is
542 shown in Figure 7C (right panel), and the left two panels extend this information into the
543 periphery. Here we include the GR+ innervation of the V glomerulus. However, a knock-in line
544 for either *Gr21a* or *Gr63a* does not currently exist; thus, it is possible these receptors (as well as
545 other poorly characterized antennal GRs) might also be more broadly expressed than previous
546 transgenic lines indicate (Fujii et al., 2015; Menuz et al., 2014). All four OR and IR co-receptors
547 are expressed in the antenna, while olfactory neurons in the palps express *Orco* and *Ir25a*
548 (Figure 7C, left panel). In the antennae, there are many different classes of OSNs expressing
549 various combinations of chemosensory receptors and co-receptors: there are Orco+ only
550 neurons (Figure 7C, middle panel, #2), such as those innervating the VM2 and VM3 glomeruli
551 (teal); IrCo+ only neurons (purple), which include neurons expressing one, two, or all three *IR*
552 co-receptors (such as VP2, VM6v, or DP1m respectively) (Figure 7C, middle panel, #1); and
553 neurons expressing both *Orco* and *IrCo(s)* (teal and purple stripe) (Figure 7C, middle panel, #3
554 and 4).

555 The expression data suggest that different sub-populations of olfactory neurons might be
556 targeting a shared glomerulus. Our data indicate that both Orco+ and Ir25a+ neurons innervate

557 the GR+ V glomerulus (dark blue; see also Figure 7A). Based on the sparse innervation of the V
558 glomerulus by the *Orco-T2A-QF2* knock-in (Figure 3A) and the lower expression levels in the
559 snRNAseq data (Figure 4A), we hypothesize that *Orco* may be expressed in only a subset of
560 Gr21a/Gr63a+ neurons. This contrasts with the *Ir25a-T2A-QF2* knock-in, which appears to label
561 most Gr21a/Gr63a+ neurons. Thus, two sub-populations of neurons may be co-converging
562 upon the same V glomerulus: neurons that express *Gr21a/Gr63a* and *Ir25a* (dark blue and
563 purple stripes), and neurons that express *Gr21a/Gr63a, Ir25a* and *Orco* (dark blue, purple, and
564 teal stripes) (Figure 7C, middle panel, #5). Such co-convergence has recently been shown in
565 the olfactory system of *Aedes aegypti* mosquitoes (Younger et al., 2020). Similarly, the sparse
566 *Orco-T2A-QF2* knock-in innervation of the DP1l glomerulus suggests that there are OSN
567 populations expressing mostly *IRs*, but with a subset of neurons that additionally express *Orco*
568 (Figure 7C, middle panel, #3). The converse may also be possible (Figure 7C, middle panel,
569 #4): OSN populations which have some neurons expressing only *Orco*, and a subset expressing
570 both *Orco* and *IrCo(s)* co-converging onto the same glomerulus. There is some evidence for this
571 in the palps, based on our anti-Orco and anti-Ir25a antibody staining (Figure 2C and I; Figure
572 4B; Table 2). The snRNAseq data suggest this may also be the case in the antennae (see
573 Figure 4-Source Data 1).

## 574 Discussion

575 Here we present evidence in *Drosophila melanogaster* of widespread chemosensory co-
576 receptor co-expression in the olfactory system, contrasting a previously accepted view of
577 segregated, mutually exclusive olfactory domains. By generating targeted knock-ins of the four
578 main chemosensory co-receptors (*Orco*, *Ir8a*, *Ir76b, Ir25a*), we demonstrate that all four co-
579 receptors have broader olfactory neuron expression than previously appreciated. Co-expression
580 of these co-receptors was found in the periphery and in the central projections to the brain. The
581 *Ir25a* co-receptor was previously thought to be expressed only in a small subset of olfactory

582 neurons (coeloconic, sacculus, and arista neurons), but we present evidence that it is
583 expressed in subsets of nearly all OSN classes that innervate the majority of the fly ALs. We
584 further demonstrate that co-expression of chemosensory co-receptors may have functional
585 relevance for olfactory neurons, and that the *Ir25a* co-receptor may be involved in modulating
586 the activity of some Orco+ OSNs, both in the antennae and maxillary palps. We present a new
587 AL map which will aid future inquiries into the role that specific chemoreceptor co-expression
588 plays in distinct OSN populations.

589 A model for OR/IR segregation was initially supported by developmental evidence. Two
590 pro-neural genes specify the development of sensory structures on the antennae: *amos* and
591 *atonal*. *Amos* mutants lack basiconic and trichoid sensilla, while *atonal* mutants do not develop
592 coeloconic sensilla, the arista, or the sacculus (Goulding et al., 2000; Gupta and Rodrigues,
593 1997; Jhaveri et al., 2000a; Jhaveri et al., 2000b). It was observed that *amos* mutants lose *Orco*
594 expression while retaining *Ir25a* expression (Benton et al., 2009). Our results generally do not
595 conflict with this view. In the traditional segregated model of the fly olfactory system, it was
596 presumed that *atonal* mutant antennae would show the reverse pattern: loss or *IrCo* expression
597 but not *Orco* expression. However, our co-receptor knock-in expression results suggest that
598 *atonal* mutants should have significant *IrCo* expression, particularly of *Ir25a*. This was indeed
599 found to be the case in RNAseq analyses performed on *atonal* mutant antennae, which showed
600 that both *Ir25a* and *Ir76b* expression, but not *Ir8a* expression, remained (Menuz et al., 2014).
601 Based upon the strength of the corresponding glomerular innervations, it does appear that the
602 previously reported Ir25a+ neurons have stronger or more consistent *Ir25a* expression, while
603 the new Ir25a+ olfactory neurons in the antennae reported here (e.g. *OR*-expressing OSNs) are
604 often weakly or stochastically labeled. This might also explain why *Ir25a* expression was initially
605 overlooked in these Orco+ neural populations. The developmental pattern is different in the
606 maxillary palps, where it is *atonal* and not *amos* which is required for development of the
607 basiconic sensilla (Gupta and Rodrigues, 1997). Interestingly, the *Ir25a* knock-in expression

608 corresponds well with the *atonal* developmental program across the olfactory appendages: the
609 strongest expression of *Ir25a* is in coeloconic sensilla, but outside of these sensilla the strongest
610 and most consistent *Ir25a* expression is in palp basiconic sensilla.

611 Chemosensory co-receptor co-expression may help clarify previously confounding
612 observations regarding *Drosophila* odor coding. For example, olfactory neurons in the sacculus
613 that express the *Ir64a* tuning receptor along with the *Ir8a* co-receptor project to two different
614 glomeruli: DC4 and DP1m (Ai et al., 2013; Ai et al., 2010). These two glomeruli exhibit different
615 olfactory response profiles, with DC4 being narrowly tuned to acids or protons, while DP1m is
616 more broadly tuned. The molecular mechanism for these differences was previously unclear as
617 it was thought these neurons expressed the same receptors. However, the co-receptor knock-in
618 data presented here reveal that the Ir64a+ OSN sub-populations do in fact express different
619 combinations of chemoreceptors: in addition to the *Ir8a* co-receptor, neurons innervating DC4
620 express *Ir25a* (and occasionally *Orco*) (see Figure 7). In contrast, neurons innervating DP1m
621 express *Ir8a*, *Ir25a*, and *Ir76b*. Thus, perhaps it is *Ir76b* expression in DP1m-targeting Ir64a+
622 neurons which makes them olfactory generalists. This idea is supported by experiments in
623 which *Ir64a* was misexpressed in neurons targeting the VM4 glomerulus, conferring a DP1m-
624 like, rather than a DC4-like, response profile to VM4 (Ai et al., 2010). We show here that VM4-
625 targeting neurons express *Ir8a*, in addition to *Ir25a* and *Ir76b* (as well as *Orco*): thus,
626 molecularly, the VM4 neuron profile is more similar to DP1m (co-expressing all *IrCos*) than DC4
627 (co-expressing two *IrCos*), and the key distinguishing component appears to be *Ir76b*. It would
628 be interesting to repeat such misexpression experiments in an *Ir76b*$^{-}$ mutant background to test
629 this hypothesis.

630 The widespread expression of *Ir25a* in the fly olfactory system raises the possibility that
631 it might have roles in addition to its function as an IrX co-receptor. For example, *Ir25a* has been
632 found to play a developmental role in forming the unique structure of Cold Cells in the arista
633 (Budelli et al., 2019). Evolutionary studies also suggest that *Ir25a* is the most ancient of all the

634 insect chemosensory receptors (Croset et al., 2010), and the currently broad expression might
635 reflect its previous ubiquitous role in chemosensory signaling. *Ir25a* may also be involved in
636 downstream olfactory signal transduction or amplification, as suggested by the work presented
637 here, and as has recently been shown for a pickpocket ion channel (Ng et al., 2019).
638 Experiments addressing potentially expanded roles for *Ir25a* in olfactory neurons will be aided
639 by the new chemosensory co-receptor map presented here.

640 While we demonstrate here that multiple chemosensory co-receptors can be co-
641 expressed in the same olfactory neurons, it remains to be determined if this also applies to
642 tuning (odor-binding) receptors. Previous studies suggest that OrX tuning receptors are
643 generally limited to a single class of olfactory neurons, with the sole exception being *Or33b*
644 (Couto et al., 2005; Fishilevich and Vosshall, 2005). However, many IrX tuning receptors remain
645 to be characterized and could be co-expressed in multiple olfactory neurons. For example,
646 recordings from ab1, ab3, and ab6 sensilla indicate responses to the typical IR odors 1,4-
647 diaminobutane, ammonia, and butyric acid, respectively (de Bruyne et al., 2001), suggesting
648 tuning IrXs may be involved. We show that *Ir25a* plays a functional role in Orco+ neurons in the
649 antennae and palps; this suggests that these Orco+ neurons could also express as yet
650 unidentified ligand binding IrXs. The recent release of the whole fly single-cell atlas, which
651 includes RNAseq data from maxillary palps, allowed us to identify 6 IRs that might be expressed
652 in palpal OSNs (*Ir40a*, *Ir51a*, *Ir60a*, *Ir62a*, *Ir76a*, *Ir93a*) (Li et al., 2021). However, *in situ*
653 analyses for these 6 IRs in the maxillary palps did not detect a signal (see Figure 6-Figure
654 Supplement 2 and Figure 6-Source Data 2). This suggests that *Ir25a* in the palps may be
655 playing a role independent of its role as a co-receptor, as discussed above, or that a tuning IrX
656 was missed by the RNAseq analyses. In antennal ab3 sensilla, we did find one odorant
657 (propionic acid) which elicited a small response in *wildtype* neurons, and no response in $Ir25a^2$
658 mutant neurons. It is possible that other antennal Orco+ OSNs might utilize IR chemoreceptors
659 for signaling. For example, the ac3B neuron, which expresses Or35a/Orco and all IR co-

660 receptors, has recently been suggested to utilize an unidentified IrX to mediate responses to
661 phenethylamine (Vulpe et al., 2021b). The chemoreceptor expression patterns revealed in this
662 work will help the search for olfactory neurons that may utilize multiple chemosensory families
663 for odor detection.

664 Based on the co-receptor innervation patterns in the antennal lobes, we identified a
665 glomerulus, VM6, that is uniquely partitioned by different olfactory sensory neurons (Figure 5)
666 (also see Schlegel et al., 2021). The co-receptor expression patterns allowed us to pinpoint the
667 likely origin of the innervating OSNs. Since the VM6 glomerulus was labeled by both the *Ir25a-*
668 *T2A-QF2* and *Ir8a-T2A-QF2* knock-in lines, the cell bodies of these neurons had to reside in the
669 antenna; furthermore, since we did not find *Ir8a-T2A-QF2* labeling of the arista, these neurons
670 were likely to be either in coeloconic sensilla or in the sacculus. Indeed, we determined the VM6
671 glomerulus to be innervated by the newly discovered Rh50+ Amt+ olfactory neurons which
672 originate in the sacculus and ac1 sensilla (Vulpe et al., 2021a). Based on our results, Rh50+
673 Amt+ sacculus neurons are further subdivided into those that strongly express Ir8a, which
674 innervate the VM6l region, and those that weakly or infrequently express Ir8a, which innervate
675 VM6m. The functional consequences of this unusual subdivision by olfactory neurons for a
676 glomerulus, and how this relates to the fly's olfactory perception of ammonia or other odorants,
677 remains to be determined. These results also highlight the value of exploring chemosensory
678 receptor expression patterns even in the era of connectomics, as the VM6 glomerulus and its
679 subdivisions were not easily identifiable in prior connectomics reconstructions of the entire
680 antennal lobe (Bates et al., 2020; Scheffer et al., 2020; Schlegel et al., 2021).

681 Co-expression of chemosensory co-receptors might function to increase the signaling
682 capabilities of an olfactory neuron. For example, the signaling of an Orco+ olfactory neuron may
683 be guided primarily by the tuning OrX, and the sensitivity range extended to include odors
684 detectable by an IrX. Co-expression might also allow synergism, such that weak activation of a
685 co-expressed receptor could increase neuronal activity to levels sufficient to drive behavior. This

686 might be useful in tuning behavioral response to complex odors, such that certain combinations
687 of odors lead to stronger olfactory neuron responses. Alternatively, a co-expressed receptor
688 inhibited by odorants might be able to attenuate a neuron's response to odor mixtures. Co-
689 expressed chemosensory receptors might also modulate the perceived valence of an olfactory
690 stimulus through the same olfactory circuit or channel. For example, a recent study showed that
691 $CO_2$, which is normally aversive to flies, can be attractive in certain contexts (van Breugel et al.,
692 2018). While the aversive response requires the known $CO_2$ receptors, *Gr21a* and *Gr63a*, the
693 attractive response was shown to be *Ir25a*-dependent. However, previous calcium imaging
694 experiments in the AL have shown that $CO_2$ primarily activates a single glomerulus, the V
695 glomerulus, which receives inputs from the Gr21a+/Gr63a+ neurons (Suh et al., 2004). Our
696 *Ir25a-T2A-QF2* knock-in line reveals that *Ir25a* is expressed in this OSN class. This raises the
697 possibility that the same neurons, through a different chemoreceptor, could drive both attractive
698 and aversive behavior in different contexts (MacWilliam et al., 2018). Co-expression of
699 chemosensory receptors could be a mechanism to increase the functional flexibility of a
700 numerically limited olfactory system.

701 *Drosophila* often serve as a model for many other insect olfactory systems, and
702 information gleaned from *Drosophila* is frequently extrapolated to other insects (for example,
703 DeGennaro et al., 2013; Fandino et al., 2019; Riabinina et al., 2016; Trible et al., 2017; Yan et
704 al., 2017). The work presented here raises the possibility that other insects may also exhibit co-
705 expression of chemosensory co-receptors. New work in *Aedes aegypti* mosquitoes suggests
706 that this may indeed be the case: mosquito olfactory neurons can co-express Orco/IrCo/Gr
707 receptors; in the $CO_2$-sensing olfactory neuron, this co-expression functionally expands the
708 range of activating odors (Younger et al., 2020). This suggests that co-expression of
709 chemosensory co-receptors may be an important feature of insect olfactory neurons.

710 # Acknowledgements

711 We thank E. Marr and K. Robinson for splinkerette genetic mapping, Y.-T. Chang for cloning of
712 *pHACK*$^{Ir8a}$ components, O. Riabinina for initial *QUAS-CsChrimson* characterization, S. Maguire
713 for preliminary SSR experiments, P. Mohapatra for RNAseq insights, D. Baktash for help with
714 figures, J. Konopka for advice on statistical analyses, S. Shankar for discussion of AL mapping,
715 and R. Mann for providing lab resources. We would like to thank E.C. Marin and M. Costa for
716 discussions regarding posterior AL glomeruli. We are also grateful to the Seung and Murthy labs
717 for access to the flywire.ai reconstruction community. Many thanks to the following labs for
718 sharing antibody and fly stock reagents: Leslie B. Vosshall (Rockefeller), Richard Benton
719 (UNIL), Paul Garrity (Brandeis), Marco Gallio (Northwestern), Greg Suh (NYU/KAIST), and
720 Thomas R. Clandinin (Stanford). We are grateful for *in situ* advice from Richard Benton/Steeve
721 Cruchet and Margo Herre. We thank the Center for Sensory Biology Imaging Facility (NIH
722 P30DC005211) for use of the LSM700 confocal microscope, and the Johns Hopkins School of
723 Public Health Malaria Research Institute for use of the Olympus SZX7 microscope equipped
724 with QImaging QIClick Cooled digital CCD camera. We thank J. Raji, S. Maguire, and J.
725 Konopka for comments on the manuscript and members of the Potter and Menuz labs for
726 discussion. We thank the Vosshall lab for sharing their *Aedes* findings before publication. This
727 work was supported by a Shelanski award to C.-C. L; a Wellcome Trust Collaborative Award
728 (203261/Z/16/Z) and an NIH BRAIN Initiative grant (1RF1MH120679-01) to G.S.X.E. Jefferis;
729 grants from the National Institutes of Health to H.L. (R00 AG062746); grants from the National
730 Institutes of Health to K.M. (NIGMS R35GM133209; NIDCD 1R21DC017868); grants from the
731 Department of Defense to C.J.P. (W81XWH-17-PRMRP) and from the National Institutes of
732 Health to C.J.P. (NIAID R01AI137078; NIDCD R01DC013070).
733 Portions of this work appear in Chapter 3 of D.T.'s doctoral dissertation.

## Author Contributions

**Conceptualization**: D.T. (knock-in analysis, SSR, AL maps and glomerular analyses), C-C.L. (HACK development, knock-in analysis, SSR, optogenetics), A.V. (SSR), M.B. (snRNAseq), P.S. (EM reconstruction and analyses), H.L. (snRNAseq), K.M. (SSR, IRs, palp analysis), C.J.P. (all aspects); **Methodology**: D.T. (cloning and generation of knock-ins (*Ir25a*, *Ir8a*, *Ir76b*), immunohistochemistry, SSR, statistics, AL maps), C-C.L. (HACK, genetics, cloning and generation of knock-ins (*Orco*, *Ir8a*, *Ir76b*), cloning and generation of *QUAS-CsChrimson*, SSR, optogenetics), A.V. (SSR), A.A. (SSR), S.B. (immunohistochemistry), M.B. (snRNAseq), P.S. (EM reconstruction and analyses), H.L. (snRNAseq), K.M. (SSR, IR expression), C.J.P. (all aspects); **Formal Analysis**: D.T. (knock-ins, SSR, cell counts), C-C.L. (knock-ins, SSR), A.V. (SSR), A.A. (SSR), S.B. (cell counts), M.B. (snRNAseq), P.S. (EM analyses), H.L. (snRNAseq); **Investigation**: D.T. (knock-in generation and validation (*Ir25a*, *Ir8a*, *Ir76b*), immunohistochemistry, AL analyses), C-C.L. (HACK development, knock-in generation and validation (*Orco*, *Ir8a*, *Ir76b*), *QUAS-CsChrimson* generation and validation, optogenetics, SSR – palp, ab2), A.V. (SSR – coeloconic), A.A. (SSR – ab3), S.B. (immunohistochemistry), M.B. (snRNAseq), P.S. (EM reconstruction and analyses), H.L. (snRNAseq); **Writing, Original Draft**: D.T. and C.J.P.; **Writing, Review & Editing**: All Authors; **Visualization**: D.T. (olfactory system/fly cartoons, AL maps, microscopy images, SSR, Venn diagram, tables), C-C.L. (genetics cartoons, crossing schemes, SSR, optogenetics), M.B. (snRNAseq), P.S. (EM traces and dendrograms), H.L. (snRNAseq), C.J.P. (all aspects); **Supervision**: G.S.X.E.J., K.M. and C.J.P.; **Funding Acquisition**: C.J.P.

## Declaration of Interests

The authors declare no competing interests.

# Figures and Tables

**Figure 1**

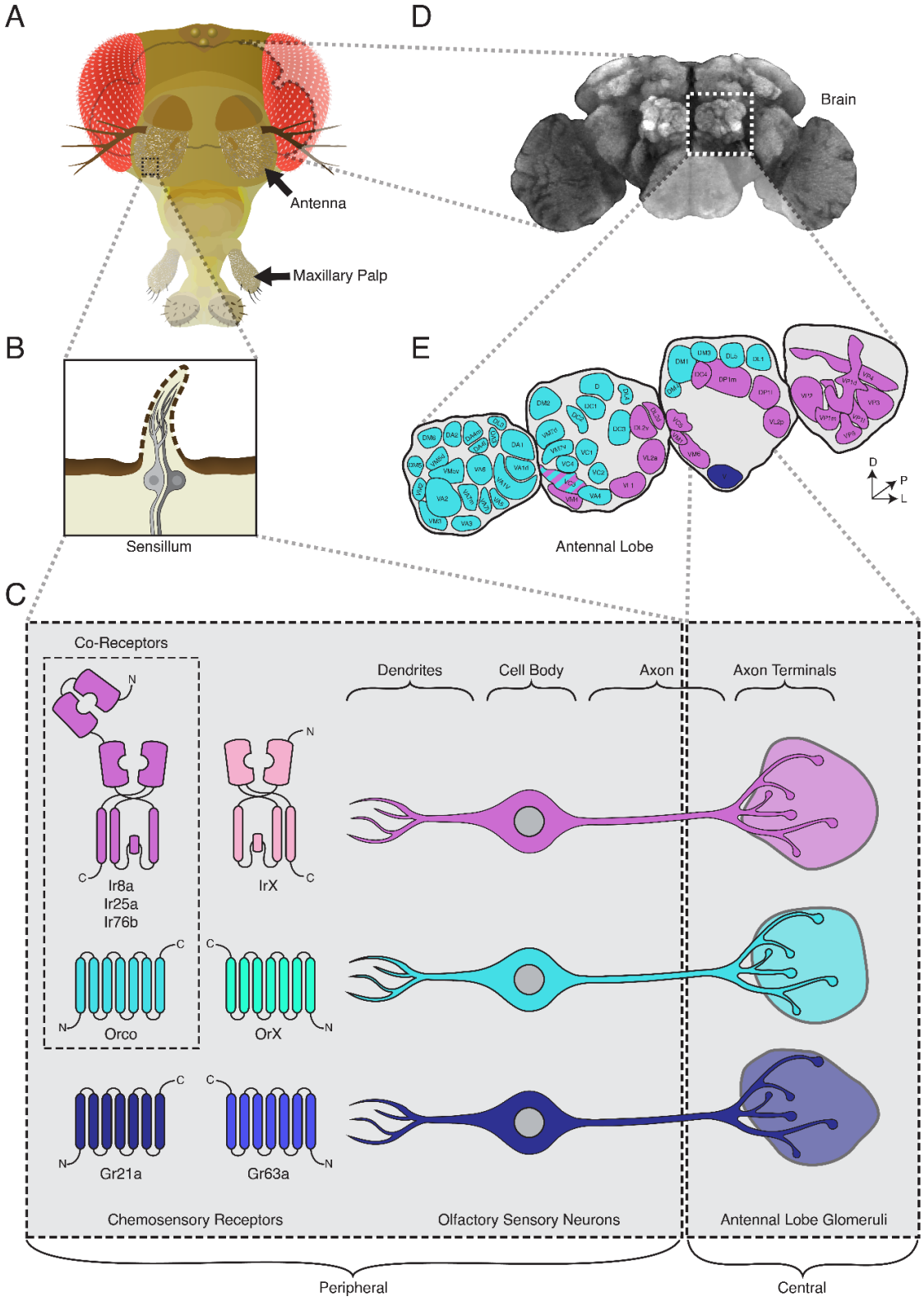

759 **Figure 1. The Standard View of Olfactory Receptor Expression in *Drosophila***
760 ***melanogaster*.**
761 **A.** The adult fly head (left) has two olfactory organs: the antennae and the maxillary palps
762 (arrows). Olfactory neurons from these organs project to the fly brain (D), to the first center
763 involved in processing of olfactory information, the antennal lobes (E). **B.** The olfactory organs
764 are covered by sensory hairs called sensilla (left). Each sensillum contains between one and
765 four olfactory sensory neurons (two example neurons are shown in grey). The dendrites of
766 these neurons extend into the sensilla, and the axons target discrete regions of the antennal
767 lobes called glomeruli (E). Neuronal compartments (dendrites, cell body, axon, axon terminals)
768 are labeled in (C). **C.** Left: in the periphery, each olfactory sensory neuron is traditionally thought
769 to express chemosensory receptors from only one of three gene families on its dendrites:
770 Ionotropic Receptors (IRs, pink and purple), Odorant Receptors (ORs, teal and green), or
771 Gustatory Receptors (GRs, light and dark blue). IRs and ORs require obligate co-receptors
772 (dotted box outline) to form functional ion channels. All ORs utilize a single co-receptor, Orco
773 (teal), while IRs can utilize one (or a combination) of three possible co-receptors (purple): Ir8a,
774 Ir25a, or Ir76b. The two GRs form a functional carbon dioxide detecting channel expressed in
775 only one class of neurons. All other olfactory neurons express one of the four co-receptors.
776 Right: olfactory sensory neurons expressing ORs, IRs, and GRs are thought to project to
777 mutually exclusive glomeruli in the AL of the central brain, forming the olfactory map shown in
778 (E). **D.** Fly brain stained with anti-brp synaptic marker (nc82), with left antennal lobe (AL)
779 outlined by dotted white box. **E.** AL map with glomeruli color-coded by the chemosensory
780 receptors (ORs, IRs, or GRs) expressed in the olfactory sensory neurons projecting to them.
781 Only one glomerulus (VC3, striped) receives inputs from neurons expressing chemoreceptors
782 from multiple gene families (ORs and IRs). Compass: D = dorsal, L = lateral, P = posterior.

783 **Figure 2**

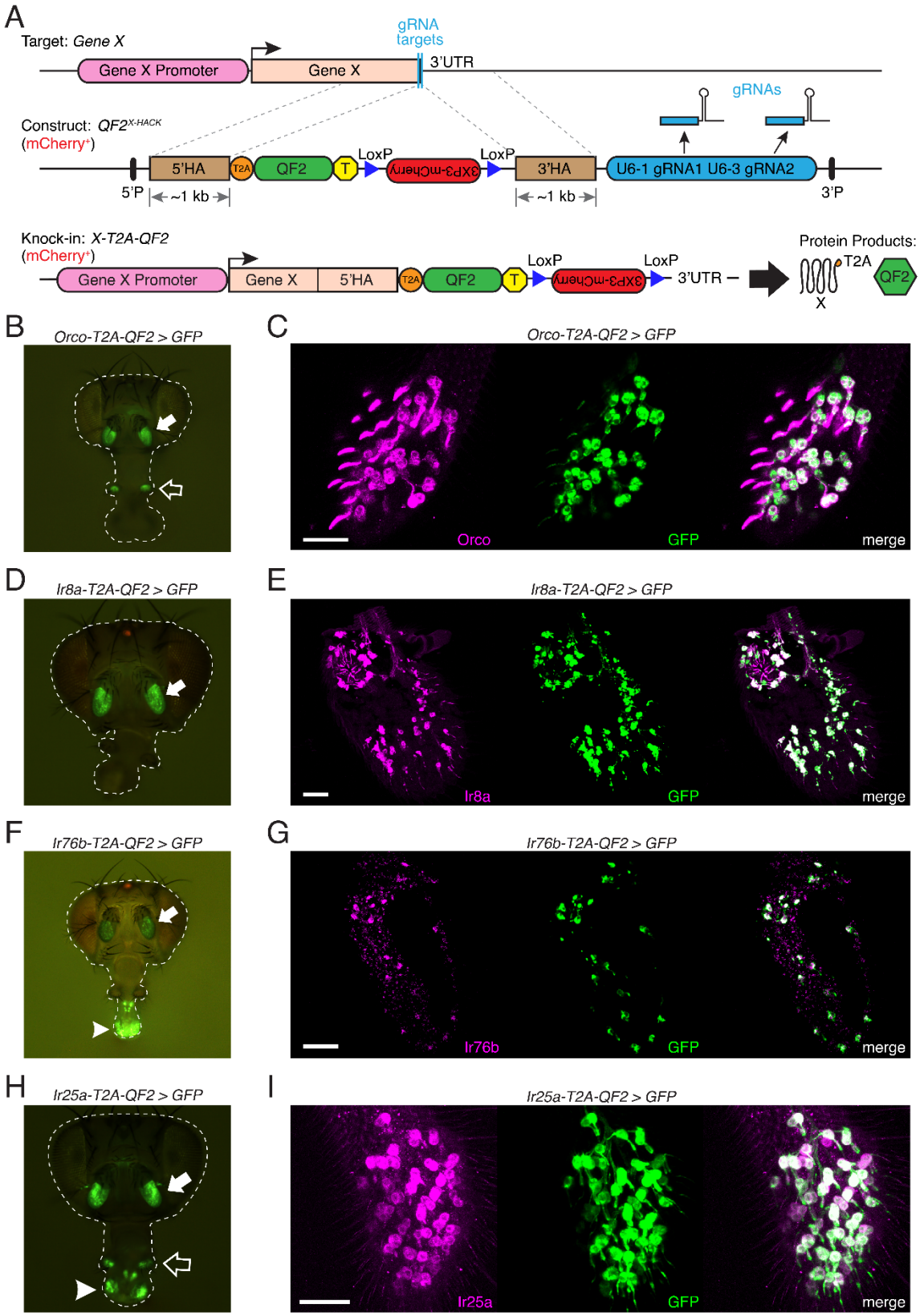
A
Target: Gene X
gRNA targets
Gene X Promoter
Gene X
3'UTR
gRNAs
Construct: QF2X-HACK (mCherry+)
5'HA
T2A
QF2
T
LoxP
3XP3-mCherry
LoxP
3'HA
U6-1 gRNA1 U6-3 gRNA2
5'P
~1 kb
~1 kb
3'P
Knock-in: X-T2A-QF2 (mCherry+)
Gene X Promoter
Gene X
5'HA
T2A
QF2
T
LoxP
3XP3-mCherry
LoxP
3'UTR
Protein Products:
T2A
QF2
X
B
Orco-T2A-QF2 > GFP
C
Orco-T2A-QF2 > GFP
Orco
GFP
merge
D
Ir8a-T2A-QF2 > GFP
E
Ir8a-T2A-QF2 > GFP
Ir8a
GFP
merge
F
Ir76b-T2A-QF2 > GFP
G
Ir76b-T2A-QF2 > GFP
Ir76b
GFP
merge
H
Ir25a-T2A-QF2 > GFP
I
Ir25a-T2A-QF2 > GFP
Ir25a
GFP
merge

784 **Figure 2. Generation and Validation of Chemosensory Co-Receptor Knock-in Lines.**
785 **A.** Schematic of HACK knock-in approach. Top: two double-stranded breaks are induced on
786 either side of the target gene stop codon with gRNAs (blue) expressed from the *QF2*$^{X\text{-}HACK}$
787 construct (middle) in the presence of Cas9. The construct includes *T2A-QF2* and a floxed *3XP3-*
788 *mCherry* marker. The knock-in introduces a transcriptional stop (yellow T) after QF2. Bottom:
789 the knock-in produces two protein products (right) from the targeted mRNA: target X and the
790 *QF2* transcription factor (Diao and White, 2012). The *X-T2A-QF2* knock-in can be crossed to a
791 reporter (e.g. *QUAS-GFP*) to examine the endogenous expression pattern of the target gene. **B.**
792 *Orco-T2A-QF2* driving *QUAS-GFP* in adult fly head. GFP expression is found in the antennae
793 (filled arrow) and maxillary palps (hollow arrow), as previously reported (Larsson et al., 2004).
794 **C.** Whole-mount anti-Orco antibody staining in *Orco-T2A-QF2>GFP* maxillary palps reveals a
795 high degree of overlap of Orco+ and GFP+ cells. N = 3. **D.** *Ir8a-T2A-QF2* drives GFP in the
796 antennae (arrow), as previously reported (Abuin et al., 2011). **E.** Anti-Ir8a antibody staining of
797 *Ir8a-T2A-QF2>GFP* antennal cryosections shows high correspondence between Ir8a+ and
798 GFP+ cells. N = 7. **F.** *Ir76b-T2A-QF2* drives GFP expression in the antennae (filled arrow) and
799 labella (hollow arrow), reflecting *Ir76b*'s role in olfaction and gustation, respectively (Benton et
800 al., 2009; Zhang et al., 2013). **G.** *In situs* on *Ir76b-T2A-QF2>GFP* antennal cryosections to
801 validate that the knock-in faithfully recapitulates the endogenous expression pattern. N = 3. **H.**
802 *Ir25a-T2A-QF2* drives GFP in the antennae (filled arrow) and labella (hollow arrow), which has
803 been reported previously (Benton et al., 2009; Croset et al., 2010). Expression in the maxillary
804 palps (arrowhead) has not been previously reported. **I.** Whole-mount maxillary palp staining with
805 an anti-Ir25a antibody in *Ir25a-T2A-QF2>GFP* flies. The knock-in and Ir25a antibody co-labeled
806 the majority of olfactory neurons in the palps. N = 5. Scale bars = 25 μm. In (D) and (F), the
807 *3XP3-mCherry* knock-in marker can be weakly detected in the eyes and ocelli (red spot) of both
808 *Ir8a-T2A-QF2* and *Ir76b-T2A-QF2*. See also Figure 2-Figure Supplements 1-4, Tables 1 and 2,
809 Table 1-Source Data 1, Figure 2-Source Data 1, and Methods.

810 **Figure 3**

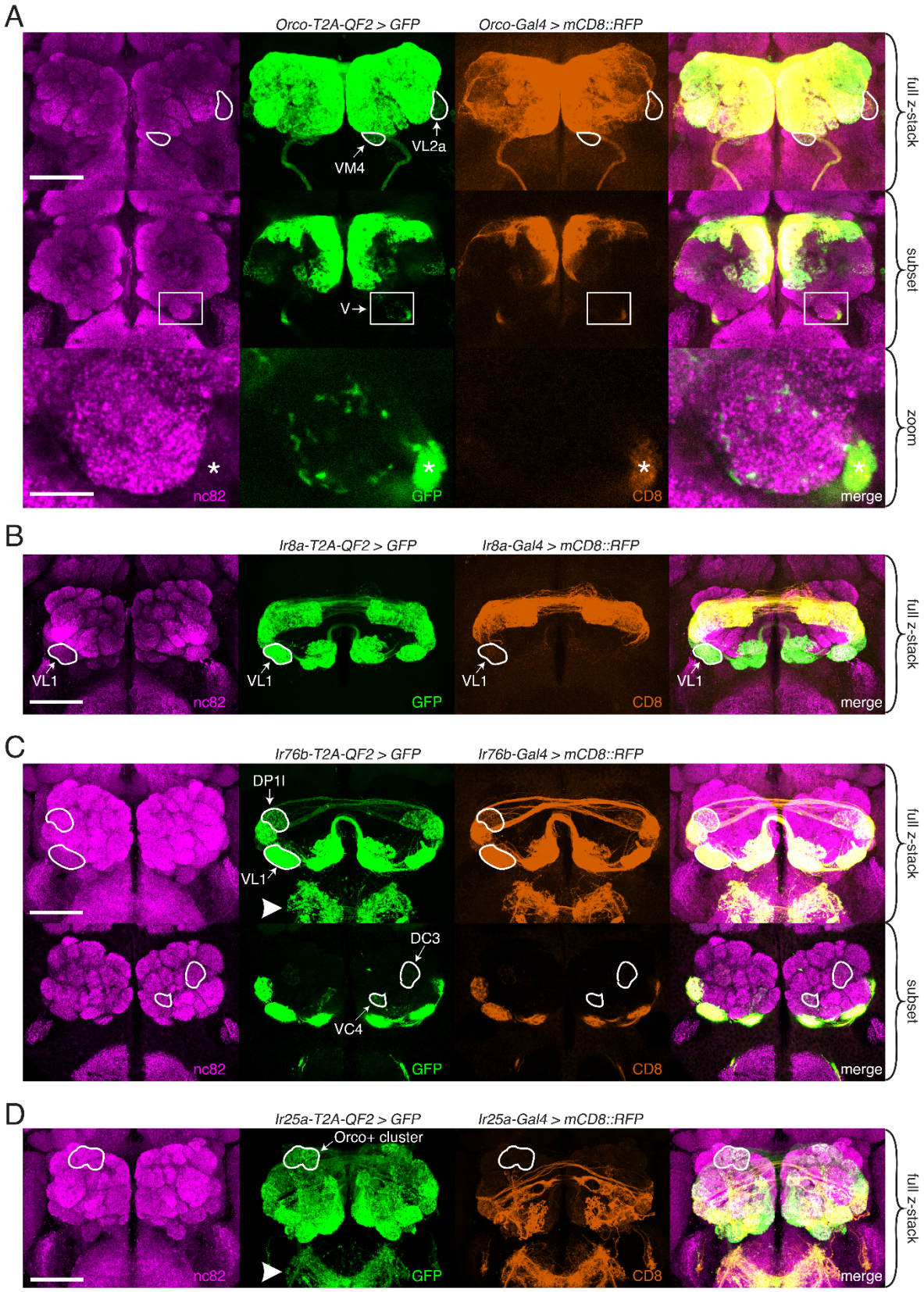
A
Orco-T2A-QF2 > GFP
Orco-Gal4 > mCD8::RFP
VM4
VL2a
V
nc82
GFP
CD8
merge
full z-stack
subset
zoom
B
Ir8a-T2A-QF2 > GFP
Ir8a-Gal4 > mCD8::RFP
VL1
nc82
GFP
CD8
merge
full z-stack
C
Ir76b-T2A-QF2 > GFP
Ir76b-Gal4 > mCD8::RFP
DP1l
VL1
DC3
VC4
nc82
GFP
CD8
merge
full z-stack
subset
D
Ir25a-T2A-QF2 > GFP
Ir25a-Gal4 > mCD8::RFP
Orco+ cluster
nc82
GFP
CD8
merge
full z-stack

811 **Figure 3. Expanded Expression of Olfactory Co-Receptors.**

812 **A-D.** Comparing knock-in innervation patterns of the AL with what has previously been reported
813 for each co-receptor. Co-labeling experiments with each co-receptor knock-in line driving
814 *QUAS-GFP* (green) and the corresponding transgenic co-receptor *Gal4* line driving *UAS-*
815 *mCD8::RFP* (anti-CD8, orange). The nc82 antibody labels synapses (magenta) and is used as a
816 brain counterstain in these and all subsequent brain images. **A.** The *Orco-T2A-QF2* knock-in
817 labels more glomeruli than the *Orco-Gal4* line. Top: maximum intensity projection of full z-stack
818 showing two additional glomeruli labeled by the knock-in, VM4 (Ir8a+/Ir76b+/Ir25a+) and VL2a
819 (Ir8a+). Middle: subset of z-stack with a box around the V glomerulus. Bottom: zoom of boxed
820 region showing sparse innervation of the V glomerulus (Gr21a+/Gr63a+) by the knock-in but not
821 the *Gal4* line. Asterisk indicates antennal nerve which is outside the V glomerulus. In the sub z-
822 stack and zoom panel, gain has been increased in the GFP channel to visualize weak labeling
823 more clearly. **B.** The *Ir8a-T2A-QF2* knock-in also drives GFP expression in more glomeruli than
824 previously reported, including the outlined VL1 glomerulus (Ir25a+). **C.** In the brain, *Ir76b-T2A-*
825 *QF2 > GFP* olfactory neurons innervate the antennal lobes (AL), while gustatory neurons from
826 the labella innervate the subesophageal zone (SEZ, arrowhead). Top: Both the *Ir76b* knock-in
827 and transgenic *Gal4* line label more glomeruli than previously reported, including VL1 (Ir25a+)
828 and DP1l (Ir8a+). Bottom: The *Ir76b-T2A-QF2* knock-in labels several Orco+ glomeruli, such as
829 DC3 and VC4 (outlined). In the subset, gain has been increased in the GFP channel to visualize
830 weakly labeled glomeruli more clearly. **D.** The *Ir25a-T2A-QF2* knock-in drives GFP expression
831 broadly in the antennal lobes and SEZ (arrowhead). Ir25a+ neurons innervate many Orco+
832 glomeruli, such as those outlined. The transgenic *Ir25a-Gal4* line labels a subset of the knock-in
833 expression pattern. N = 3 – 10 for co-labeling experiments, N = 5 – 15 for additional analyses of
834 the knock-in lines alone. Scale bars = 25 μm, except zoom panel scale bar = 10 μm. See also
835 Figure 3-Figure Supplements 1 and 2, Table 3, and Figure 3-Source data 1 and 2.

836 **Figure 4**

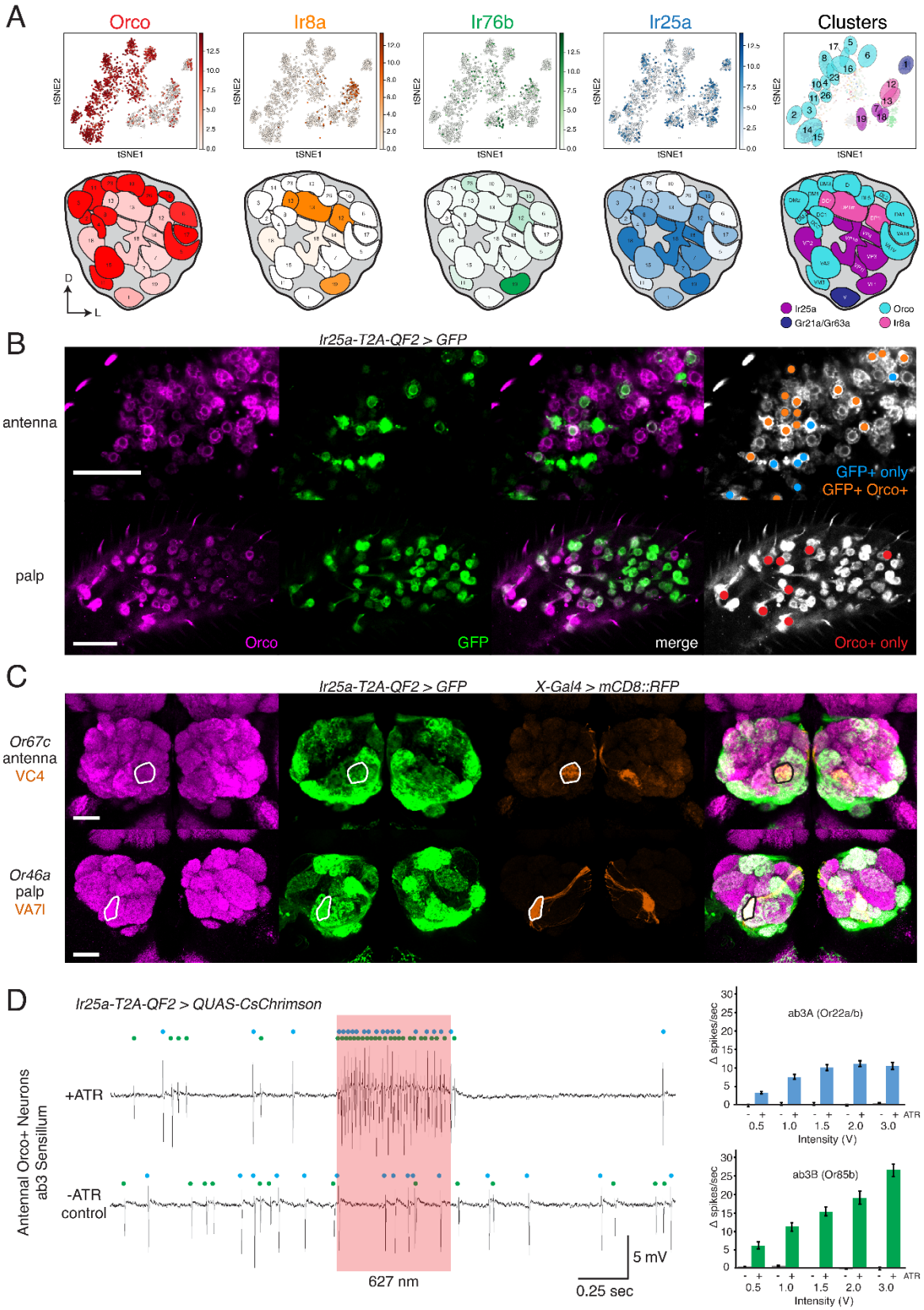
A
Orco
Ir8a
Ir76b
Ir25a
Clusters
tSNE1
tSNE2
D
L
Ir25a
Gr21a/Gr63a
Orco
Ir8a
B
Ir25a-T2A-QF2 > GFP
antenna
palp
GFP+ only
GFP+ Orco+
Orco
GFP
merge
Orco+ only
C
Ir25a-T2A-QF2 > GFP
X-Gal4 > mCD8::RFP
Or67c
antenna
VC4
Or46a
palp
VA7l
D
Ir25a-T2A-QF2 > QUAS-CsChrimson
Antennal Orco+ Neurons
ab3 Sensillum
+ATR
-ATR
control
627 nm
5 mV
0.25 sec
ab3A (Or22a/b)
ab3B (Or85b)
Δ spikes/sec
Intensity (V)
ATR

837 **Figure 4. Confirmation of Co-Receptor Co-Expression.**

838 **A.** snRNAseq of adult fly antennae (McLaughlin et al., 2021) confirms expanded expression of
839 olfactory co-receptors. Top: tSNE plots show expression of each co-receptor in 20 decoded
840 OSN clusters. Bottom: clusters were mapped to 24 glomeruli. Opacity of fill in each glomerulus
841 indicates the proportion of cells in that cluster expressing the given co-receptor, normalized to
842 total expression for that co-receptor gene (see Figure 4-Source Data 1). Right column: clusters
843 color-coded according to original chemoreceptor gene family. Compass: D = dorsal, L = lateral.
844 **B.** Anti-Orco antibody staining in antennal cryosections (top) and whole-mount palps (bottom)
845 confirms co-expression of Orco and Ir25a in the periphery (genotype: *Ir25a-T2A-QF2* > *GFP*).
846 Right panels show cells pseudo-colored grey with specific single- or double-labeled cells
847 indicated by colored cell markers (GFP+ only in blue, GFP+ Orco+ in orange, Orco+ only in
848 red). **C.** Co-labeling experiments with various transgenic *Gal4* lines driving mCD8::RFP (orange)
849 and the *Ir25a-T2A-QF2* knock-in driving GFP (green). *Ir25a-T2A-QF2* labels glomeruli
850 innervated by both antennal (top) and palpal (bottom) OSNs. **D.** Verification of *Ir25a* expression
851 in antennal ab3 sensilla using optogenetics. SSR recordings from ab3 Orco+ neurons in *Ir25a-*
852 *T2A-QF2* > *QUAS-CsChrimson* flies. Representative traces from ab3 using 1.5V of 627 nm LED
853 light (red box) to activate *CsChrimson*. Bottom trace is control animal which was not fed the
854 required all-trans retinal cofactor (-ATR). Spikes from the ab3A and ab3B neurons are indicated
855 by blue and green dots, respectively. Right: Quantification of neuronal activity in response to
856 light at various LED intensities (N = 7 – 12). These optogenetic experiments support *Ir25a*
857 expression in both ab3A neurons (*Or22a/b*, top; corresponding to DM2 glomerulus) and ab3B
858 neurons (*Or85b*, bottom; corresponding to VM5d glomerulus). Scale bars = 25 μm. See also
859 Figure 4-Figure Supplement 1, Table 3, and Figure 4-Source Data 1 – 3.

860 **Figure 5**

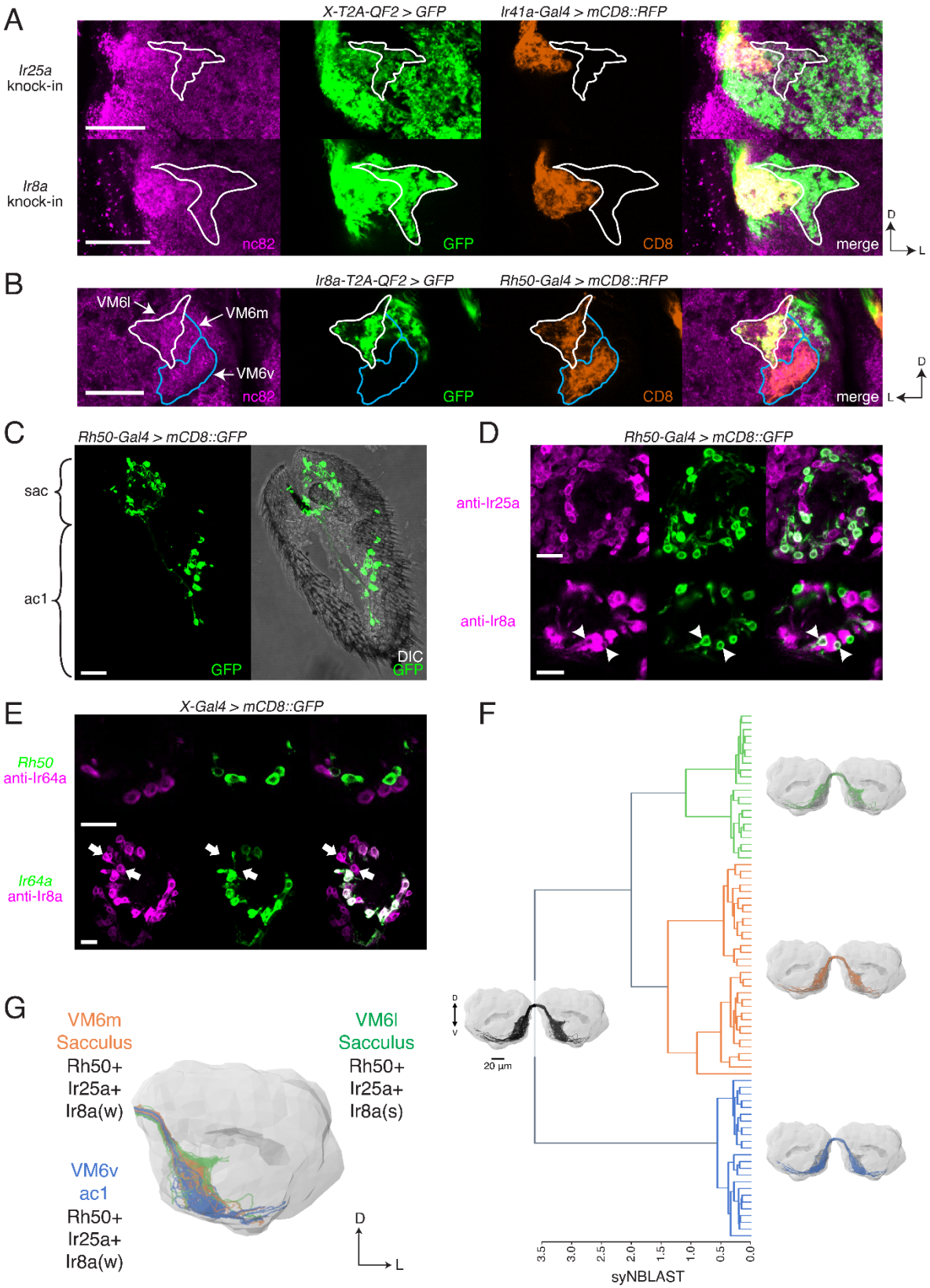
A
X-T2A-QF2 > GFP
Ir41a-Gal4 > mCD8::RFP
Ir25a knock-in
Ir8a knock-in
nc82
GFP
CD8
merge
D
L
B
Ir8a-T2A-QF2 > GFP
Rh50-Gal4 > mCD8::RFP
VM6l
VM6m
VM6v
nc82
GFP
CD8
merge
C
Rh50-Gal4 > mCD8::GFP
sac
ac1
GFP
DIC
GFP
D
Rh50-Gal4 > mCD8::GFP
anti-Ir25a
anti-Ir8a
E
X-Gal4 > mCD8::GFP
Rh50
anti-Ir64a
Ir64a
anti-Ir8a
F
20 µm
syNBLAST
3.5
3.0
2.5
2.0
1.5
1.0
0.5
0.0
G
VM6m
Sacculus
Rh50+
Ir25a+
Ir8a(w)
VM6l
Sacculus
Rh50+
Ir25a+
Ir8a(s)
VM6v
ac1
Rh50+
Ir25a+
Ir8a(w)
D
L

861 **Figure 5. Identification of New OSN Classes.**

862 **A.** Co-labeling experiments with *Ir41a-Gal4* show that both *Ir25a-T2A-QF2* and *Ir8a-T2A-QF2*
863 label the VC5 glomerulus (orange), and also a previously unidentified AL region (outline). **B.**
864 The new innervation pattern corresponds to the 'horn' (white outline) of the VM6 glomerulus
865 labeled by Rh50+ neurons (orange). One portion of VM6 is strongly Ir8a+ (VM6l), while two
866 other portions show little to no Ir8a expression (VM6m and VM6v, blue outlines). **C.** *Rh50-Gal4*
867 > *GFP* labels neurons in the sacculus (sac) and antennal coeloconic ac1 sensilla. **D.** In the
868 sacculus, all Rh50+ neurons appear to be Ir25a+ (top), and a subset are Ir8a+ (bottom,
869 arrowheads). **E.** Top: Rh50+ neurons in the sacculus do not overlap with Ir64a+ neurons.
870 Bottom: there are two distinct populations of Ir8a+ neurons in the sacculus – those that are
871 Ir64a+ and those that are Ir64a- (arrows). The latter likely correspond to Rh50+ neurons. **F.** EM
872 reconstructions of VM6 OSNs in a full brain volume (Dorkenwald et al., 2020) reveal three
873 distinct subpopulations. **G.** Model of OSN innervation of the VM6 region. VM6 can be
874 subdivided into three OSN populations based on anatomical location in the periphery and
875 chemoreceptor expression: VM6v (blue) OSNs originate in ac1, strongly (s) express Rh50 and
876 Ir25a, and weakly (w) or infrequently express Ir8a; VM6m (orange) neurons originate in the
877 sacculus and have a similar chemoreceptor expression profile to VM6v; VM6l (green) OSNs
878 originate in the sacculus but strongly express Ir8a in addition to Rh50 and Ir25a. Compass: D =
879 dorsal, L = lateral. Scale bars: 20 μm in (A-C) and (F), 10 μm in (D-E). See also Figure 5-Figure
880 Supplement 1 and Tables 3 and 4.

881 **Figure 6**

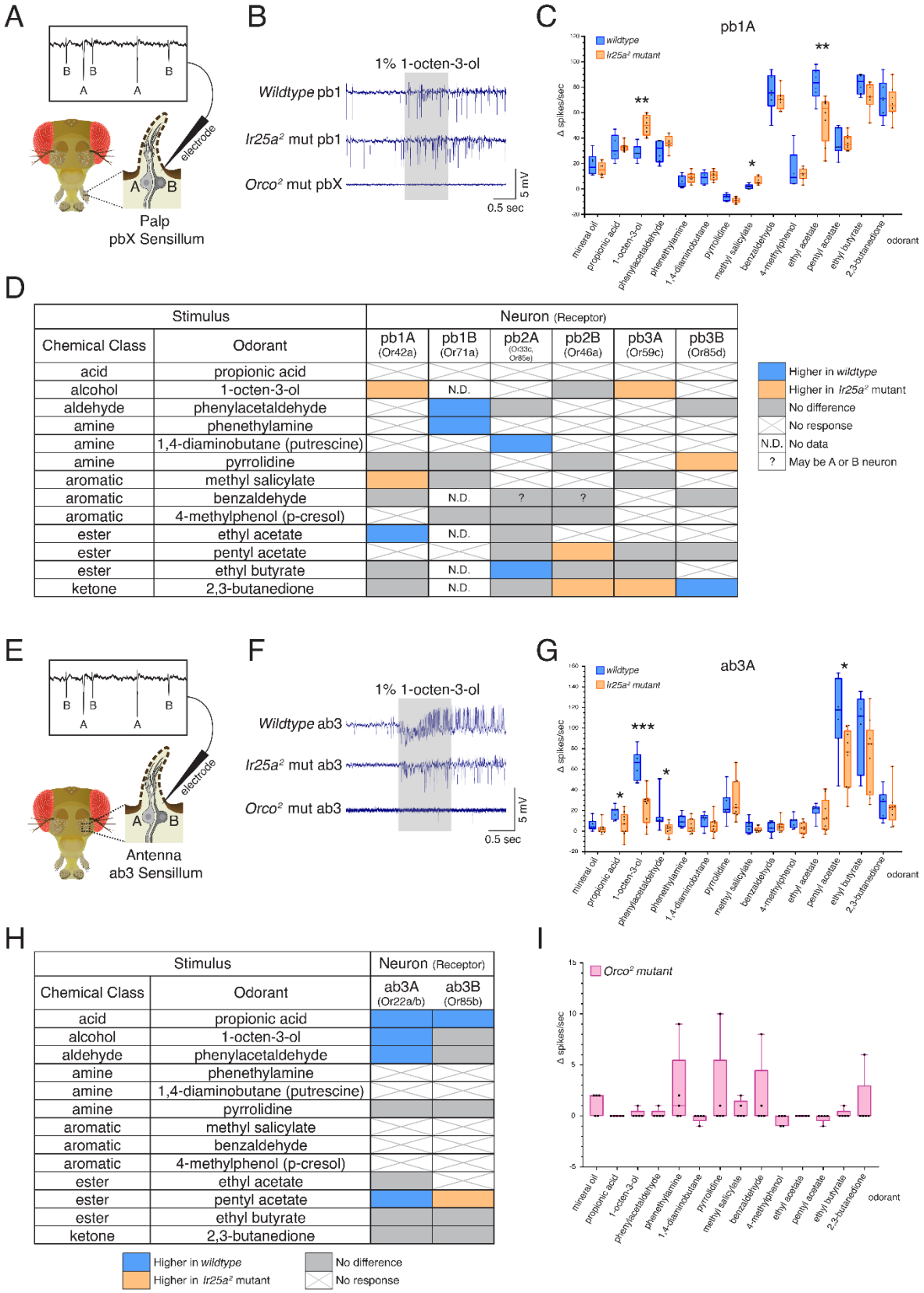


| Stimulus | | Neuron (Receptor) | | | | | |
|---|---|---|---|---|---|---|---|
| Chemical Class | Odorant | pb1A (Or42a) | pb1B (Or71a) | pb2A (Or33c, Or85e) | pb2B (Or46a) | pb3A (Or59c) | pb3B (Or85d) |
| acid | propionic acid | | | | | | |
| alcohol | 1-octen-3-ol | | N.D. | | | | |
| aldehyde | phenylacetaldehyde | | | | | | |
| amine | phenethylamine | | | | | | |
| amine | 1,4-diaminobutane (putrescine) | | | | | | |
| amine | pyrrolidine | | | | | | |
| aromatic | methyl salicylate | | | | | | |
| aromatic | benzaldehyde | | N.D. | ? | ? | | |
| aromatic | 4-methylphenol (p-cresol) | | | | | | |
| ester | ethyl acetate | | N.D. | | | | |
| ester | pentyl acetate | | | | | | |
| ester | ethyl butyrate | | N.D. | | | | |
| ketone | 2,3-butanedione | | N.D. | | | | |

| Stimulus | | Neuron (Receptor) | |
|---|---|---|---|
| Chemical Class | Odorant | ab3A (Or22a/b) | ab3B (Or85b) |
| acid | propionic acid | | |
| alcohol | 1-octen-3-ol | | |
| aldehyde | phenylacetaldehyde | | |
| amine | phenethylamine | | |
| amine | 1,4-diaminobutane (putrescine) | | |
| amine | pyrrolidine | | |
| aromatic | methyl salicylate | | |
| aromatic | benzaldehyde | | |
| aromatic | 4-methylphenol (p-cresol) | | |
| ester | ethyl acetate | | |
| ester | pentyl acetate | | |
| ester | ethyl butyrate | | |
| ketone | 2,3-butanedione | | |

Higher in wildtype
Higher in Ir25a² mutant
No difference
No response

882 **Figure 6. Co-Receptor Contributions to Olfactory Neuron Physiology.**

883 **A-I.** SSR experiments were performed in three genetic backgrounds: *wildtype*, *Ir25a*$^2$ mutant,
884 and *Orco*$^2$ mutant flies. A panel of 13 odorants was tested. In all box plots, * $p < 0.05$, ** $p <$
885 $0.01$, and *** $p < 0.001$. **A.** Cartoon of a fly head, zooming in on a single sensillum in the palp.
886 Each palpal sensillum (pbX) contains two neurons, A and B. An electrode is inserted into the
887 sensillum, and neuronal activity is recorded in response to odorants. Activity of the A and B
888 neurons can be distinguished based on their spike amplitudes (top). **B.** Representative traces
889 from recordings in palp basiconic pb1 sensilla in the three genotypes in response to 1% 1-
890 octen-3-ol. Sensilla were identified based on responses to reference odorants (de Bruyne et al.,
891 1999). The *Orco*$^2$ mutant did not exhibit odor-evoked activity nor spontaneous activity making it
892 difficult to determine the identity of the recorded sensillum. *Orco*$^2$ mutant sensilla are thus
893 denoted pbX. **C.** Quantification of responses to the panel of odorants in *wildtype* (blue; N = 5 – 9
894 flies) and *Ir25a*$^2$ mutant (orange; N = 6 – 10 flies) pb1A neurons. Responses were higher in the
895 *Ir25a*$^2$ mutant than in the *wildtype* for 1-octen-3-ol and methyl salicylate, and lower in the *Ir25a*$^2$
896 mutant for ethyl acetate. Mann-Whitney U tests indicated these differences were statistically
897 significant: 1-octen-3-ol: $Mdn_{Ir25amut} = 50$, $Mdn_{wildtype} = 28$, $U(N_{Ir25amut} = 8, N_{wildtype} = 5) = 0$, $p =$
898 $0.0016$; methyl salicylate: $Mdn_{Ir25amut} = 5$, $Mdn_{wildtype} = 2$, $U(N_{Ir25amut} = 7, N_{wildtype} = 5) = 3$, $p =$
899 $0.0177$; ethyl acetate: $Mdn_{Ir25amut} = 63.5$, $Mdn_{wildtype} = 83.5$, $U(N_{Ir25amut} = 8, N_{wildtype} = 6) = 4$, $p =$
900 $0.008$. **D.** Summary of differences in responses across all six neuron classes in the palps
901 between *wildtype* and *Ir25a*$^2$ mutant flies. Comparisons were made using Mann-Whitney *U*
902 tests. Orange indicates higher response in *Ir25a*$^2$ mutant, blue indicates higher response in
903 *wildtype*. Grey is no difference between genotypes, X indicates no response to the given
904 stimulus, and N.D. is no data (strong A neuron response obscured B neuron spikes preventing
905 quantification). In the *wildtype*, for one sensillum-odorant combination (pb2 and benzaldehyde),
906 it could not be distinguished if responses arose from the A or B neuron or both (indicated by a
907 question mark). **E.** Fly head cartoon, zooming in on a single sensillum in the antenna. We

908 recorded from antennal ab3 sensilla, each of which contains two neurons, A and B. As in the
909 palps, responses from these neurons can be distinguished based upon their spike amplitude
910 (top). **F.** Representative traces from recordings in antennal basiconic ab3 sensilla in the three
911 genotypes in response to 1% 1-octen-3-ol. In *Orco*$^2$ mutant ab3 sensilla spontaneous activity
912 was observed, but there was no significant odor-evoked activity. *Wildtype* N = 7 sensilla from 5
913 flies; *Ir25a*$^2$ mutant N = 10 sensilla from 5 flies. **G.** Quantification of responses in *wildtype* (blue;
914 N = 7) and *Ir25a*$^2$ mutant (orange; N = 9) ab3A neurons. Responses were significantly higher in
915 *wildtype* compared to *Ir25a*$^2$ mutant ab3A neurons for four odorants (Mann-Whitney *U* results in
916 parentheses; all $N_{wildtype}$ = 7 and $N_{Ir25amut}$ = 9): propionic acid ($Mdn_{wildtype}$ = 21, $Mdn_{Ir25amut}$ = 7, $U$ =
917 12.5, $p$ = 0.0441); 1-octen-3-ol ($Mdn_{wildtype}$ = 67, $Mdn_{Ir25amut}$ = 29, $U$ = 1.5, $p$ = 0.0004);
918 phenylacetaldehyde ($Mdn_{wildtype}$ = 10, $Mdn_{Ir25amut}$ = 3, $U$ = 9, $p$ = 0.015); and pentyl acetate
919 ($Mdn_{wildtype}$ = 118, $Mdn_{Ir25amut}$ = 77, $U$ = 9, $p$ = 0.0164). Difference between *wildtype* and *Ir25a*$^2$
920 mutant to phenylacetaldehyde is significant even with the large *wildtype* outlier removed ($p$ =
921 0.0336). **H.** Summary of differences in responses in the two neuron classes in ab3 between
922 *wildtype* and *Ir25a*$^2$ mutant flies. Comparisons were made using Mann-Whitney *U* tests. Orange
923 indicates higher response in *Ir25a*$^2$ mutant, blue indicates higher response in *wildtype*, grey is
924 no difference between genotypes, and X is no response to the given stimulus. One *Ir25a*$^2$
925 mutant fly was excluded from analyses as it had high responses to the mineral oil control (40 –
926 53 Δ spikes/sec), not seen in any other animal of any genotype. **I.** Weak responses in *Orco*$^2$
927 mutant flies to certain stimuli (≤ 10 Δ spikes/sec) were occasionally detected. While there were
928 some statistically significant differences from mineral oil control (pentyl acetate $p$ = 0.0109,
929 propionic acid $p$ = 0.0434, ethyl acetate $p$ = 0.0434, 1,4-diaminobutane $p$ = 0.0109, p-cresol $p$ =
930 0.0021), these were not deemed biologically significant due to very small Δ spike values relative
931 to zero. For more details, see Methods. N = 5 flies. See also Figure 6-Figure Supplements 1
932 and 2, and Figure 6-Source Data 1 and 2.

933 **Figure 7**

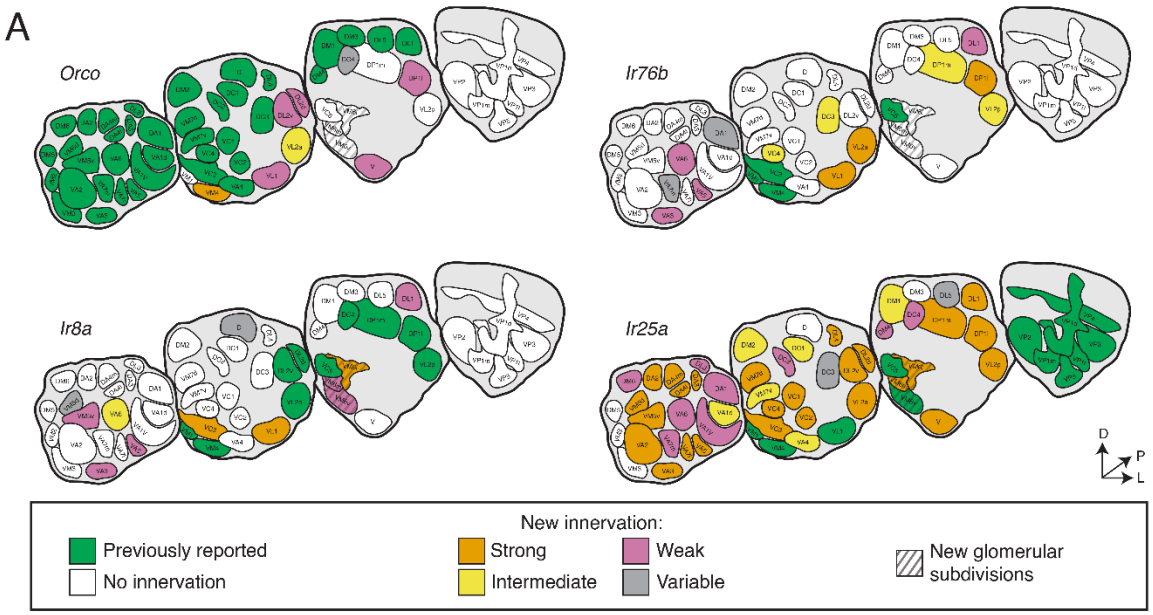


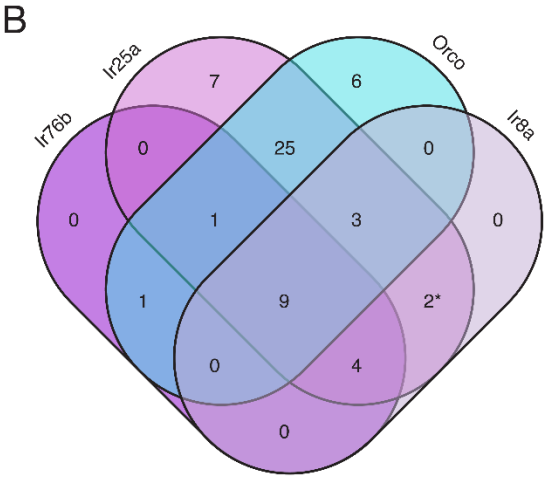


| Co-Receptor(s) | Total | Glomeruli |
|---|---|---|
| Orco, Ir8a, Ir76b, Ir25a | 9 | DP1l, VA3, VC3, VL1, VL2a, VM4, DL1, VA5, VA6 |
| Ir8a, Ir76b, Ir25a | 4 | DP1m, VC5, VL2p, VM1 |
| Orco, Ir8a, Ir25a | 3 | DL2d, DL2v, VM5v |
| Orco, Ir76b, Ir25a | 1 | VC4 |
| Orco, Ir25a | 25 | DA1, DA2, DA3, DA4l, DA4m, DC1, DC2, DL3, DL4, DM1, DM2, DM4, DM6, V, VA1d, VA1v, VA2, VA4, VA7l, VA7m, VC1, VC2, VM5d, VM7d, VM7v |
| Ir8a, Ir25a | 2* | DC4, VM6(l, m, and v)* |
| Orco, Ir76b | 1 | DC3 |
| Ir25a | 7 | VP1d, VP1l, VP1m, VP2, VP3, VP4, VP5 |
| Orco | 6 | D, DL5, DM3, DM5, VM2, VM3 |

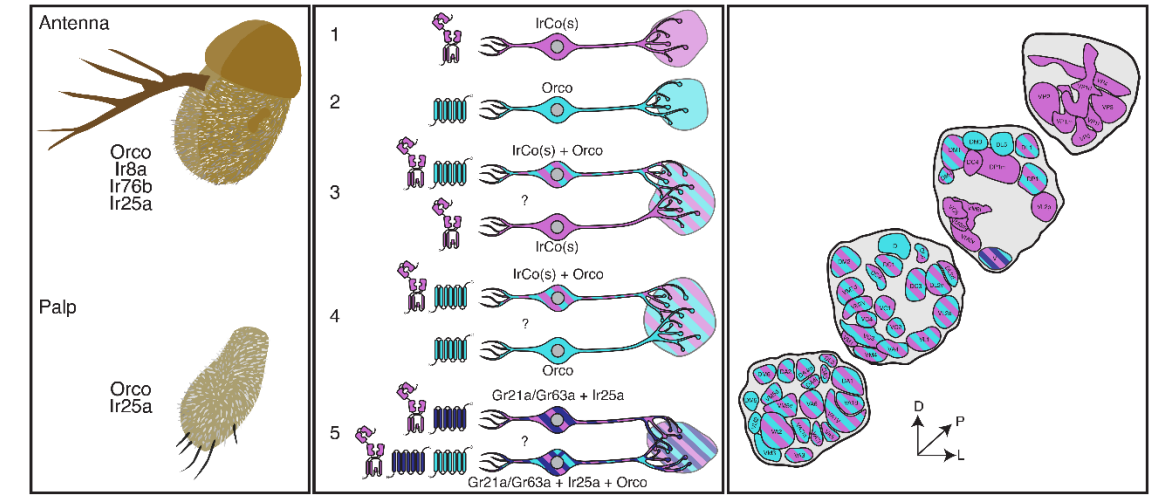

934 **Figure 7. The Co-Receptor Co-Expression Map of Olfaction in *Drosophila*.**

935 **A.** Summary of AL expression for all co-receptor knock-in lines (from all brains examined in
936 Figure 3 – 5; *Orco* N = 8, *Ir8a* N = 15, *Ir76b* N = 11, *Ir25a* N = 15). The previously reported
937 innervation pattern for each co-receptor is shown in green; new innervation reported here is
938 color-coded according to strength of glomerular labeling, from strong (orange), to intermediate
939 (yellow), to weak (pink). Glomeruli labeled in <50% of brains examined for a given knock-in line
940 are designated variable (grey); glomeruli not labeled are white. The novel VM6 glomerular
941 subdivisions reported here are indicated by grey stripes. **B.** Overlap of chemosensory modalities
942 in the AL. In the Venn diagram (left), *IR* co-receptors are color-coded in shades of purple, while
943 *Orco* is in teal, as in Figure 1. Numbers indicate how many glomeruli are found in the given
944 intersection of co-receptors out of 58 total glomeruli. Variably labeled glomeruli were excluded
945 from these analyses. The table lists the names of the glomeruli in each section of the Venn
946 diagram. The new glomerular subdivisions are indicated with an asterisk. **C.** New view of
947 olfaction in *Drosophila*. Left: in the periphery, all four co-receptors are expressed in the antenna
948 (top), while palpal neurons express *Orco* and *Ir25a* (bottom). Middle: Many different classes of
949 OSNs express various combinations of chemosensory receptors and co-receptors. While some
950 neurons express only *IrCos* (purple, #1) or *Orco* (teal, #2), many neurons co-express these
951 chemoreceptors (indicated with striped fill, #3 and 4). Within the latter group, there may be OSN
952 populations in which *IRs* are the dominant receptors, and *OR* expression is sparse (#3), and
953 other populations where *ORs* are the primary receptors and *IR* expression is infrequent (#4).
954 GR+ neurons (dark blue) also express *Ir25a* (#5, dark blue and purple striped fill), and some of
955 these neurons additionally express *Orco* (#5, dark blue, purple, and teal striped fill). Question
956 marks indicate potential instances of co-convergence of different sub-types of OSNs onto the
957 same glomeruli. Right: a comprehensive map of the antennal lobe shows that most glomeruli
958 are innervated by OSNs that co-express multiple chemoreceptors. Compass in (A) and (C): D =
959 dorsal, L = lateral, P = posterior. See also Table 3 and Figure 3-Source Data 1 and 2.

960 **Table 1**

| Gene | Approach | mCherry+ | mCherry- | Total | Efficiency | Founders Producing Knock-in (#/Total) | Knock-ins Sampled | False Positives | Confirmed | Correct |
|---|---|---|---|---|---|---|---|---|---|---|
| ***Orco*** | Direct Injection | 180 | 365 | 545 | 33% | 43% (3/7) | 30 | 0 | 30 | 100% |
| ***Ir8a*** | Direct Injection | 53 | 609 | 662 | 8% | 20% (4/20) | 5 | 0 | 5 | 100% |
| ***Ir76b*** | Direct Injection | 79 | 184 | 263 | 30% | 100% (2/2) | 10 | 0 | 10 | 100% |
| ***Ir25a*** | Direct Injection | 82 | 268 | 350 | 23% | 40% (2/5) | 6 | 0 | 6 | 100% |
| ***Orco*** | Cross | 37 | 96 | 133 | 28% | 100% (3/3) | 2 | 1 | 1 | 50% |
| ***Ir25a*** | Cross | 30 | 95 | 125 | 24% | 100% (2/2) | 30 | 5 | 25 | 83% |

961 **Table 1. Summary of HACK Knock-in Efficiency. Related to Figure 2.**

962 There are two ways to generate knock-ins via the HACK technique: by direct injection or by genetic cross (see Figure 2-Figure
963 Supplement 1 and Methods for details) (Lin and Potter, 2016a). All four co-receptor genes were targeted using the direct injection
964 approach; additionally, the crossing approach was tested with *Orco* and *Ir25a*. Knock-in efficiency, as measured by the number of
965 flies having the mCherry+ marker divided by the total number of potentially HACKed flies, was high for all genes tested and both
966 approaches. Efficiency appears to depend on the genetic locus, as has been previously demonstrated (Lin and Potter, 2016a). To
967 further estimate the effort required to generate a HACK knock-in, we calculated the percentage of founder flies producing knock-in
968 lines; this gives an indication of the number of independent crosses needed to successfully create a knock-in line. Two to five

969 individual $G_0$ starting crosses were sufficient to produce a knock-in. For each gene, a sample of individual knock-in lines were tested
970 via PCR genotyping, sequencing, and by crossing to a reporter line to confirm brain expression (knock-ins sampled). For all knock-
971 ins generated via the direct injection method, every fly tested represented a correctly targeted knock-in. However, for the cross
972 method, some lines had the mCherry+ marker and yet did not drive GFP expression in the brain when crossed to a reporter line
973 (labeled here as false positives). See also Table 1-Source Data 1 and Figure 2-Figure Supplement 1.

974 **Table 2**

| Knock-in | Sample* | Antibody† (Ab) | Ab+ cells | GFP+ cells | Double-labeled cells | Total cells |
|---|---|---|---|---|---|---|
| ***Orco*** | Palp 1 (WM) | anti-Orco | 125 | 127 | 125 | 127 |
| ***Orco*** | Palp 2 (WM) | anti-Orco | 112 | 111 | 108 | 115 |
| ***Orco*** | Palp 6 (WM) | anti-Orco | 125 | 126 | 123 | 128 |
| | | Total across samples: | 362 | 364 | 356 | 370 |
| | | | Proportion of Ab+ cells that are GFP+: | Proportion of GFP+ cells that are Ab+: | Proportion of all cells that are double labeled: | |
| | | | **0.98** | **0.98** | **0.96** | |
| ***Ir8a*** | Antenna 1 (Cryo) | anti-Ir8a | 20 | 21 | 20 | 21 |
| ***Ir8a*** | Antenna 2 (Cryo) | anti-Ir8a | 24 | 24 | 24 | 24 |
| ***Ir8a*** | Antenna 6 (Cryo) | anti-Ir8a | 40 | 43 | 40 | 43 |
| ***Ir8a*** | Antenna 7 (Cryo) | anti-Ir8a | 12 | 13 | 12 | 13 |
| ***Ir8a*** | Antenna 8 (Cryo) | anti-Ir8a | 16 | 16 | 16 | 16 |
| ***Ir8a*** | Antenna 9 (Cryo) | anti-Ir8a | 42 | 42 | 41 | 43 |
| ***Ir8a*** | Antenna 10 (Cryo) | anti-Ir8a | 41 | 40 | 40 | 41 |
| | | Total across samples: | 195 | 199 | 193 | 201 |
| | | | Proportion of Ab+ cells that are GFP+: | Proportion of GFP+ cells that are Ab+: | Proportion of all cells that are double labeled: | |
| | | | **0.99** | **0.97** | **0.96** | |
| ***Ir25a*** | Palp 1 (WM) | anti-Ir25a | 107 | 105 | 104 | 108 |
| ***Ir25a*** | Palp 2 (WM) | anti-Ir25a | 86 | 85 | 85 | 86 |
| ***Ir25a*** | Palp 3 (WM) | anti-Ir25a | 111 | 111 | 110 | 112 |
| ***Ir25a*** | Palp 4 (WM) | anti-Ir25a | 94 | 94 | 94 | 94 |
| ***Ir25a*** | Palp 5 (WM) | anti-Ir25a | 83 | 83 | 81 | 85 |
| | | Total across samples: | 481 | 478 | 474 | 485 |
| | | | Proportion of Ab+ cells that are GFP+: | Proportion of GFP+ cells that are Ab+: | Proportion of all cells that are double labeled: | |
| | | | **0.99** | **0.99** | **0.98** | |

975 **Table 2. Validation of *T2A-QF2* Knock-in Expression in the Antennae and Maxillary Palps.**

976 **Related to Figure 2.**

977 To verify that the knock-in lines recapitulate the endogenous expression patterns of the target

978 genes, antennae or maxillary palps of flies containing the knock-ins driving GFP expression

979 were co-stained with the corresponding antibody (Ab) (anti-Orco, anti-Ir8a, or anti-Ir25a). The

980 overlap of Ab+ and GFP+ cells was examined, and a high correspondence between antibody

981 staining and knock-in driven GFP was found. *WM = whole-mount, Cryo = cryosection. See also

982 Figure 2-Figure Supplement 3.

983 **Table 3**

| Glomerulus† | Sensillum | Tuning Receptor(s) | Original Co-receptor(s) | *Orco-T2A-QF2* | *Ir8a-T2A-QF2* | *Ir76b-T2A-QF2* | *Ir25a-T2A-QF2* | References |
|---|---|---|---|---|---|---|---|---|
| D | Ab9A | Or69aA, Or69aB | Orco | Yes | Variable | No | No | (Couto et al., 2005; Fishilevich and Vosshall, 2005) |
| DA1 | At1A | Or67d | Orco | Yes | No | Variable | Yes | (Couto et al., 2005; Fishilevich and Vosshall, 2005; Kurtovic et al., 2007) |
| DA2 | Ab4B | Or56a, Or33a | Orco | Yes | No | No | Yes | (Couto et al., 2005; Fishilevich and Vosshall, 2005) |
| DA3 | Ai2B (At2B) | Or23a | Orco | Yes | No | No | Yes | (Couto et al., 2005; Fishilevich and Vosshall, 2005; Lin and Potter, 2015) |
| DA4l | Ai3C (At3C) | Or43a | Orco | Yes | No | No | Yes | (Couto et al., 2005; Fishilevich and Vosshall, 2005; Lin and Potter, 2015) |
| DA4m | Ai3B (At3B) | Or2a | Orco | Yes | No | No | Yes | (Couto et al., 2005; Lin and Potter, 2015) |
| DC1 | Ai3A (At3A) | Or19a, Or19b | Orco | Yes | No | No | Yes | (Couto et al., 2005; Fishilevich and Vosshall, 2005; Lin and Potter, 2015) |
| DC2 | Ai1A (Ab6A) | Or13a | Orco | Yes | No | No | Yes | (Couto et al., 2005; Fishilevich and Vosshall, 2005; Lin and Potter, 2015) |
| DC3 | Ai2A (At2A) | Or83c | Orco | Yes | No | Yes | Variable | (Couto et al., 2005; Fishilevich and Vosshall, 2005; Lin and Potter, 2015) |
| DL1 | Ab1D | Or10a, Gr10a | Orco | Yes | Yes | Yes | Yes | (Couto et al., 2005; Fishilevich and Vosshall, 2005) |
| DL3 | At4B | Or65a, Or65b, Or65c | Orco | Yes | No | No | Yes | (Couto et al., 2005; Fishilevich and Vosshall, 2005) |
| DL4 | Ab10B | Or49a, Or85f | Orco | Yes | No | No | Yes | (Couto et al., 2005; Fishilevich and Vosshall, 2005) |
| DL5 | Ab4A | Or7a | Orco | Yes | No | No | Variable | (Couto et al., 2005) |

| | | | | | | | | |
|---|---|---|---|---|---|---|---|---|
| DM1 | Ab1A | Or42b | Orco | Yes | No | No | Yes | (Couto et al., 2005; Fishilevich and Vosshall, 2005) |
| DM2 | Ab3A | Or22a, Or22b | Orco | Yes | No | No | Yes | (Couto et al., 2005; Fishilevich and Vosshall, 2005) |
| DM3 | Ab5B | Or47a, Or33b | Orco | Yes | No | No | No | (Couto et al., 2005; Fishilevich and Vosshall, 2005) |
| DM4 | Ab2A | Or59b | Orco | Yes | No | No | Yes | (Couto et al., 2005) |
| DM5 | Ab2B | Or85a, Or33b | Orco | Yes | No | No | No | (Couto et al., 2005; Fishilevich and Vosshall, 2005) |
| DM6 | Ab10A | Or67a | Orco | Yes | No | No | Yes | (Couto et al., 2005) |
| VA1d | At4C | Or88a | Orco | Yes | No | No | Yes | (Couto et al., 2005; Fishilevich and Vosshall, 2005) |
| VA1v | At4A | Or47b | Orco | Yes | No | No | Yes | (Couto et al., 2005; Fishilevich and Vosshall, 2005) |
| VA2 | Ab1B | Or92a | Orco | Yes | No | No | Yes | (Couto et al., 2005; Fishilevich and Vosshall, 2005) |
| VA3 | Ab9B | Or67b | Orco | Yes | Yes | Yes | Yes | (Couto et al., 2005; Fishilevich and Vosshall, 2005) |
| VA4 | Pb3B | Or85d | Orco | Yes | No | No | Yes | (Couto et al., 2005) |
| VA5 | Ai1B (Ab6B) | Or49b | Orco | Yes | Yes | Yes | Yes | (Couto et al., 2005; Lin and Potter, 2015) |
| VA6 | Ab5A | Or82a | Orco | Yes | Yes | Yes | Yes | (Couto et al., 2005; Fishilevich and Vosshall, 2005) |
| VA7l | Pb2B | Or46a | Orco | Yes | No | No | Yes | (Couto et al., 2005; Fishilevich and Vosshall, 2005) |
| VA7m | UNK | UNK | Orco | Yes | No | Variable | Yes | (Couto et al., 2005) |

| | | | | | | | | |
|---|---|---|---|---|---|---|---|---|
| VC1 | Pb2A | Or33c, Or85e | Orco | Yes | No | No | Yes | (Couto et al., 2005; Fishilevich and Vosshall, 2005) |
| VC2 | Pb1B | Or71a | Orco | Yes | No | No | Yes | (Couto et al., 2005; Fishilevich and Vosshall, 2005) |
| VC4 | Ab7B | Or67c | Orco | Yes | No | Yes | Yes | (Couto et al., 2005) |
| VM2 | Ab8A | Or43b | Orco | Yes | No | No | No | (Couto et al., 2005) |
| VM3 | Ab8B | Or9a | Orco | Yes | No | No | No | (Couto et al., 2005) |
| VM5d | Ab3B | Or85b?, Or98b? | Orco | Yes | Variable | No | Yes | (Couto et al., 2005) |
| VM5v | Ab7A | Or98a | Orco | Yes | Yes | No | Yes | (Couto et al., 2005; Fishilevich and Vosshall, 2005) |
| VM7d | Pb1A | Or42a | Orco | Yes | No | No | Yes | (Couto et al., 2005; Endo et al., 2007; Fishilevich and Vosshall, 2005) |
| VM7v (1) | Pb3A | Or59c | Orco | Yes | No | No | Yes | (Couto et al., 2005; Endo et al., 2007) |
| VC3 | Ac3B | Or35a | Orco, Ir76b | Yes | Yes | Yes | Yes | (Couto et al., 2005; Fishilevich and Vosshall, 2005; Silbering et al., 2011) |
| V | Ab1C | Gr21a, Gr63a | N/A | Yes | No | No | Yes | (Couto et al., 2005; Jones et al., 2007; Kwon et al., 2007) |
| DC4 | Sacculus, Chamber III | Ir64a | Ir8a | Variable | Yes | No | Yes | (Ai et al., 2013; Ai et al., 2010; Silbering et al., 2011) |
| DL2d | Ac3A | Ir75b | Ir8a | Yes | Yes | No | Yes | (Prieto-Godina et al., 2017; Silbering et al., 2011) |
| DL2v | Ac3A | Ir75c | Ir8a | Yes | Yes | No | Yes | (Prieto-Godina et al., 2017; Silbering et al., 2011) |
| DP1l | Ac2 | Ir75a | Ir8a | Yes | Yes | Yes | Yes | (Silbering et al., 2011) |
| DP1m | Sacculus, Chamber III | Ir64a | Ir8a | No | Yes | Yes | Yes | (Ai et al., 2013; Ai et al., 2010; Silbering et al., 2011) |
| VL2a | Ac4 | Ir84a | Ir8a | Yes | Yes | Yes | Yes | (Silbering et al., 2011) |

| | | | | | | | | |
|---|---|---|---|---|---|---|---|---|
| VL2p | Ac1 | Ir31a | Ir8a | No | Yes | Yes | Yes | (Silbering et al., 2011) |
| VC5 | Ac2 | Ir41a | Ir8a, Ir25a, Ir76b | No | Yes | Yes | Yes | (Hussain et al., 2016; Min et al., 2013; Silbering et al., 2011) |
| VM1 | Ac1 | Ir92a | Ir8a, Ir25a, Ir76b | No | Yes | Yes | Yes | (Min et al., 2013; Silbering et al., 2011) |
| VM4 | Ac4 | Ir76a | Ir8a, Ir25a, Ir76b | Yes | Yes | Yes | Yes | (Benton et al., 2009; Min et al., 2013; Silbering et al., 2011) |
| VL1 | Ac1, Ac2, Ac4 | Ir75d | Ir25a | Yes | Yes | Yes | Yes | (Silbering et al., 2011) |
| VM6v (VM6) | Ac1 | Rh50, Amt | Ir25a | No | Yes (weak) | No | Yes | (Chai et al., 2019; Li et al., 2016; Schlegel et al., 2021; Vulpe et al., 2021), This paper |
| VM6m (new) | Sacculus, Chamber III | Rh50, Amt | N/A (this paper) | No | Yes (weak) | No | Yes | (Chai et al., 2019; Li et al., 2016; Schlegel et al., 2021; Vulpe et al., 2021), This paper |
| VM6l* (new) | Sacculus, Chamber III | Rh50, Amt | N/A (this paper) | No | Yes (strong) | No | Yes | (Chai et al., 2019; Li et al., 2016; Schlegel et al., 2021; Vulpe et al., 2021), This paper |
| VP1d | Sacculus, Chamber II | Ir40a, Ir93a | Ir25a | No | No | No | Yes | (Enjin et al., 2016; Frank et al., 2017; Knecht et al., 2017; Knecht et al., 2016; Marin et al., 2020; Silbering et al., 2011) |
| VP1l | Sacculus, Chamber I | Ir21a, Ir93a | Ir25a | No | No | No | Yes | (Frank et al., 2017; Knecht et al., 2017; Knecht et al., 2016; Marin et al., 2020; Silbering et al., 2011) |
| VP1m | Sacculus, Chamber I | Ir68a, Ir93a | Ir25a | No | No | No | Yes | (Frank et al., 2017; Knecht et al., 2017; Knecht et al., 2016; Marin et al., 2020; Silbering et al., 2011) |
| VP2 | Arista | Gr28b.d, Ir93a | Ir25a | No | No | No | Yes | (Enjin et al., 2016; Frank et al., 2017; Marin et al., 2020; Miwa et al., 2018; Ni et al., 2013) |

| | | | | | | | | |
|---|---|---|---|---|---|---|---|---|
| VP3 | Arista | Ir21a, Ir93a | Ir25a | No | No | No | Yes | (Budelli et al., 2019; Enjin et al., 2016; Frank et al., 2017; Silbering et al., 2011) |
| VP4 | Sacculus, Chambers I + II | Ir40a, Ir93a | Ir25a | No | No | No | Yes | (Enjin et al., 2016; Frank et al., 2017; Knecht et al., 2017; Knecht et al., 2016; Marin et al., 2020; Silbering et al., 2011) |
| VP5 | Sacculus, Chamber II | Ir68a, Ir93a | Ir25a | No | No | No | Yes | (Frank et al., 2017; Knecht et al., 2017; Marin et al., 2020) |

984 **Table 3. Summary of Expression Patterns for All Knock-in Lines. Related to Figures 3 – 5.**

985 Summarized here are all of the OSN classes innervating the 58 antennal lobe glomeruli[†]; their corresponding sensilla and tuning
986 receptors; the previously reported (original) co-receptors they express; and whether or not each of the co-receptor knock-in lines
987 labels those glomeruli. Variable indicates that the glomerulus was labeled in <50% of brains examined in the given knock-in line.
988 Sensilla or glomeruli that have been renamed or reclassified have their former nomenclature listed in parentheses. Question marks
989 indicate expression that has been reported but not functionally validated. [†]The VM6 subdivisions (VM6v, VM6m, VM6l) are separated
990 in this table for clarity but counted together as one glomerulus in accordance with Schlegel et al., 2021. *VM6l was initially named
991 VC6 in version 1 of our pre-print (Task et al., 2020) but was reclassified using additional data from EM reconstructions in the AL and
992 immunohistochemical experiments in the periphery (see Figure 5). See also Figure 3-Source Data 1 and 2.

993 **Table 4**

| Genotype | Sample | Ir8a+ cells | GFP+ cells | Double-labeled cells | Total cells |
|---|---|---|---|---|---|
| **Rh50-Gal4 > GFP** | 20210226 a1 | 18 | 9 | 2 | 25 |
| **Rh50-Gal4 > GFP** | 20210226 a2 | 22 | 15 | 4 | 33 |
| **Rh50-Gal4 > GFP** | 20210226 a3 | 41 | 22 | 7 | 56 |
| **Rh50-Gal4 > GFP** | 20210226 a4 | 41 | 14 | 5 | 50 |
| **Rh50-Gal4 > GFP** | 20210129 a1 | 26 | 20 | 9 | 37 |
| **Rh50-Gal4 > GFP** | 20210129 a2 | 32 | 24 | 7 | 49 |
| **Rh50-Gal4 > GFP** | 20210129 a3 | 29 | 19 | 7 | 41 |
| **Rh50-Gal4 > GFP** | 20210216 a1 | 26 | 21 | 8 | 39 |
| **Rh50-Gal4 > GFP** | 20210216 a2 | 30 | 18 | 7 | 41 |
| **Rh50-Gal4 > GFP** | 20210216 a3 | 34 | 23 | 8 | 49 |
| **Rh50-Gal4 > GFP** | 20210216 a4 | 34 | 23 | 9 | 48 |
| | Total across samples: | 333 | 208 | 73 | 468 |
| | | Proportion of Ir8a+ cells that are GFP+: | Proportion of GFP+ cells that are Ir8a+: | Proportion of all cells that are double labeled: | |
| | | **0.22** | **0.35** | **0.16** | |

994 **Table 4. Co-expression of Rh50 and Ir8a in the Sacculus. Related to Figure 5.**

995 Antennal cryosections of *Rh50-Gal4>GFP* flies were stained with an anti-Ir8a antibody and the

996 overlap of Ir8a+ and GFP+ cells was quantified in the sacculus. 22% of Ir8a+ cells expressed

997 Rh50, 35% of Rh50+ cells expressed Ir8a, and 16% of all cells were double labeled. N = 11.

# Figure Supplements

## Figure 2-Figure Supplement 1

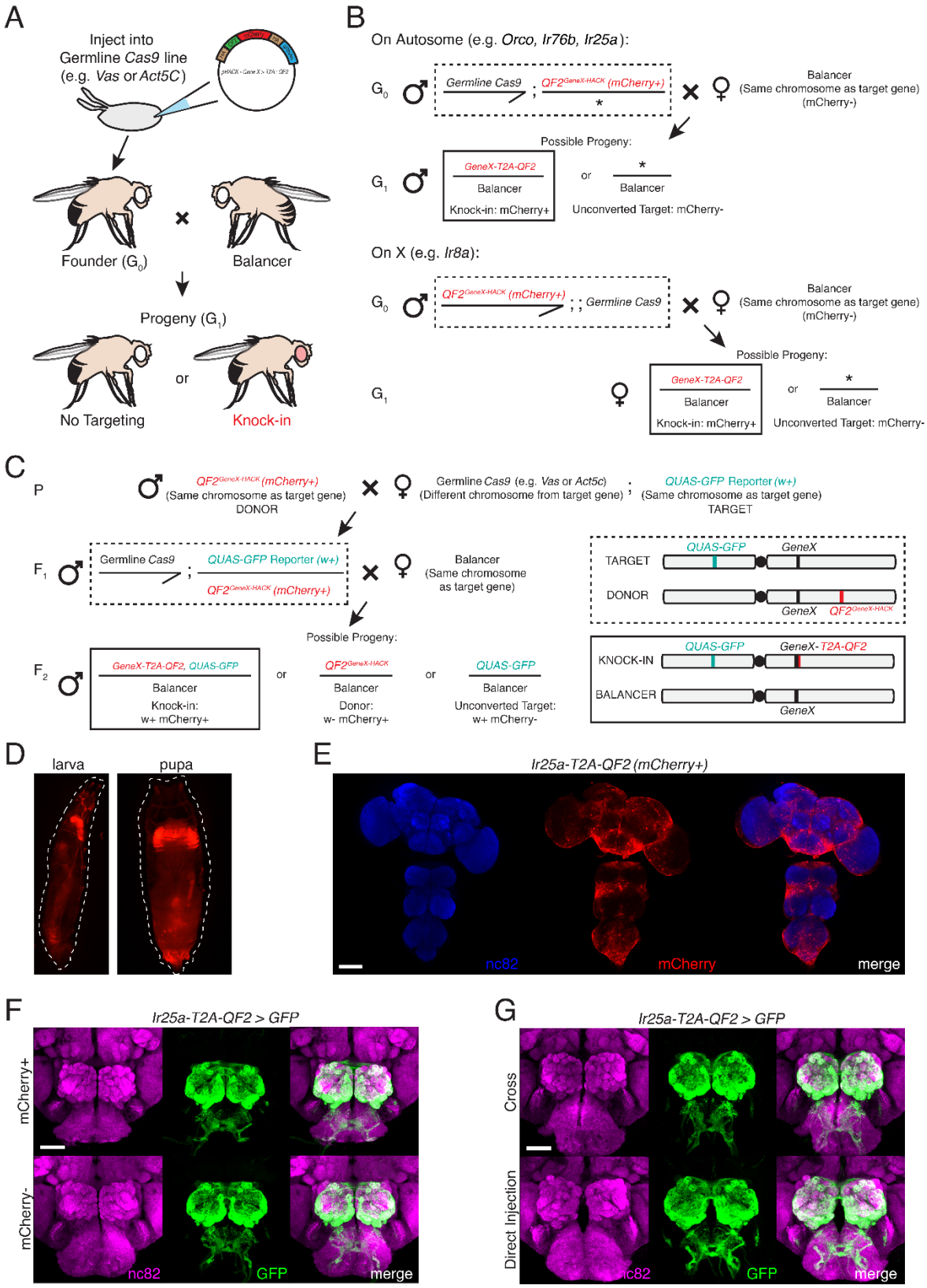

1000 **Figure 2-Figure Supplement 1. HACK Crossing Schematics, Marker Expression and**
1001 **Approach Comparison.**
1002 **A.** Schematic of the direct injection method to generate a HACK knock-in. The HACK KI
1003 construct is injected into a germline Cas9 expressing embryo (both *Act5C-Cas9* and *Vas-Cas9*
1004 yielded successful knock-ins; see Methods for more details). This approach requires one
1005 genetic cross to generate a knock-in: injected founder flies ($G_0$) are individually crossed to
1006 balancer flies, and progeny ($G_1$) are screened for the mCherry knock-in marker. Each mCherry+
1007 $G_1$ represents an independent knock-in event; thus, single mCherry+ flies are used to establish
1008 knock-in lines. **B.** Details of the genetic crosses used to establish knock-in lines for each target
1009 gene using the direct injection approach. For genes on autosomes (*Orco* and *Ir76b*, 3$^{rd}$
1010 chromosome; *Ir25a*, 2$^{nd}$ chromosome), a *Cas9* line on the X chromosome was used, and
1011 mCherry+ male progeny selected to remove the *Cas9* after successful HACKing. For *Ir8a* on the
1012 X chromosome, a *Cas9* line on the 3$^{rd}$ chromosome was used which was marked with GFP to
1013 facilitate its removal in subsequent generations. In addition to mCherry marker screening, PCR
1014 genotyping, and sequencing, knock-in lines were confirmed by crossing to a *QUAS* reporter line
1015 and checking brain expression, either at the $G_2$ stage, or by crossing $G_0$ flies to balanced
1016 reporter lines to immediately check $G_1$ brain expression. **C.** Details of using the crossing method
1017 to generate HACK knock-ins. This involves the creation of donor lines, in which the HACK
1018 targeting construct is inserted into the genome, such as through *P*-element insertion or *ΦC31*
1019 integration. Donor lines are crossed to a germline *Cas9* line (Parental). The progeny, $F_1$, have
1020 all the components necessary for a knock-in to occur (gRNAs, Cas9, HDR cassette). An
1021 additional cross is required to select germline HACKing events at the $F_2$ generation. Because
1022 the donor lines also express mCherry, as do the knock-ins, the target chromosome must be
1023 marked with a different marker (such as w+) for knock-in selection (see chromosome
1024 schematics at the right, illustrating the locations of the genetic elements in the $F_1$ and $F_2$
1025 generations). $F_2$ knock-ins will have both markers (in this case, mCherry+ w+), while donor flies

1026 will only have one (mCherry+ w-). The cross approach was tested with two of the four genetic
1027 targets (*Orco* and *Ir25a*) and successfully produced knock-in lines for both. However, the cross
1028 approach can produce false positives (see Table 1 and Table 1-Source Data 1) and is more
1029 time consuming. The direct injection approach is recommended for generation of targeted
1030 knock-ins. **D.** Knock-in screening can be performed at the larval (left) and pupal (right) stages.
1031 **E.** The *3XP3-mCherry* marker is expressed throughout the adult fly brain and ventral nerve
1032 cord. Nc82 channel has been pseudo-colored blue for clarity. **F.** The marker cassette is flanked
1033 by *loxP* sites and can be removed through *Cre* recombination (see Methods for details) (Siegal
1034 and Hartl, 1996). The *3XP3-mCherry* marker does not affect knock-in expression. *Ir25a-T2A-*
1035 *QF2*-driven GFP expression in the brain was similar before (top row) and after (bottom row)
1036 *Cre*-mediated removal of the mCherry marker. **G.** No difference was found in the expression
1037 patterns of *Ir25a-T2A-QF2* knock-in lines generated by the two HACK methods, genetic cross
1038 (top) and direct injection (bottom). For (F) and (G): N = 5 for direct injection; N = 4 for cross,
1039 mCherry+; N = 3 for cross, mCherry-. Expression patterns were comparable across all three
1040 groups. See also Table 1 and Table 1-Source Data 1. Scale bars: 100 μm in (E), 50 μm in (F-
1041 G).

1042 **Figure 2-Figure Supplement 2**

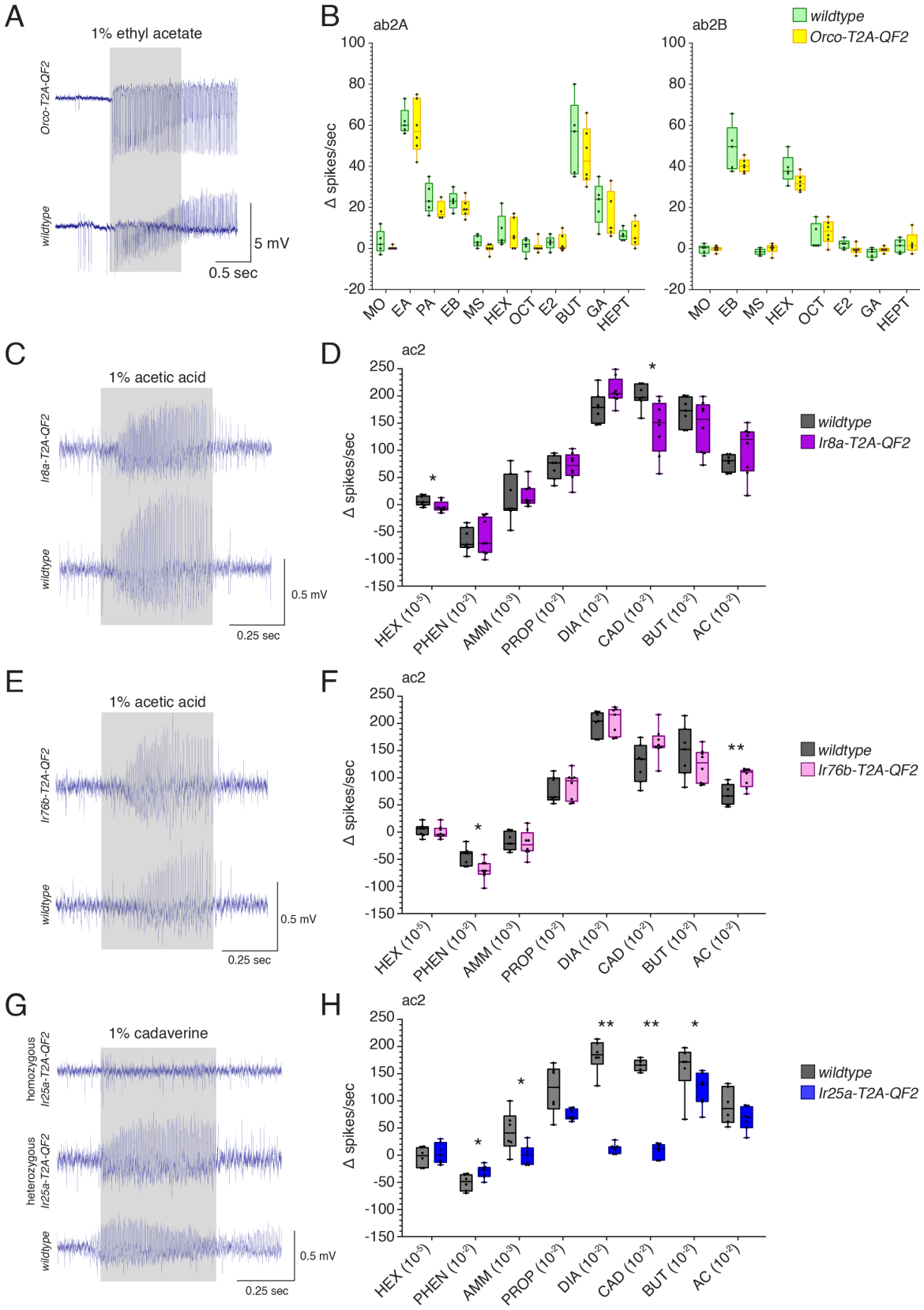

1043 **Figure 2-Figure Supplement 2. *T2A-QF2 HACK knock-in Effects on Target Gene Function*.**
1044 **A.** *Orco* knock-in SSR experiments were performed in ab2 sensilla. Responses to ten odorants
1045 plus mineral oil control were compared in *wildtype* and homozygous *Orco-T2A-QF2* sensilla.
1046 Shown are example responses to 1% ethyl acetate. **B.** ab2 sensilla contain two neurons: A (left)
1047 and B (right). No differences were found in the responses of these neurons between the two
1048 genotypes across all odorants tested (Mann-Whitney *U* test, $p > 0.05$). A small difference in
1049 baseline (pre-stimulus) activity was observed, which can be seen in (A). Fewer stimuli are
1050 shown for ab2B because odorants strongly activating the A neuron obscured the B neuron
1051 responses. N = 5 for *wildtype*, N = 6 for *Orco-T2A-QF2*. Abbreviations: MO mineral oil, EA ethyl
1052 acetate, PA pentyl acetate, EB ethyl butyrate, MS methyl salicylate, HEX hexanol, OCT 1-octen-
1053 3-ol, E2 e2-hexenal, BUT 2,3-butanedione, GA geranyl acetate, HEPT 2-heptanone. **C**.-**H**. *IrCo*
1054 knock-in SSR experiments were performed in ac2 sensilla. Responses to eight odorants were
1055 compared in *wildtype* and homozygous knock-in flies. **C.** Example responses to 1% acetic acid
1056 in *Ir8a-T2A-QF2* and *wildtype* sensilla. **D.** There was a small but significant difference in
1057 responses between the two genotypes to hexanol (Mann-Whitney *U* test, $p = 0.0286$) and
1058 cadaverine (Mann-Whitney *U* test, $p = 0.0106$), which are not typically considered to be Ir8a-
1059 dependent odorants (Silbering et al., 2011). Responses to all other stimuli were not significantly
1060 different between genotypes. N = 7 for *wildtype*, N = 8 for *Ir8a-T2A-QF2*. **E.** Example responses
1061 to 1% acetic acid in *Ir76b-T2A-QF2* and *wildtype* flies. **F.** There were small but significant
1062 differences in responses to phenethylamine (Mann-Whitney *U* test, $p = 0.012$) and acetic acid
1063 (Mann-Whitney *U* test, $p = 0.0087$) between *Ir76b-T2A-QF2* and *wildtype* flies. Responses to
1064 the other stimuli were not significantly different between genotypes. N = 7 for *wildtype*, N = 8 for
1065 *Ir76b-T2A-QF2*. **G.** Homozygous *Ir25a-T2A-QF2* flies lost responses to most amines,
1066 recapitulating an *Ir25a* mutant phenotype (Abuin et al., 2011; Silbering et al., 2011).
1067 Heterozygous *Ir25a-T2A-QF2* flies with one *wildtype* copy of *Ir25a* had normal responses.
1068 Shown are example responses to 1% cadaverine in homozygous *Ir25a-T2A-QF2*, heterozygous

1069 *Ir25a-T2A-QF2*, and *wildtype* ac2 sensilla. **H.** Homozygous *Ir25a-T2A-QF2* flies had strongly
1070 reduced or abolished responses to phenethylamine (Mann-Whitney *U* test, $p = 0.039$), ammonia
1071 (Mann-Whitney *U* test, $p = 0.0338$), 1,4-diaminobutane (Mann-Whitney *U* test, $p = 0.0012$),
1072 cadaverine (Mann-Whitney *U* test, $p = 0.0025$), and 2,3-butanedione (Mann-Whitney *U* test, $p =$
1073 $0.0472$). Responses to the other stimuli were not significantly different between genotypes. N =
1074 6 for *wildtype*, N = 7 for homozygous *Ir25a-T2A-QF2*. Abbreviations in (D-H): PO paraffin oil,
1075 HEX hexanol, PHEN phenethylamine, AMM ammonia, PROP propanal, DIA 1,4-diaminobutane,
1076 CAD cadaverine, BUT 2,3-butanedione, AC acetic acid. See Figure 2-Source Data 1 for all *U*
1077 and *p* values.

1078 **Figure 2-Figure Supplement 3**

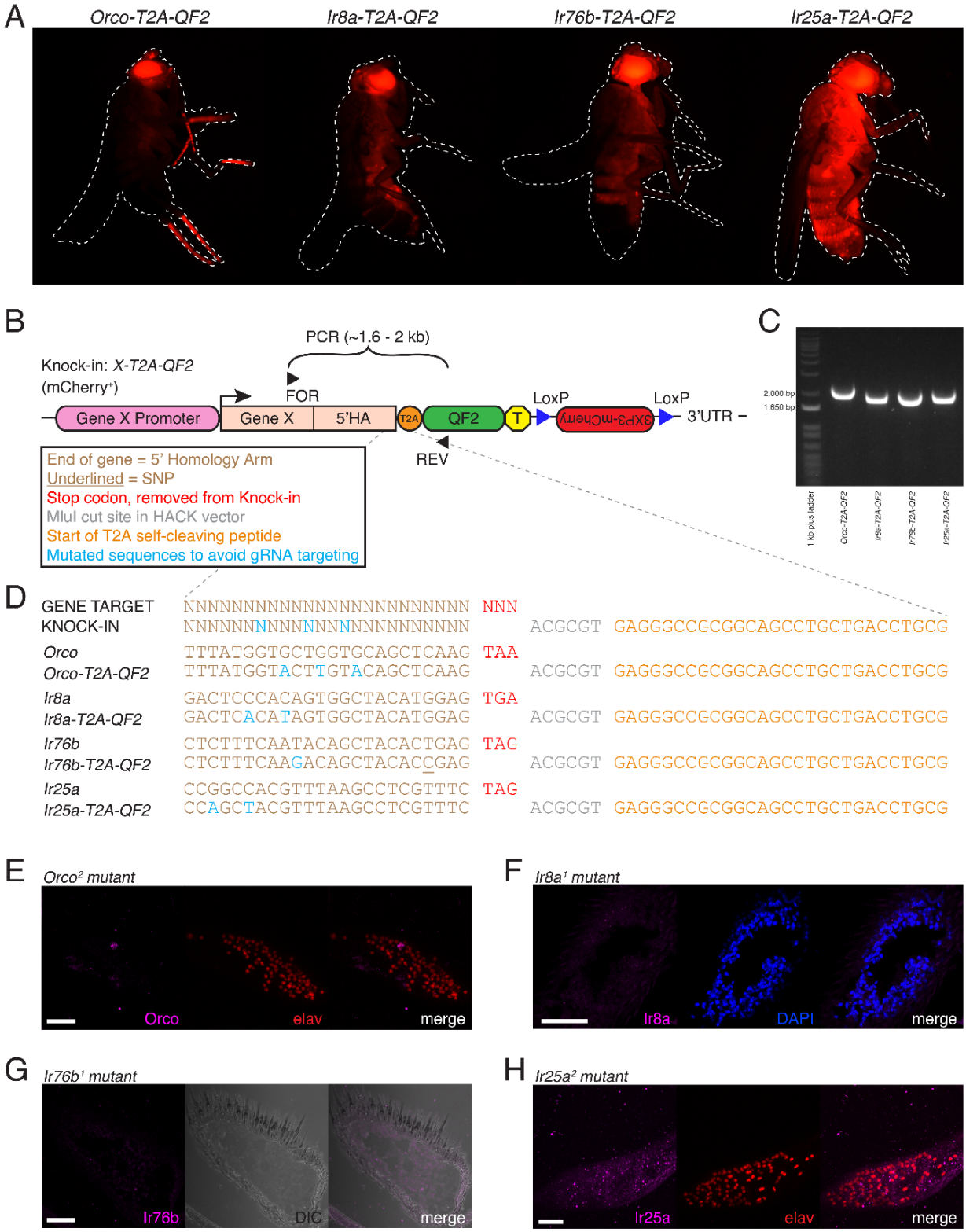

1079 **Figure 2-Figure Supplement 3. Additional Validation of Co-Receptor Knock-in Lines.**
1080 **A.** The HACK *3XP3-mCherry* marker is expressed in the eyes and broadly throughout the fly
1081 nervous system and is subject to positional effects in expression. **B.** Each knock-in line is
1082 generated by CRISPR-Cas9 mediated homology-directed insertion of a *T2A-QF2* cassette
1083 marked by mCherry in front of the translational stop codon of the target gene. The 5' homology
1084 arm (5'HA) is ~1kb of the gene just before the stop codon. Successful knock-in lines were
1085 confirmed using forward primers upstream of the 5'HA (FOR), and a reverse primer within the
1086 *QF2* sequence (REV). Amplification of a ~1.6 to 2 kb sequence occurs only if a knock-in is
1087 present. See Figure 2A for target and donor construct schematics. **C.** PCR genotyping using the
1088 primers shown in (B) confirms successful knock-in of the four targeted genes. **D.** Knock-ins
1089 were confirmed with sequencing of the targeted genomic site. For each co-receptor, the first line
1090 shows the target sequence (based on the FlyBase reference genome) (Thurmond et al., 2019),
1091 and the second line shows the verified sequence of the knock-in. The stop codon (red) has
1092 been replaced with the HACK *T2A-QF2* cassette. The portion shown here includes the *MluI*
1093 restriction site used for cloning the 5'HA (grey), as well as the start of the *T2A* sequence
1094 (orange). In each knock-in construct, synonymous substitutions (blue) have been made to
1095 prevent the gRNA/Cas9 from cutting the donor construct. Each knock-in construct was designed
1096 with three substitutions. The underlined base pair in the *Ir76b* knock-in is a SNP discovered in
1097 the lab *wildtype* stock and considered when designing the knock-in construct. **E.-H.** Antibody
1098 and *in situ* probe validation. **E.** No anti-Orco expression in $Orco^2$ mutant palps. elav is used as a
1099 pan-neuronal counterstain. **F.** No anti-Ir8a expression in $Ir8a^1$ mutant antennae. DAPI is used as
1100 a cellular counterstain. **G.** No *Ir76b* probe signal in $Ir76b^1$ mutant antennae. DIC used to
1101 visualize tissue. **H.** No anti-Ir25a expression in $Ir25a^2$ mutant palps (elav counterstain). Scale
1102 bars = 25 μm. See also Table 2.

1103 **Figure 2-Figure Supplement 4**

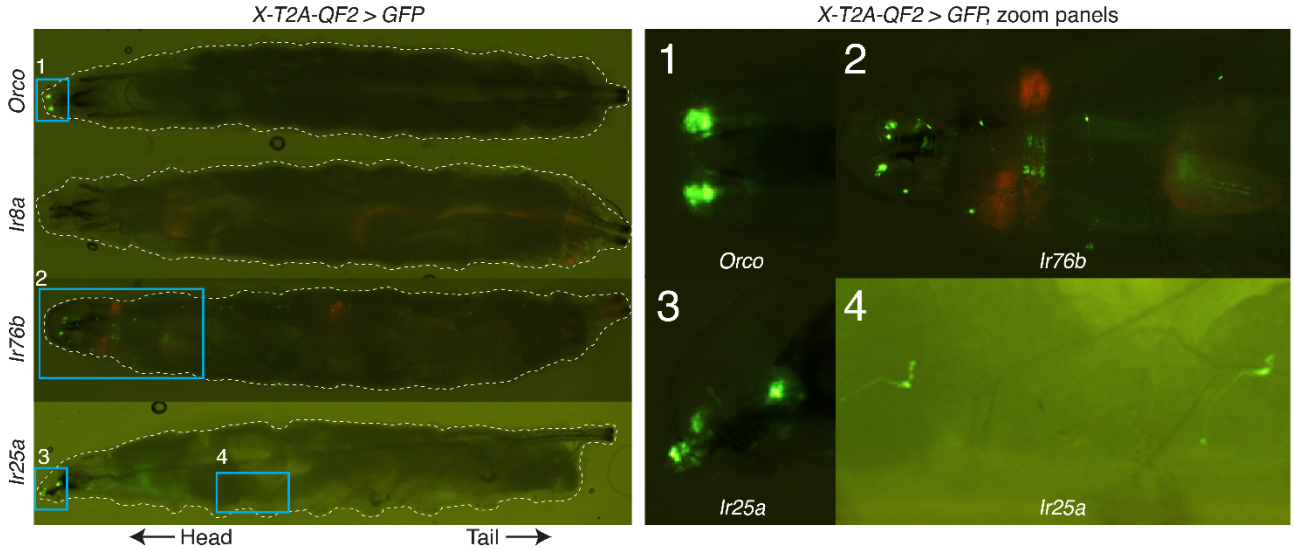


1104 **Figure 2-Figure Supplement 4. Knock-in Expression in the Larva.**

1105 In the larval stage, *Orco-T2A-QF2* (first row) appears to drive expression only in the dorsal
1106 organs (zoom panel 1), as previously described (Larsson et al., 2004); *Ir8a-T2A-QF2* (second
1107 row) does not appear to drive GFP expression in the larva (although very weak expression may
1108 not be visible at this magnification); and both *Ir76b-T2A-QF2* (third row) and *Ir25a-T2A-QF2*
1109 (fourth row) drive GFP expression in the larval head as well as throughout the body wall (zoom
1110 panel 2 for *Ir76b*; zoom panels 3 and 4 for *Ir25a*), reflecting the role of these genes in additional,
1111 non-olfactory modalities. Weak red fluorescence from the *3XP3-mCherry* knock-in marker can
1112 be detected in the *Ir8a-T2A-QF2* and *Ir76b-T2A-QF2* larvae. This is due to channel bleed-
1113 through and is not seen in the other knock-in lines (*Orco-T2A-QF2* and *Ir25a-T2A-QF2*) that
1114 have had the marker removed (see Methods for details).

1115 **Figure 3-Figure Supplement 1**

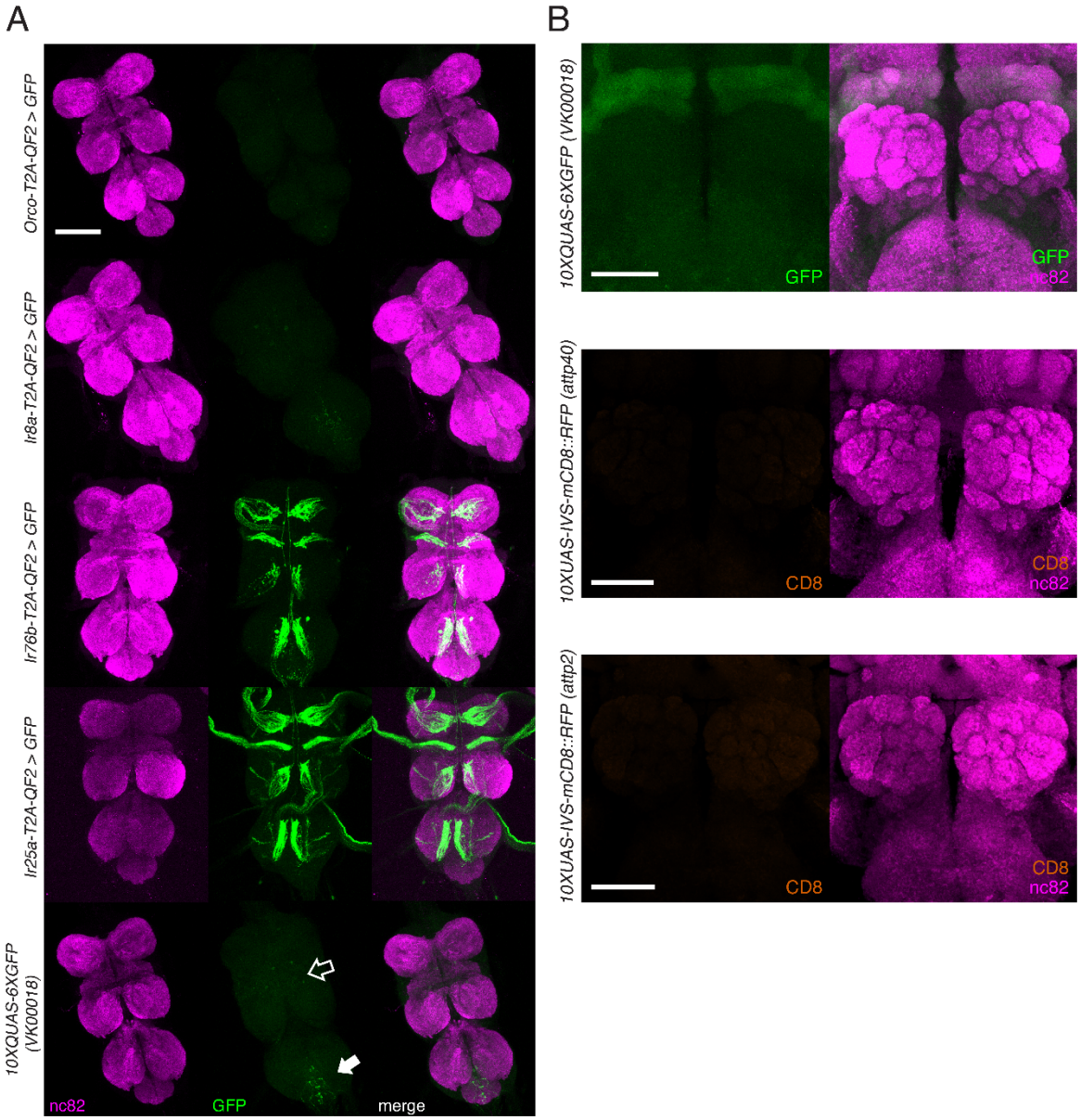


1116 **Figure 3-Figure Supplement 1. Knock-in Expression in the Adult Ventral Nerve Cord and**

1117 **Reporter Expression in the Brain.**

1118 **A.** In adult flies, two of the four knock-ins (*Ir76b-T2A-QF2*, third row, and *Ir25a-T2A-QF2*, fourth

1119 row) drive GFP expression in neurons innervating the ventral nerve cord (VNC). This likely

1120 reflects the role of these co-receptors in gustation. There is weak GFP expression in the

1121 reporter control (bottom row) in the abdominal neuromere (filled arrow), as well as the

1122 accessory mesothoracic neuropil (empty arrow), which can be seen in the two other knock-ins

1123 (*Orco-T2A-QF2*, first row, and *Ir8a-T2A-QF2*, second row). This non-specific expression is likely

1124 from the reporter itself rather than driven by the two knock-ins. **B.** Control brains showing the

1125 *QUAS-GFP* reporter alone (top) and the *UAS-mCD8::RFP* reporters alone (middle and bottom).

1126 These reporters were used for all brain images in Figures 3 – 5. The *QUAS* reporter weakly

1127 labels the mushroom bodies. The ventral nerve cord from the fly in (A, fourth row) is also used

1128 in Figure 2-Figure Supplement 1E. Scale bars: 100 μm in (A), 50 μm in (B).

1129 **Figure 3-Figure Supplement 2**

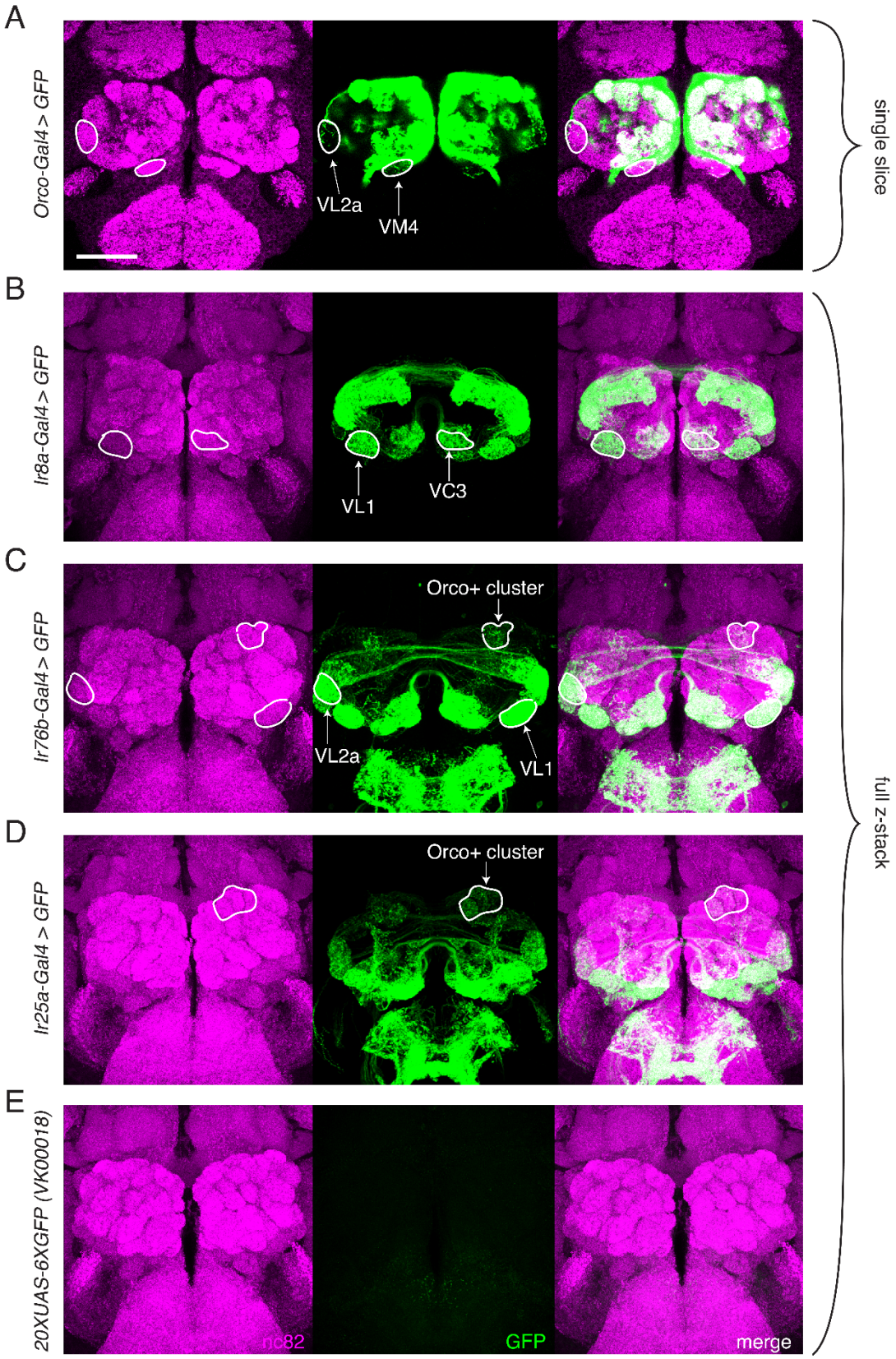

1130 **Figure 3-Figure Supplement 2. Transgenic Co-Receptor *Gal4* Lines Do Not Fully**
1131 **Recapitulate Knock-in Expression.**

1132 **A.-E.** Transgenic co-receptor *Gal4* lines crossed to a strong *UAS* reporter reveal expression in
1133 some, but not all, of the additional glomeruli labeled by the respective knock-ins. Some
1134 discrepancies between the *Gal4* and knock-in lines are enumerated here, but do not represent a
1135 comprehensive list. **A.** *Orco-Gal4* drives weak GFP expression in VL2a and VM4 glomeruli
1136 (outlined), but lacks expression in DL2, V, and VL1 glomeruli, which are labeled by the knock-in.
1137 **B.** *Ir8a-Gal4>GFP* labels VC3 and VL1 (outlined), but lacks expression in the VM4 and VA3
1138 glomeruli, which are labeled in the knock-in. **C.** *Ir76b-Gal4* labels the VL1 and VL2a glomeruli
1139 (outlined), but lacks expression in the VA5 and DC3 glomeruli which are consistently labeled in
1140 the knock-in. Additionally, it drives GFP expression in Orco+ glomeruli not seen in the knock-in
1141 (outlined). **D.** *Ir25a-Gal4* labels some Orco+ glomeruli (outline includes DA2, DA3, DA4m, and
1142 DA4l), but is lacking expression in many glomeruli labeled by the knock-in. **E.** The *UAS-GFP*
1143 control line has weak leaky expression in the SEZ but no expression in the AL. (A) shows single
1144 slice to visualize weakly labeled glomeruli; (B-E) are maximum intensity projections of z-stacks.
1145 Scale bar = 50 μm. See also Figure 3-Source Data 1.

1146 **Figure 4-Figure Supplement 1**

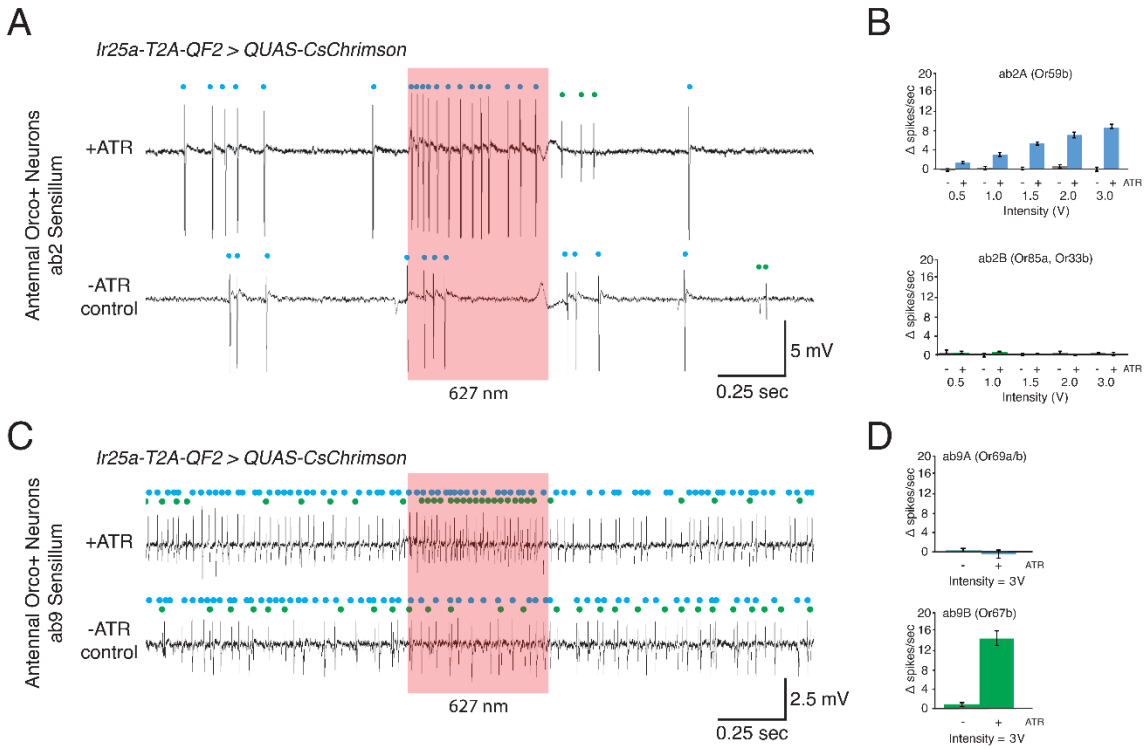


1147

1148 **Figure 4-Figure Supplement 1. Optogenetic Experiments to Examine *Ir25a* Expression in**

1149 **Orco+ Neurons.**

1150 **A-D.** Confirmation of *Ir25a* expression in ab2 and ab9 sensilla using optogenetic stimulation.

1151 *CsChrimson* expression is driven by *Ir25a-T2A-QF2*, and recordings are performed in neurons

1152 previously determined to express only *Orco*. **A.** Representative SSR traces from ab2 using 1.5V

1153 of a 627 nm LED light (red box) to activate *CsChrimson*. Bottom trace is control animal which

1154 was not fed the necessary cofactor all-trans retinal (-ATR). ab2 has two neurons: blue dots

1155 indicate A neuron spikes, while green dots indicate B neuron spikes (genotype: *Ir25a-T2A-QF2*;

1156 *QUAS-CsChrimson*). **B.** Quantification of neuronal activity in response to light stimulation at

1157 various intensities (N = 7 – 12). Optogenetic experiments confirm *Ir25a* expression in ab2A

1158 (expressing *Or59b*, top; DM4 glomerulus) but not ab2B (expressing *Or85a* and *Or33b*, bottom;

1159 DM5 glomerulus). **C.** Combination of optogenetics and fluorescent guided SSR (Lin and Potter,

1160 2015) to examine *Ir25a* expression in ab9 sensilla (genotype: *Ir25a-T2A-QF2*; *QUAS-*

1161 *CsChrimson/Or67b-Gal4, 15XUAS-IVS-mcd8::GFP)*. Representative traces from ab9 in
1162 response to 3V of 627 nm LED light (red box). As in (A), -ATR indicates the inactive
1163 *CsChrimson* control; blue dots indicate A neuron spikes, green dots indicate B neuron. **D.**
1164 Quantification of activity in response to light stimulation verified that *Ir25a* is expressed in ab9B
1165 (*Or67b*, bottom; VA3 glomerulus) but not in ab9A neurons (*Or69aA/aB*, top; D glomerulus). N =
1166 5.
1167

1168 **Figure 5-Figure Supplement 1**

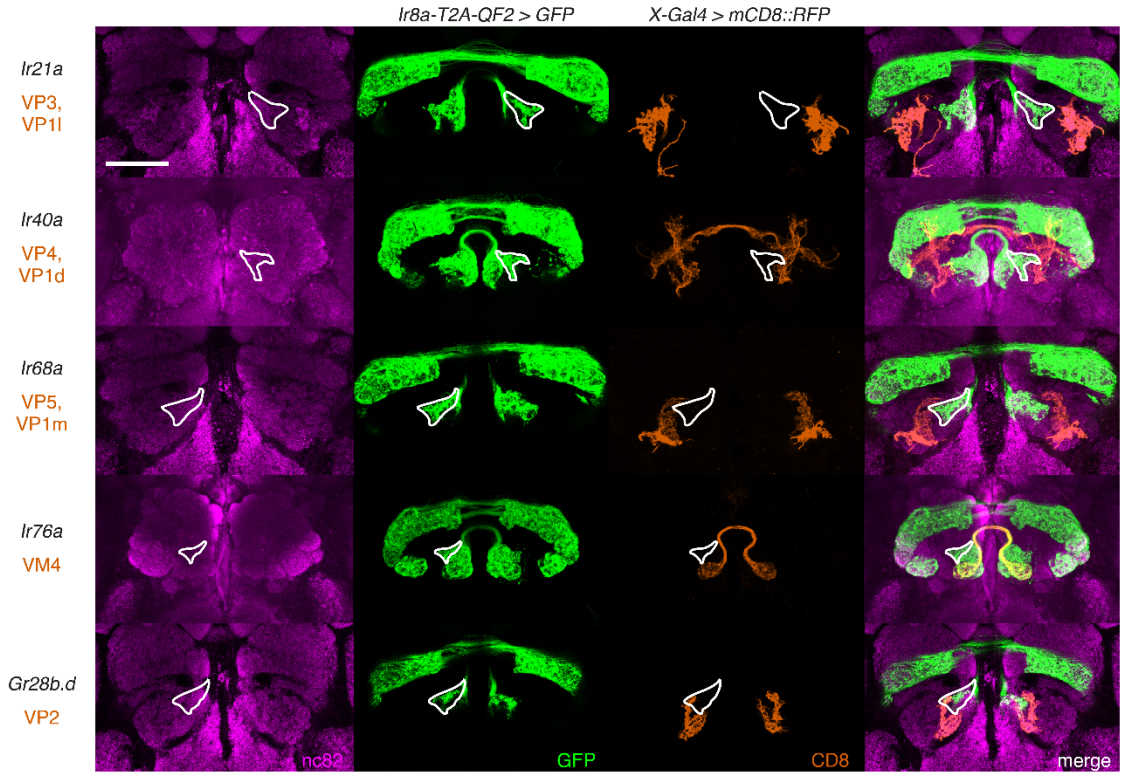


1169 **Figure 5-Figure Supplement 1. The New Glomerular Region Labeled by the *Ir8a* Knock-in**

1170 **Does Not Correspond to Previously Identified Posterior Glomeruli.**

1171 Co-labeling experiments with *Ir8a-T2A-QF2 > GFP* (green) and various *Gal4* lines driving

1172 *mCD8::RFP* (orange) confirm that the outlined region does not correspond to any of the VP

1173 glomeruli nor to VM4. Scale bar: 50 μm.

1174 **Figure 6-Figure Supplement 1**

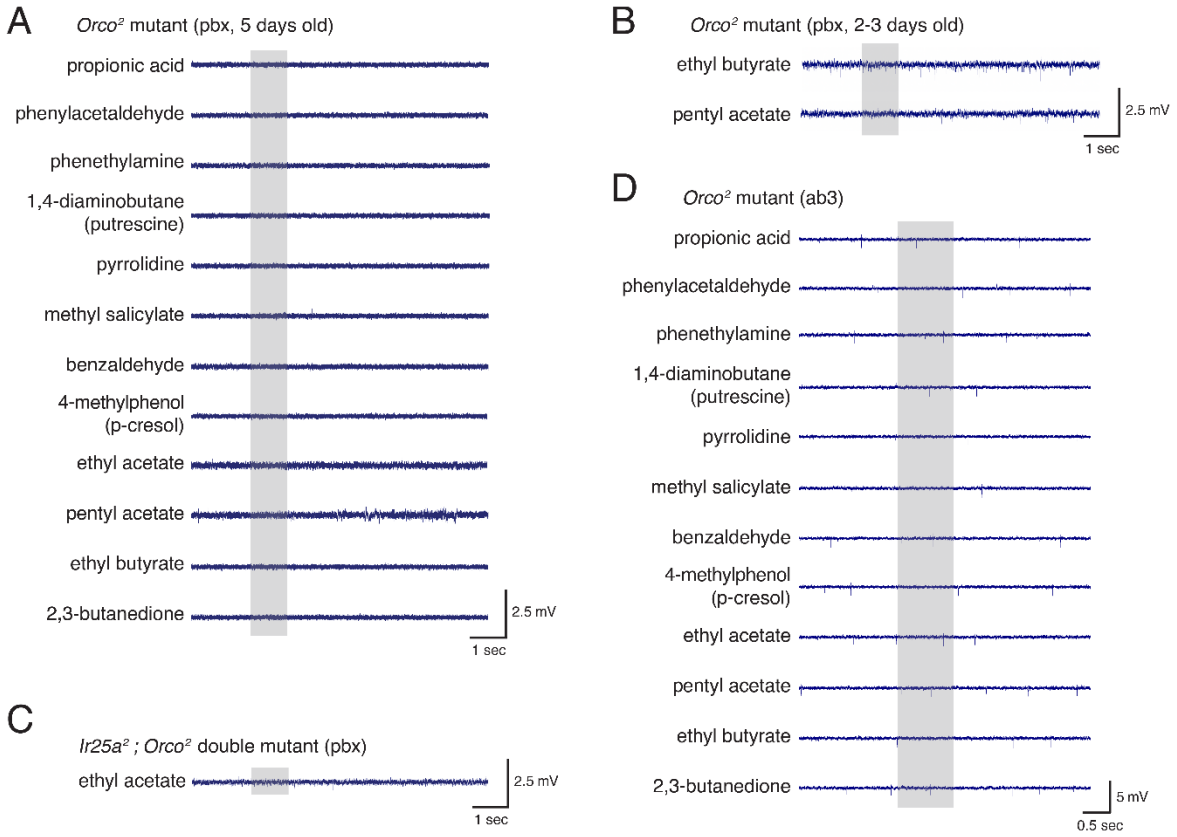


1175 **Figure 6-Figure Supplement 1. Electrophysiological Experiments to Examine *Ir25a***

1176 **Function in Orco+ Neurons.**

1177 **A.** SSR recordings in *Orco*$^2$ mutant palpal sensilla show neither baseline nor odor-evoked

1178 activity in response to a panel of odorants in 5-day old flies. N = 20 sensilla, 4 animals (3 male,

1179 1 female). **B.** Young *Orco*$^2$ mutant palpal neurons also do not have spontaneous or odor-evoked

1180 activity. **C.** *Ir25a*$^2$*; Orco*$^2$ double mutant palpal sensilla show neither baseline nor odor-evoked

1181 activity. N = 42 sensilla from 5 animals (3 male, 2 female). **D.** Antennal ab3 sensilla do

1182 occasionally show baseline activity in the *Orco*$^2$ mutant, but generally do not show odor-evoked

1183 activity (N = 5 flies; see also Figure 6). Grey box indicates the time of stimulus delivery. See

1184 also Figure 6-Source Data 1.

1185 **Figure 6-Figure Supplement 2**

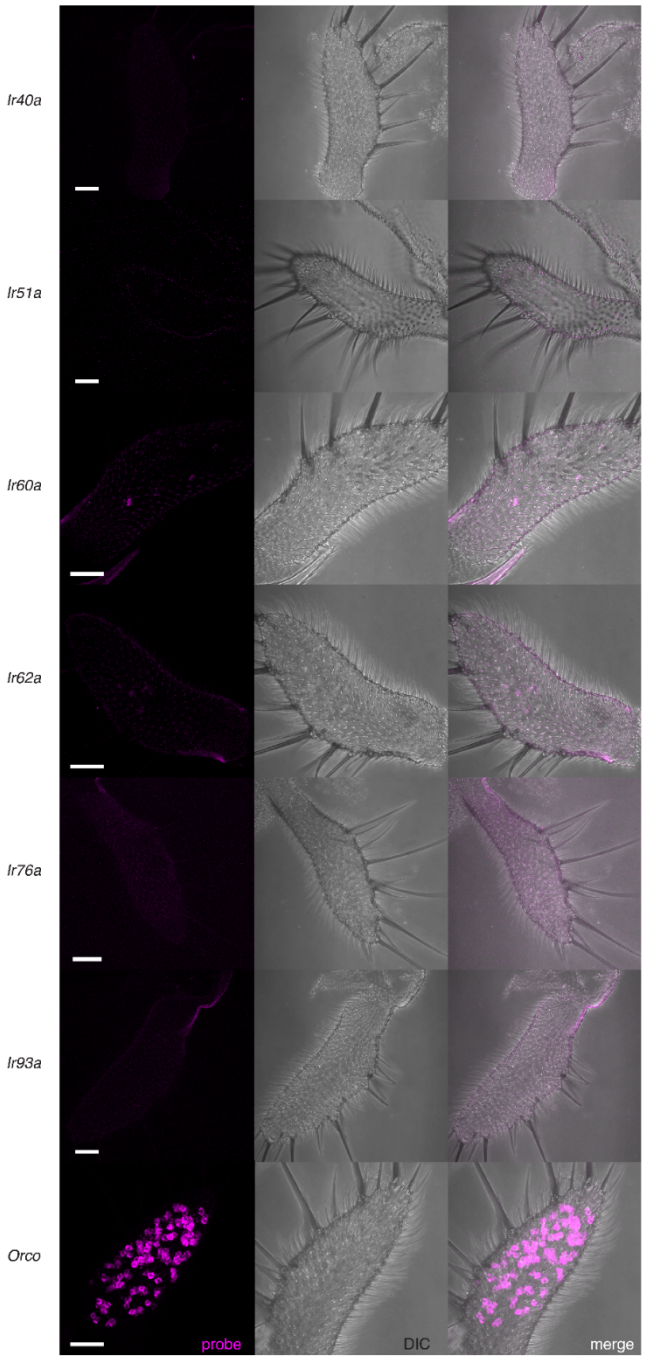


1186 **Figure 6-Figure Supplement 2. No IrX Expression of the Top Candidates in the Maxillary**

1187 **Palps.**

1188 The recent fly cell atlas (Li et al., 2021) was used to identify potential IrX tuning receptors in the

1189 palps. *In situ* experiments did not reveal strong expression of any of these target genes. Orco

1190 (bottom) was used as a positive control. See also Figure 6-Source Data 2. Scale bars = 25 μm.

1191 # Materials and Methods

1192 ## *Key Resources Table*

| REAGENT or RESOURCE | SOURCE | IDENTIFIER |
|---|---|---|
| Antibodies | | |
| Mouse anti-nc82 | DSHB | Cat# nc82; RRID: AB_2314866 |
| Rat anti-cd8 | Thermo Fisher Scientific | Cat# 14-0081-82; RRID: AB_467087 |
| Rat anti-elav | DSHB | Cat# Rat-Elav-7E8A10; RRID: AB_528218 |
| Rabbit anti-Orco | Gift from Leslie Vosshall; (Larsson et al., 2004) | N/A |
| Rabbit anti-Ir25a | Gift from Richard Benton; (Benton et al., 2009) | RRID: AB_2567027 |
| Guinea pig anti-Ir8a | Gift from Richard Benton; (Abuin et al., 2011) | RRID:AB_2566833 |
| Rabbit anti-Ir64a | Gift from Greg Suh; (Ai et al., 2010) | RRID:AB_2566854 |
| Goat anti-guinea pig Alexa 568 | Thermo Fisher Scientific | Cat# A11075; RRID: AB_141954 |
| Goat anti-rabbit Cy3 conjugated AffiniPure 568 | Jackson ImmunoResearch | Cat# 111-165-144; RRID: AB_2338006 |
| Goat anti-mouse Cy3 | Jackson ImmunoResearch | Cat# 115-165-166; RRID: AB_2338692 |
| Goat anti-mouse Alexa 647 | Jackson ImmunoResearch | Cat# 115-605-166; RRID: AB_2338914 |
| Donkey anti-guinea pig Cy3 | Jackson ImmunoResearch | Cat# 706-165-148; RRID: AB_2340460 |
| Goat anti-rat Cy3 | Jackson ImmunoResearch | Cat# 112-165-167; RRID: AB_2338251 |
| Goat anti-rat Alexa 647 | Jackson ImmunoResearch | Cat# 112-605-167; RRID: AB_2338404 |
| Goat anti-rabbit Cy3 | Jackson ImmunoResearch | Cat# 111-165-144; RRID: AB_2338006 |
| Goat anti-rabbit Alexa 647 | Jackson ImmunoResearch | Cat# 111-605-144; RRID: AB_2338078 |
| Chemicals, Peptides, and Recombinant Proteins | | |
| Mineral oil | Sigma-Aldrich | CAS# 8042-47-5 |
| Ethyl acetate | Sigma-Aldrich | CAS# 141-78-6 |
| Pentyl acetate | Sigma-Aldrich | CAS# 628-63-7 |
| Benzaldehyde | Sigma-Aldrich | CAS# 100-52-7 |
| Ethyl butyrate | Sigma-Aldrich | CAS# 105-54-4 |
| Hexanol | Sigma-Aldrich | CAS# 111-27-3 |
| E2-hexenal | Sigma-Aldrich | CAS# 6728-26-3 |
| Geranyl acetate | Sigma-Aldrich | CAS# 105-87-3 |
| 2-heptanone | Sigma-Aldrich | CAS# 110-43-0 |
| 1-octen-3-ol | Sigma-Aldrich | CAS# 3391-86-4 |

| | | |
|---|---|---|
| 2,3-butanedione | Sigma-Aldrich | CAS# 431-03-8 |
| Phenylacetaldehyde | Sigma-Aldrich | CAS# 122-78-1 |
| Phenethylamine | Sigma-Aldrich | CAS# 64-04-0 |
| Propionic acid | Sigma-Aldrich | CAS# 79-09-4 |
| 1,4-diaminobutane | Sigma-Aldrich | CAS# 110-60-1 |
| Pyrrolidine | Sigma-Aldrich | CAS# 123-75-1 |
| P-cresol | Sigma-Aldrich | CAS# 106-44-5 |
| Methyl salicylate | Sigma-Aldrich | CAS# 119-36-8 |
| Paraffin Oil | ACROS Organics | CAS# 8012-95-1 |
| Water | SIGMA Life Science | CAS# 7732-18-5 |
| Acetic acid | Fisher Scientific | CAS# 64-19-7 |
| Ammonium hydroxide | Fisher Scientific | CAS# 7664-41-7 |
| Cadaverine | Sigma-Aldrich | CAS# 462-94-2 |
| Hexanol | ACROS Organics | CAS# 111-27-3 |
| 2,3-butanedione | ACROS Organics | CAS# 431-03-8 |
| Phenethylamine | ACROS Organics | CAS# 64-04-0 |
| Propanal | ACROS Organics | CAS# 123-38-6 |
| 1,4-diaminobutane | ACROS Organics | CAS# 110-60-1 |
| All trans-retinal | Sigma-Aldrich | CAS# 116-31-4 |
| Critical Commercial Assays | | |
| HCR v3.0 | Molecular Instruments | N/A |
| In-Fusion Cloning | Clontech Labs | Cat# 639645 |
| DNeasy Blood and Tissue Kit | Qiagen | Cat# 69506 |
| Deposited Data | | |
| Raw and analyzed data | This paper | Available upon request |
| snRNAseq data | (McLaughlin et al., 2021) | GSE162121; https://github.com/colleen-mclaughlin/ORN_seq/ |
| EM reconstructions | This paper | https://flywire.ai/#links/Task2021a/all |
| Experimental Models: Organisms/Strains | | |
| *D. melanogaster*: *Orco-T2A-QF2* knock-in | This paper | BDSC: 92400, 92401, 92402 |
| *D. melanogaster*: *Ir8a-T2A-QF2* knock-in | This paper | BDSC: 92398, 92399 |
| *D. melanogaster*: *Ir76b-T2A-QF2* knock-in | This paper | BDSC: 92396, 92397 |
| *D. melanogaster*: *Ir25a-T2A-QF2* knock-in | This paper | BDSC: 92392, 92393, 92394, 92395 |
| *D. melanogaster: y[1] w[*]; Pin[1]/CyO; P(w[+mC]=10XQUAS-CsChrimson.mVenus)11c* | This paper | BDSC: 91996; FlyBase: FBst0091996 |
| *D. melanogaster*: *Ir21a-T2A-Gal4* knock-in | Gift from Paul Garrity; (Marin et al., 2020) | N/A |
| *D. melanogaster*: *Ir68a-T2A-Gal4* knock-in | Gift from Paul Garrity; (Marin et al., 2020) | N/A |

| | | |
|---|---|---|
| *D. melanogaster: Ir64a-Gal4* | Gift from Greg Suh lab; (Ai et al., 2010) | N/A |
| *D. melanogaster: Rh50-Gal4* | (Vulpe et al., 2021a) | N/A |
| *D. melanogaster: Amt-Gal4* | (Menuz et al., 2014) | N/A |
| *D. melanogaster: Repo-Gal80* | (Awasaki et al., 2011) | FlyBase: FBtp0067904 |
| *D. melanogaster: wCS (Cantonized $w^{1118}$)* | (Koh et al., 2014) | FlyBase: FBrf0226011 |
| *D. melanogaster: Or35a-Gal4* | (Yao et al., 2005) | N/A |
| *D. melanogaster: y[1] w[67c23] P(y[+mDint2]=Crey)1b; sna[Sco]/CyO* | Bloomington *Drosophila* Stock Center | BDSC: 766; FlyBase: FBti0012692 |
| *D. melanogaster: w[*]; l(2)*[*]/CyO; P(w[+mC]=Or10a-GAL4.C)134t1.3* | Bloomington *Drosophila* Stock Center | BDSC: 23885; FlyBase: FBti0102042 |
| *D. melanogaster: w[*]; P(w[+mC]=Or22a-GAL4.7.717)14.2* | Bloomington *Drosophila* Stock Center | BDSC: 9951; FlyBase: FBti0101805 |
| *D. melanogaster: w[*]; P(w[+mC]=Or22a-GAL4.7.717)14.21* | Bloomington *Drosophila* Stock Center | BDSC: 9952; FlyBase: FBti0101805 |
| *D. melanogaster: w[*]; P(w[+mC]=Or33c-GAL4.F)78.3* | Bloomington Drosophila Stock Center | BDSC: 9966; FlyBase: FBti0101843 |
| *D. melanogaster: w[*]; P(w[+mC]=Or35a-GAL4.F)109.2A* | Bloomington *Drosophila* Stock Center | BDSC: 9967; FlyBase: FBti0101810 |
| *D. melanogaster: w[*]; P(w[+mC]=Or35a-GAL4.F)109.3* | Bloomington *Drosophila* Stock Center | BDSC: 9968; FlyBase: FBti0101844 |
| *D. melanogaster: w[*]; P(w[+mC]=Or42a-GAL4.F)48.3B* | Bloomington *Drosophila* Stock Center | BDSC: 9970; FlyBase: FBti0101811 |
| *D. melanogaster: w[*]; P(w[+mC]=Or42b-GAL4.F)64.3* | Bloomington *Drosophila* Stock Center | BDSC: 9971; FlyBase: FBti0101812 |
| *D. melanogaster: w[*]; P(w[+mC]=Or47a-GAL4.8.239)15.4A* | Bloomington *Drosophila* Stock Center | BDSC: 9982; FlyBase: FBti0101851 |
| *D. melanogaster: w[*]; P(w[+mC]=Or49b-GAL4.F)80.1* | Bloomington *Drosophila* Stock Center | BDSC: 9986; FlyBase: FBti0101853 |
| *D. melanogaster: w[*]; Bl[1]/SM1; P(w[+mC]=Or65a-GAL4.F)72.1* | Bloomington *Drosophila* Stock Center | BDSC: 9994; FlyBase: FBti0101857 |
| *D. melanogaster: w[*]; P(w[+mC]=Or67b-GAL4.F)68.3/TM6B, Tb[1]* | Bloomington *Drosophila* Stock Center | BDSC: 9995; FlyBase: FBti0101858 |
| *D. melanogaster: w[*]; P(w[+mC]=Or71a-GAL4.F)30.4* | Bloomington *Drosophila* Stock Center | BDSC: 23122; FlyBase: FBti0101860 |
| *D. melanogaster: w[*]; P(w[+mC]=Or83c-GAL4.F)73.3B* | Bloomington *Drosophila* Stock Center | BDSC: 23131; FlyBase: FBti0101829 |

| | | |
|---|---|---|
| *D. melanogaster: w[*]; P(w[+mC]=Or85a-GAL4.F)67.2* | Bloomington *Drosophila* Stock Center | BDSC: 23133; FlyBase: FBti0101830 |
| *D. melanogaster: w[*]; P(w[+mC]=Or92a-GAL4.F)62.1* | Bloomington *Drosophila* Stock Center | BDSC: 23139; FlyBase: FBti0101867 |
| *D. melanogaster: w[*]; P(w[+mC]=Or98a-GAL4.F)115.1* | Bloomington *Drosophila* Stock Center | BDSC: 23141; FlyBase: FBti0101868 |
| *D. melanogaster: w[1118]; P(w[+mC]=Or46a-GAL4.G)32.1.y* | Bloomington *Drosophila* Stock Center | BDSC: 23291; FlyBase: FBti0076800 |
| *D. melanogaster: w[*]; P(w[+mC]=Or13a-GAL4.C)229t56.2/TM3, Sb[1]* | Bloomington *Drosophila* Stock Center | BDSC: 23886; FlyBase: FBti0102056 |
| *D. melanogaster: w[*]; P(w[+mC]=Or43b-GAL4.C)110t8.1* | Bloomington Drosophila Stock Center | BDSC: 23894; FlyBase: FBti0102047 |
| *D. melanogaster: w[*]; P(w[+mC]=Or59b-GAL4.C)114t2.2* | Bloomington Drosophila Stock Center | BDSC: 23897; FlyBase: FBti0102060 |
| *D. melanogaster: w[*]; P(w[+mC]=Or59c-GAL4.C)129t1.1* | Bloomington *Drosophila* Stock Center | BDSC: 23899; FlyBase: FBti0102061 |
| *D. melanogaster: w[*]; P(w[+mC]=Or67a-GAL4.C)137t3.3* | Bloomington *Drosophila* Stock Center | BDSC: 23904; FlyBase: FBti0102049 |
| *D. melanogaster: w[*]; P(w[+mC]=Or67c-GAL4.C)116t3.2/CyO* | Bloomington *Drosophila* Stock Center | BDSC: 23905; FlyBase: FBti0102050 |
| *D. melanogaster: w[*]; P(w[+mC]=Or85b-GAL4.C)179t5.1* | Bloomington *Drosophila* Stock Center | BDSC: 23911; FlyBase: FBti0102053 |
| *D. melanogaster: w[*]; P(w[+mC]=Or85d-GAL4.C)143t2.1* | Bloomington *Drosophila* Stock Center | BDSC: 24148; FlyBase: FBti0102066 |
| *D. melanogaster: w[*]; P(w[+mC]=Orco-GAL4.W)11.17; TM2/TM6B, Tb[1]* | Bloomington *Drosophila* Stock Center | BDSC: 26818; FlyBase: FBti0101150 |
| *D. melanogaster: w[*]; P(w[+mC]=Ir40a-GAL4.3011)214.1; TM2/TM6B, Tb[1]* | Bloomington *Drosophila* Stock Center | BDSC: 41727; FlyBase: FBst0041727 |
| *D. melanogaster: w[*]; P(w[+mC]=Ir25a-GAL4.A)236.1; TM2/TM6B, Tb[1]* | Bloomington *Drosophila* Stock Center | BDSC: 41728; FlyBase: FBti0148895 |
| *D. melanogaster: w[*]; P(w[+mC]=Ir76b-GAL4.916)226.8; TM2/TM6B, Tb[+]* | Bloomington *Drosophila* Stock Center | BDSC: 41730; FlyBase: FBti0153291 |
| *D. melanogaster: w[*]; P(w[+mC]=Ir8a-GAL4.A)204.8; TM2/TM6B, Tb[1]* | Bloomington *Drosophila* Stock Center | BDSC: 41731; FlyBase: FBti0148897 |
| *D. melanogaster: w[*]; P(w[+mC]=Ir64a-GAL4.A)183.8; TM2/TM6B, Tb[1]* | Bloomington *Drosophila* Stock Center | BDSC: 41732; FlyBase: FBti0148898 |

| | | |
|---|---|---|
| *D. melanogaster: w[*]; P(w[+mC]=Ir76a-GAL4.PB)292.3B; TM2/TM6B, Tb[1]* | Bloomington *Drosophila* Stock Center | BDSC: 41735; FlyBase: FBst0041735 |
| *D. melanogaster: w[*]; P(y[+t7.7] w[+mC]=Ir41a-GAL4.2474)attP40; TM2/TM6B, Tb[1]* | Bloomington *Drosophila* Stock Center | BDSC: 41749; FlyBase: FBst0041749 |
| *D. melanogaster: w[*]; P(w[+mC]=Or35a-Mmus\Cd8a.GFP)3/TM3, Sb[1]* | Bloomington *Drosophila* Stock Center | BDSC: 52624; FlyBase: FBti0156834 |
| *D. melanogaster: w[*]; P(w[+mC]=Gr21a-GAL4.9.323)2/CyO; Dr[1]/TM3, Sb[+]* | Bloomington *Drosophila* Stock Center | BDSC: 57600; FlyBase: FBti0162643 |
| *D. melanogaster: w[*]; P(w[+mC]=Gr28b.d-GAL4)B27; Dr[1]/TM3, Sb[1]* | Bloomington *Drosophila* Stock Center | BDSC: 57620; FlyBase: FBst0057620 |
| *D. melanogaster: y[1] w[*] TI(GAL4)Or7a[KI-GAL4.w-]* | Potter lab | BDSC: 91991; FlyBase: FBti0214362 |
| *D. melanogaster: QUAS* reporter*: y[1] w[1118]; P(w[+mC]=QUAS-mCD8::GFP.P)5B/TM6B, Tb[1]* | Bloomington *Drosophila* Stock Center | BDSC: 30003; FlyBase: FBti0129937 |
| *D. melanogaster: QUAS* reporter*: y[1] w[*]; PBac(y[+mDint2] w[+mC]=10XQUAS-6XGFP)VK00018/CyO, P(Wee-P.ph0)Bacc[Wee-P20]* | Bloomington *Drosophila* Stock Center | BDSC: 52264; FlyBase: FBti0162759 |
| *D. melanogaster: UAS* reporter*: w[*]; P(y[+t7.7] w[+mC]=10XUAS-IVS-mCD8::GFP)attP40* | Bloomington *Drosophila* Stock Center | BDSC: 32186; FlyBase: FBti0131963 |
| *D. melanogaster: UAS* reporter*: w[*]; P(y[+t7.7] w[+mC]=15XUAS-IVS-mCD8::GFP)attP2* | Bloomington *Drosophila* Stock Center | BDSC: 32193; FlyBase: FBti0131935 |
| *D. melanogaster: UAS* reporter*: w[*]; P(y[+t7.7] w[+mC]=10XUAS-IVS-mCD8::RFP)attP2* | Bloomington *Drosophila* Stock Center | BDSC: 32218; FlyBase: FBti0131950 |
| *D. melanogaster: UAS* reporter*: w[*]; P(y[+t7.7] w[+mC]=10XUAS-IVS-mCD8::RFP)attP40* | Bloomington *Drosophila* Stock Center | BDSC: 32219; FlyBase: FBti0131967 |
| *D. melanogaster: UAS* reporter*: y[1] w[*]; PBac(y[+mDint2] w[+mC]=20XUAS-6XGFP)VK00018/CyO, P(Wee-P.ph0)Bacc[Wee-P20]* | Bloomington *Drosophila* Stock Center | BDSC: 52261; FlyBase: FBti0162758 |
| *D. melanogaster: UAS* reporter (sacculus experiments)*: UAS-mCD8::GFP (2nd)* | (Lee and Luo, 1999) | FlyBase: FBti0012685 |
| *D. melanogaster: UAS* reporter (sacculus experiments)*: UAS-mCD8::GFP (3rd)* | (Lee and Luo, 1999) | FlyBase: FBti0012686 |
| *D. melanogaster: Orco$^2$* mutant*: w[*]; TI(w[+m*]=TI)Orco[2]* | Bloomington *Drosophila* Stock Center | BDSC: 23130; FlyBase: FBti0168777 |
| *D. melanogaster: Ir25a$^2$* mutant*: w[*]; TI(w[+m*]=TI)Ir25a[2]/CyO* | Bloomington *Drosophila* Stock Center | BDSC: 41737; FlyBase: FBti0168524 |
| *D. melanogaster: Ir8a$^1$* mutant*: w[*] TI(w[+mW.hs]=TI)Ir8a[1]; Bl[1] L[2]/CyO* | Bloomington *Drosophila* Stock Center | BDSC: 41744; FlyBase: FBst0041744 |

| | | |
|---|---|---|
| *D. melanogaster: Ir76b*[1] mutant*: w[*]; Ir76b[1]* | Bloomington *Drosophila* Stock Center | BDSC: 51309; FlyBase: FBst0051309 |
| *D. melanogaster:* germline *Cas9*: *y[1] M(RFP[3xP3.PB] GFP[E.3xP3]=vas-Cas9)ZH-2A w[1118]/FM7c* | Bloomington *Drosophila* Stock Center | BDSC: 51323; FlyBase: FBti0154823 |
| *D. melanogaster:* germline *Cas9: w[1118]; PBac(y[+mDint2]=vas-Cas9)VK00027* | Bloomington *Drosophila* Stock Center | BDSC: 51324; FlyBase: FBti0154822 |
| *D. melanogaster:* germline *Cas9: y[1] M(w[+mC]=Act5C-Cas9.P)ZH-2A w[*]* | Bloomington *Drosophila* Stock Center | BDSC: 54590; FlyBase: FBti0159182 |
| *D. melanogaster:* double balancer: *19ADrok/FM7c; Pin/CyO* | N/A (Potter lab stock) | Derived from BDSC 6666, FBba0000009, FBal0013831, FBba0000025 |
| *D. melanogaster:* double balancer: *y,w; Pin/CyO; Dh/TM6B* | N/A (Potter lab stock) | Derived from FBal0013831, FBba0000025, FBti0004009, FBba0000057, FBal0016730 |
| *D. melanogaster:* double balancer: *y,w; S/CyO; Pr/TM6B* | N/A (Potter lab stock) | Derived from FBal0015108, FBba0000025, FBal0013944, FBba0000057, FBal0016730 |
| *D. melanogaster:* single balancer: *y,w; +/+; Pr/TM6B* | N/A (Potter lab stock) | Derived from FBal0013944, FBba0000057, FBal0016730 |
| *D. melanogaster:* single balancer: *y,w; S/CyO; +/+* | N/A (Potter lab stock) | Derived from FBal0015108, FBba0000025 |
| *D. melanogaster:* wildtype: *w*[1118] *IsoD1* | Gift from Thomas R. Clandinin | Derived from FBal0018186 |
| Oligonucleotides | | |
| Orco_gRNA_FOR: TCCGGGTGAACTTCGCACAGTGCGGAGGGGGC AAGTTTTAGAGCTAGAAATAGCAAGTTA | Integrated DNA Technologies; This paper | N/A |
| Orco_gRNA_REV: TTCTAGCTCTAAAACACTTTATGGTGCTGGTGCA GCGACGTTAAATTGAAAATAGGTC | Integrated DNA Technologies; This paper | N/A |
| Orco_5HA_FOR: CCCTTACGTAACGCGTCAGCTTGTTTGACTTACT TGATTAC | Integrated DNA Technologies; This paper | N/A |
| Orco_5HA_REV: CGCGGCCCTCACGCGTCTTGAGCTGTACAAGTA CCATAAAGT | Integrated DNA Technologies; This paper | N/A |
| Orco_3HA_FOR: GTTATAGATCACTAGTCTCAGTACTATGCAACCA GCAATA | Integrated DNA Technologies; This paper | N/A |

| | | |
|---|---|---|
| Orco_3HA_REV: AATTCAGATCACTAGTGTTTTATGAAAGCTGCAAGAAATAA | Integrated DNA Technologies; This paper | N/A |
| Ir8a_gRNA_FOR: TCCGGGTGAACTTCGTTTGTTTGTTCGGCCATGTGTTTTAGAGCTAGAAATAGCAAGTTA | Integrated DNA Technologies; This paper | N/A |
| Ir8a_gRNA_REV: TTCTAGCTCTAAAACCTGTGGGAGTCAGAGGCACCGACGTTAAATTGAAAATAGGTC | Integrated DNA Technologies; This paper | N/A |
| Ir8a_5HA_FOR: CCCTTACGTAACGCGtCTATTGGCTATTCGTCGTACTCATGC | Integrated DNA Technologies; This paper | N/A |
| Ir8a_5HA_REV: CGCGGCCCTCACGCGtCTCCATGTAGCCACTATGTGAGTCAGAT | Integrated DNA Technologies; This paper | N/A |
| Ir8a_3HA_FOR: GTTATAGATCACTAGtGTTTCTTGTCGCACCTAATTAACAAGTG | Integrated DNA Technologies; This paper | N/A |
| Ir8a_3HA_REV: AATTCAGATCACTAGtCATACTTAAGCTCCTTGAGGTCCAGC | Integrated DNA Technologies; This paper | N/A |
| Ir76b_gRNA_FOR: TCCGGGTGAACTTCGCAGTGATGCGAACTTCATAGTTTTAGAGCTAGAAATAGCAAGTTA | Integrated DNA Technologies; This paper | N/A |
| Ir76b_gRNA_REV: TTCTAGCTCTAAAACCGGCGGCCCTCTTTCAATACGACGTTAAATTGAAAATAGGTC | Integrated DNA Technologies; This paper | N/A |
| Ir76b_5HA_FOR: CCCTTACGTAACGCGtACCAATGAATCCTTGTCCATGCTAAA | Integrated DNA Technologies; This paper | N/A |
| Ir76b_5HA_REV: CGCGGCCCTCACGCGtCTCGGTGTAGCTGTCTTGAAGGAA | Integrated DNA Technologies; This paper | N/A |
| Ir76b_3HA_FOR: GTTATAGATCACTAGtGCCTAATTGGAATACCTTCTACATAATGGA | Integrated DNA Technologies; This paper | N/A |
| Ir76b_3HA_REV: AATTCAGATCACTAGtGGCAAGGCACAAAATAAAACGAAG | Integrated DNA Technologies; This paper | N/A |
| Ir25a_gRNA_FOR: TCCGGGTGAACTTCGCCGGATACTGATTAAAGCGGTTTTAGAGCTAGAAATAGCAAGTTA | Integrated DNA Technologies; This paper | N/A |
| Ir25a_gRNA_REV: TTCTAGCTCTAAAACAGTGCTCATTTTACCATAATCGACGTTAAATTGAAAATAGGTC | Integrated DNA Technologies; This paper | N/A |
| Ir25a_5HA_FOR: CCCTTACGTAACGCGtTGCATGACTTCATTGACACCTCAAG | Integrated DNA Technologies; This paper | N/A |
| Ir25a_5HA_REV: CGCGGCCCTCACGCGtGAAACGAGGCTTAAACGTAGCTGGATATT | Integrated DNA Technologies; This paper | N/A |
| Ir25a_3HA_FOR: GTTATAGATCACTAGtAATATTATGGTTAAGTGAGCTCTCGG | Integrated DNA Technologies; This paper | N/A |

| | | |
|---|---|---|
| Ir25a_3HA_REV: AATTCAGATCACTAGtCAAAGCTAAGTTCATCGTCATAGAGAC | Integrated DNA Technologies; This paper | N/A |
| Orco_Seq_FOR: GATGTTCTGCTCTTGGCTGATATTC | Integrated DNA Technologies; This paper | N/A |
| Ir8a_Seq_FOR: CATCGACTTCATCATCAGGCTTTCG | Integrated DNA Technologies; This paper | N/A |
| Ir76b_Seq_FOR: CAACGATATCCTCACGAAGAACAAGC | Integrated DNA Technologies; This paper | N/A |
| Ir25a_Seq_FOR: CGAAAGGATACAAAGGATACTGCAT | Integrated DNA Technologies; This paper | N/A |
| HACK_Seq_REV: TGTATTCCGTCGCATTTCTCTC | Integrated DNA Technologies; This paper | N/A |
| IVS-FOR: TGGGTTGGACTCAGGGAATAGATCTAAAAGGTAGGTTCAACCACT | Integrated DNA Technologies; This paper | N/A |
| EcoRI-SV40-REV: GCTTACGTCAGAATTCAGATCGATCCAGACATGATAAGA | Integrated DNA Technologies; This paper | N/A |
| Tsp42Ej_FOR: GAGAAGTCGTTTCCCATAACACCCT | Integrated DNA Technologies; This paper | N/A |
| Tsp42Ej_REV: GAGGAGCAGTTTTCGGAGTCGCCTTC | Integrated DNA Technologies; This paper | N/A |
| HCR probe sets: Ir76b, Ir40a, Ir51a, Ir60a, Ir62a, Ir76a, Ir93a, Orco (see Figure 6-Source Data 2 for sequences) | Molecular Instruments; This paper | N/A |
| Recombinant DNA | | |
| *pHACK-QF2* | Addgene; (Lin and Potter, 2016a) | Plasmid# 80274; RRID: Addgene_80274 |
| *p10XQUAS-CsChrimson-SV40* | This paper | Plasmid# 163629; RRID: Addgene_163629 |
| *pHACK-QF2$^{Orco}$* | This paper | N/A |
| *pHACK-QF2$^{Ir8a}$* | This paper | N/A |
| *pHACK-QF2$^{Ir76b}$* | This paper | N/A |
| *pHACK-QF2$^{Ir25a}$* | This paper | N/A |
| Software and Algorithms | | |
| Fiji (ImageJ) | (Schindelin et al., 2012) | https://imagej.net/Fiji |
| GraphPad Prism 8.0 | GraphPad Software | www.graphpad.com |
| AutoSpike | Syntech | http://www.ockenfels-syntech.com/products/signal-acquisition-systems-2/ |
| LabChart Pro v8 | ADInstruments | https://www.adinstruments.com/support/downloads/windows/labchart |
| Adobe Illustrator CS6 | Adobe, Inc. | https://www.adobe.com/products/illustrator.html |

| | | |
|---|---|---|
| Adobe Photoshop CS6 | Adobe, Inc. | https://www.adobe.com/products/photoshop.html |
| MacVector 16.0 | MacVector, Inc. | https://macvector.com/ |
| Zen Black | Carl Zeiss Microscopy | https://www.zeiss.com/microscopy/us/products/microscope-software/zen.html |
| Venn Diagram web tool | VIB / UGent Bioinformatics & Evolutionary Genomics | http://bioinformatics.psb.ugent.be/webtools/Venn/ |
| Amira | Thermo Fisher Scientific | https://www.thermofisher.com/us/en/home/industrial/electron-microscopy/electron-microscopy-instruments-workflow-solutions/3d-visualization-analysis-software/amira-life-sciences-biomedical.html |
| Python packages | (Schlegel et al., 2021) | https://github.com/schlegelp/navis; https://github.com/flyconnectome/fafbseg-py |
| Q-Capture Pro 7 | Teledyne QImaging | https://www.qimaging.com/home |

## Resource Availability

### *Lead Contact*

Further information and requests for resources and reagents should be directed to and will be fulfilled by the Lead Contact, Christopher J. Potter (cpotter@jhmi.edu).

### *Materials Availability*

Fly lines generated in this study have been deposited to Bloomington *Drosophila* Stock Center.

### *Data and Code Availability*

snRNAseq dataset analyzed in this paper is published in (McLaughlin et al., 2021). Sequencing reads and pre-processed sequencing data are available in the NCBI Gene Expression Omnibus

1203 (GSE162121). Python code for generating figures is publicly available on GitHub
1204 (https://github.com/colleen- mclaughlin/ORN_seq/). VM6 reconstructions using FlyWire can be
1205 viewed at https://flywire.ai/#links/Task2021a/all. All other data are available upon request.

## 1206 Experimental Model and Subject Details

### 1207 *Fly Husbandry*

1208 Fly stocks were maintained at 20 – 25°C on standard cornmeal-agar food. Male and female flies
1209 used for experiments were 3 – 11 days old, unless otherwise noted.

### 1210 *Fly Stocks*

1211 Fly lines used in this paper can be found in the Key Resources Table.
1212 Generation of *QUAS-CsChrimson*: the sequence of CsChrimson.Venus was PCR
1213 amplified from the genomic DNA of *UAS-CsChrimson.mVenus* flies (Klapoetke et al., 2014) and
1214 cloned into the *10XQUAS* vector (Addgene #163629). Fly line was established through random
1215 *P*-element insertion. Cloning was confirmed with Sanger sequencing (Genewiz) before being
1216 sent for injection (Rainbow Transgenic Flies, Inc). Primers used for PCR amplification and In-
1217 Fusion cloning:
1218 IVS-FOR:
1219 TGGGTTGGACTCAGGGAATAGATCTAAAAGGTAGGTTCAACCACT
1220 EcoRI-SV40-REV:
1221 GCTTACGTCAGAATTCAGATCGATCCAGACATGATAAGA
1222 While performing co-labeling experiments, we discovered that several *OrX-Gal4* lines
1223 label multiple glomeruli, and thus do not accurately represent single OSN classes. These lines
1224 were excluded from analyses and should be used with caution: *Or33c-Gal4* (BDSC# 9966),
1225 *Or42a-Gal4* (BDSC# 9970), *Or43b-Gal4* (BDSC# 23894), *Or59b-Gal4* (BDSC# 23897), *Or65a-*
1226 *Gal4* (BDSC# 9994), *Or85a-Gal4* (BDSC# 23133), *Or85b-Gal4* (BDSC# 23911). We also found
1227 that the following *Or35a* lines label the newly identified VM6l glomerulus in addition to VC3:

1228 *Or35a-Gal4* (BDSC# 9967), *Or35a-Gal4* (BDSC# 9968), *Or35a-mCD8.GFP* (BDSC# 52624), as
1229 well as an *Or35a-Gal4* line from the Carlson lab (Yao et al., 2005).

1230 ### *Generation of HACK Knock-in Lines*

1231 The HACK knock-in approach requires two components: a donor construct and Cas9 (Lin and
1232 Potter, 2016a). The donor includes *gRNAs* specific to the target gene, as well as the template
1233 for HDR-mediated insertion of *T2A-QF2* into the genome (Figure 2A, middle row). This template
1234 includes ~1kb homology arms directly up and downstream of the gene's stop codon flanking a
1235 cassette containing *T2A-QF2* and a *3XP3-mCherry* fluorescent eye marker (see Figure 2-Figure
1236 Supplement 1D-E and Figure 2-Figure Supplement 3A-B). Outside of these homology arms, the
1237 construct has two *RNA polymerase III U6* promoters driving independent expression of two
1238 *gRNAs* specific to the region around the target gene's stop codon (Port et al., 2014). Two
1239 *gRNAs* were used to increase the probability of successfully inducing double stranded breaks in
1240 the target (Port et al., 2014). The knock-in construct replaces the target gene's stop codon
1241 (Figure 2A, bottom row), and introduces a transcriptional stop at the end of *QF2*.

1242 The donor construct can be supplied in one of two ways (Figure 2-Figure Supplement 1).
1243 The first is to inject the HACK construct directly into embryos expressing Cas9 in their germline
1244 (direct injection method) (Figure 2-Figure Supplement 1A-B). The second approach is to
1245 establish transgenic donor lines through random *P*-element insertion or *ΦC31* integration
1246 (Bischof et al., 2007; Gloor et al., 1991; Groth et al., 2004) of the construct into the genome,
1247 followed by genetic crosses with germline Cas9 flies for generation of the knock-in (cross
1248 method)(Figure 2-Figure Supplement 1C). Only one (direct injection method) or two (cross
1249 method) generations of crosses are required for the creation of a knock-in line (Figure 2-Figure
1250 Supplement 1B-C). The HACK 3XP3-mCherry selection marker is bright but shows positional
1251 effects (Figure 2-Figure Supplement 3A). Potential knock-in flies can be screened at the adult
1252 stage (Figure 2-Figure Supplement 3A), or at the larval or pupal stages (Figure 2-Figure
1253 Supplement 1D). We generated *T2A-QF2* knock-in lines for all four co-receptor genes using the

1254 direct injection method. Additionally, we tested the feasibility of the cross approach with two
1255 genes: *Orco* and *Ir25a*. Knock-ins were confirmed by PCR genotyping and sequencing (Figure
1256 2-Figure Supplement 3B-D), and by crosses to a *QUAS-GFP* reporter to check for expression in
1257 the brain (*QUAS-mCD8::GFP* was used only to establish the *Orco-T2A-QF2* knock-in line, after
1258 which the reporter was removed via genetic crosses. For all antennal lobe analyses, we used
1259 the *10XQUAS-6XGFP* reporter line). We found no difference in expression pattern in the brain
1260 between these two approaches (Figure 2-Figure Supplement 1G). After establishing a knock-in
1261 line, the 3XP3-mCherry marker can be removed via *Cre* recombination (Siegal and Hartl, 1996).
1262 This can be useful as 3XP3-mCherry is expressed broadly throughout the fly nervous system
1263 and can interfere with red fluorescent reporters (Figure 2-Figure Supplement 1E). We produced
1264 two unmarked knock-in lines (for *Orco* and *Ir25a*) and confirmed no difference in brain GFP
1265 expression between marked and unmarked lines (Figure 2-Figure Supplement 1F).
1266 Both approaches produced knock-ins at high rates (Table 1). Efficiency was calculated
1267 as the number of potentially HACKed knock-in flies (mCherry+), divided by the total number of
1268 flies from the given cross ($G_1$ or $F_2$ progeny; see Figure 2-Figure Supplement 1A-C). We further
1269 calculated the percentage of founders producing knock-in lines, as this gives an indication of
1270 effort (how many initial crosses need to be set up to produce a knock-in). The aggregate
1271 efficiency rates for a given target locus ranged from 8% for Ir8a to 33% for Orco (Table 1);
1272 however, for individual crosses, efficiency rates were as high as 100% (see Table 1-Source
1273 Data 1), meaning that all progeny were potential mCherry+ knock-ins. For the two genes for
1274 which we created knock-in lines via both direct injection and genetic cross (*Orco* and *Ir25a*), we
1275 found efficiency rates comparable between approaches (*Orco*: 33% for direct injection, 28% for
1276 cross; *Ir25a*: 23% for direct injection, 24% for cross). For the direct injection approach, we
1277 tested 51 independent knock-in lines across the four target genes and found 100% to be
1278 correctly targeted events (Table 1). However, for the genetic cross approach, of the 32

1279 independent knock-in lines tested for the two target genes, 6 (~19%) had the HACK mCherry
1280 eye marker but did not have *QF2*-driven GFP expression in the brain.
1281 Information on plasmid construction can be found in Method Details below. All
1282 *Drosophila* embryo injections were performed by Rainbow Transgenic Flies, Inc. (Camarillo,
1283 CA). For HACKing via genetic cross, *Orco-T2A-QF2* and *Ir25a-T2A-QF2* constructs were
1284 injected into $w^{1118}$ flies for *P*-element insertion, and donor lines were established on the second
1285 or third chromosomes by crossing to double balancers (see Key Resources Table). Donor lines
1286 were then crossed to *Vas-Cas9* (BDSC# 51323). Knock-in lines were established from *cis*-
1287 chromosomal HACK (donor line on same chromosome as target gene) (Lin and Potter, 2016a).
1288 For HACKing via direct injection, knock-in constructs were injected into the following lines: *Vas-*
1289 *Cas9* (BDSC# 51324) for *Ir8a*; *Act5C-Cas9* (BDSC# 54590) for *Orco*, *Ir76b*, and *Ir25a*. The
1290 following lines were used to verify knock-in expression: *QUAS-mCD8::GFP* (BDSC# 30003),
1291 *10XQUAS-6XGFP* (BDSC# 52264). Knock-in lines were confirmed by PCR genotyping
1292 (Phusion, NEB) and Sanger sequencing (Genewiz). Unmarked *Orco-T2A-QF2* and *Ir25a-T2A-*
1293 *QF2* knock-in lines were generated by crossing mCherry+ knock-in flies to the Crey+1B fly line
1294 (see Key Resources Table) (Siegal and Hartl, 1996).
1295 To investigate the effect of *T2A-QF2* knock-in on gene function, we performed single
1296 sensillum recordings (SSR) on homozygous flies for each co-receptor knock-in (Figure 2-Figure
1297 Supplement 2), comparing their responses to *wildtype* flies to panels of Orco- and Ir-dependent
1298 odorants (Abuin et al., 2011; de Bruyne et al., 2001; Lin and Potter, 2015). In ab2 basiconic
1299 sensilla, *Orco-T2A-QF2* knock-in flies had slightly lower baseline activity as compared to
1300 *wildtype* (Figure 2-Figure Supplement 2A); however, there were no significant differences in
1301 odor-evoked activity between these two genotypes across all stimuli tested (Figure 2-Figure
1302 Supplement 2B). In ac2 coeloconic sensilla, responses of *Ir8a-T2A-QF2* knock-in flies to
1303 hexanol and cadaverine were slightly lower than *wildtype* (Figure 2-Figure Supplement 2D);
1304 however, these are not typically considered Ir8a-dependent odorants. Responses of the *Ir8a-*

1305 *T2A-QF2* knock-in to Ir8a-dependent odorants (Abuin et al., 2011) were similar to *wildtype*
1306 controls (example trace in Figure 2-Figure Supplement 2C, quantification in Figure 2-Figure
1307 Supplement 2D). Responses of *Ir76b-T2A-QF2* knock-in ac2 neurons to phenethylamine and
1308 acetic acid differed slightly from *wildtype* controls (Figure 2-Figure Supplement 2E-F). The
1309 reasons for this are unclear. The largest difference in responses between a knock-in and
1310 *wildtype* were for *Ir25a-T2A-QF2* (Figure 2-Figure Supplement 2G-H); the knock-in has
1311 significantly reduced or abolished responses to Ir25a-dependent odorants, recapitulating an
1312 *Ir25a* mutant phenotype (Abuin et al., 2011; Silbering et al., 2011). See also Figure 2-Source
1313 Data 1.

1314 ## Method Details

1315 ### *Plasmid Construction*

1316 The construction of $QF2^{X\text{-}HACK}$ knock-in plasmids requires three steps of cloning, as previously
1317 described (Lin and Potter, 2016a). All knock-in constructs were created using the *pHACK-QF2*
1318 plasmid (Addgene #80274) as the backbone. The backbone was digested with the following
1319 enzymes for cloning: *MluI* for the 5' homology arms; *SpeI* for the 3' homology arms; and *BbsI* for
1320 the gRNAs. All cloning was performed using In-Fusion Cloning (Clontech #639645). The
1321 homology arms were PCR amplified from genomic DNA extracted from *wildtype* flies using the
1322 DNeasy Blood and Tissue Kit (Qiagen #69506), while the gRNAs were PCR amplified using the
1323 *pHACK-QF2* backbone as a template, with the primers themselves containing the gRNA target
1324 sequences. All homology arms were approximately 1 kb (Orco: 5HA = 1012 bp, 3HA = 1027 bp;
1325 Ir8a: 5HA = 1027 bp, 3HA = 1079 bp; Ir76b: 5HA = 997 bp, 3HA = 956 bp; Ir25a: 5HA = 1119
1326 bp, 3HA = 990 bp). gRNAs were selected by analyzing the region around the stop codon of
1327 each gene using an online tool (https://flycrispr.org/) (Gratz et al., 2014). When possible, gRNAs
1328 were chosen to minimize potential off-target cleavage sites (zero predicted for *Orco*, *Ir8a*, and
1329 *Ir76b*; one predicted for *Ir25a*, discussed below). They were selected such that: one gRNA

1330 targeted upstream of the stop codon, within the last exon of the gene; the second gRNA
1331 targeted downstream of the stop codon, within the 3'UTR; and the two gRNAs were <100 bp
1332 apart. In order to prevent the gRNAs from targeting the homology arms, three synonymous
1333 nucleotide substitutions were made in each homology arm. The final knock-in lines did not
1334 always have all three substitutions (see Figure 2-Figure Supplement 3D), possibly due to PCR
1335 or HDR error. Note that due to the way the primers are designed, each targeted gene loses a
1336 small portion of its native 3'UTR (Orco = 72 bp, Ir8a = 31 bp, Ir76b = 27 bp, Ir25a = 24 bp).
1337 Cloning was confirmed with Sanger sequencing (Genewiz) before being sent for injection
1338 (Rainbow Transgenic Flies, Inc). Below are the gRNAs used for each gene, with the PAM
1339 sequence in parentheses.
1340
1341 Orco:
1342 CTGCACCAGCACCATAAAGT (AGG)
1343 GCACAGTGCGGAGGGGGCAA (GGG)
1344
1345 Ir8a:
1346 GTTTGTTTGTTCGGCCATGT (TGG)
1347 GGTGCCTCTGACTCCCACAG (TGG)
1348
1349 Ir76b:
1350 GCAGTGATGCGAACTTCATA (TGG)
1351 GTATTGAAAGAGGGCCGCCG (AGG)
1352
1353 Ir25a:
1354 GCCGGATACTGATTAAAGCG (CGG)
1355 ATTATGGTAAAATGAGCACT (CGG)

1356

1357 PRIMERS

1358 *Italics* = In-Fusion cloning 15 b.p. overhang; **bold** = gRNA; lowercase = adding back restriction

1359 site; <u>underline</u> = synonymous substitution to prevent Cas9 targeting of donor construct.

1360

1361 PCR Primers for Cloning:

1362 Orco_gRNA_FOR:

1363 *TCCGGGTGAACTTC***GCACAGTGCGGAGGGGGCAA**GTTTTAGAGCTAGAAATAGCAAGTTA

1364 Orco_gRNA_REV:

1365 *TTCTAGCTCTAAAAC***ACTTTATGGTGCTGGTGCAG**CGACGTTAAATTGAAAATAGGTC

1366 Orco_5HA_FOR:

1367 *CCCTTACGTAACGCG*tCAGCTTGTTTGACTTACTTGATTAC

1368 Orco_5HA_REV:

1369 *CGCGGCCCTCACGCG*tCTTGAGCTG<u>T</u>AC<u>A</u>AG<u>T</u>ACCATAAAGT

1370 Orco_3HA_FOR:

1371 *GTTATAGATCACTAG*tCTC<u>A</u>G<u>T</u>ACT<u>A</u>TGCAACCAGCAATA

1372 Orco_3HA_REV:

1373 *AATTCAGATCACTAG*tGTTTTATGAAAGCTGCAAGAAATAA

1374

1375 Ir8a_gRNA_FOR:

1376 *TCCGGGTGAACTTCG***TTTGTTTGTTCGGCCATGT**GTTTTAGAGCTAGAAATAGCAAGTTA

1377 Ir8a_gRNA_REV:

1378 *TTCTAGCTCTAAAAC***CTGTGGGAGTCAGAGGCAC**CGACGTTAAATTGAAAATAGGTC

1379 Ir8a_5HA_FOR:

1380 *CCCTTACGTAACGCG*tCTATTGGCTATTCGTCGTACTCATGC

1381 Ir8a_5HA_REV:

1382 *CGCGGCCCTCACGCG*tCTCCATGTAGCCACTATGTGAGTCAGAT

1383 Ir8a_3HA_FOR:

1384 *GTTATAGATCACTAG*tGTTTCTTGTCGCACCTAATTAACAAGTG

1385 Ir8a_3HA_REV:

1386 *AATTCAGATCACTAG*tCATACTTAAGCTCCTTGAGGTCCAGC

1387

1388 Ir76b_gRNA_FOR:

1389 *TCCGGGTGAACTTCG***CAGTGATGCGAACTTCATA**GTTTTAGAGCTAGAAATAGCAAGTTA

1390 Ir76b_gRNA_REV:

1391 *TTCTAGCTCTAAAAC***CGGCGGCCCTCTTTCAATAC**GACGTTAAATTGAAAATAGGTC

1392 Ir76b_5HA_FOR:

1393 *CCCTTACGTAACGCG*tACCAATGAATCCTTGTCCATGCTAAA

1394 Ir76b_5HA_REV:

1395 *CGCGGCCCTCACGCG*tCTCGGTGTAGCTGTCTTGAAGGAA

1396 Ir76b_3HA_FOR:

1397 *GTTATAGATCACTAG*tGCCTAATTGGAATACCTTCTACATAATGGA

1398 Ir76b_3HA_REV:

1399 *AATTCAGATCACTAG*tGGCAAGGCACAAAATAAAACGAAG

1400

1401 Ir25a_gRNA_FOR:

1402 *TCCGGGTGAACTTC***GCCGGATACTGATTAAAGCG**GTTTTAGAGCTAGAAATAGCAAGTTA

1403 Ir25a_gRNA_REV:

1404 *TTCTAGCTCTAAAAC***AGTGCTCATTTTACCATAAT**CGACGTTAAATTGAAAATAGGTC

1405 Ir25a_5HA_FOR:

1406 *CCCTTACGTAACGCG*tTGCATGACTTCATTGACACCTCAAG

1407 Ir25a_5HA_REV:

1408 *CGCGGCCCTCACGCG*tGAAACGAGGCTTAAACGTAGCTGGATATT

1409 Ir25a_3HA_FOR:

1410 *GTTATAGATCACTAG*tAATATTATGGTTAAGTGAGCTCTCGG

1411 Ir25a_3HA_REV:

1412 *AATTCAGATCACTAG*tCAAAGCTAAGTTCATCGTCATAGAGAC

1413

1414 Genotyping and Sequencing Primers (PCR fragment size):

1415 Orco_Seq_FOR (~2kb):

1416 GATGTTCTGCTCTTGGCTGATATTC

1417 Ir8a_Seq_FOR (~1.9kb):

1418 CATCGACTTCATCATCAGGCTTTCG

1419 Ir76b_Seq_FOR (~1.9kb):

1420 CAACGATATCCTCACGAAGAACAAGC

1421 Ir25a_Seq_FOR (~1.9kb):

1422 CGAAAGGATACAAAGGATACTGCAT

1423 HACK_Seq_REV (same for all):

1424 TGTATTCCGTCGCATTTCTCTC

1425 ***Checking for Off-target Effects***

1426 One of the gRNAs for *QF2*$^{Ir25a\text{-}HACK}$ had one predicted potential off-target cut site in the genome,

1427 in the *tetraspanin 42ej* (*Tsp42Ej*) gene. We sequenced this locus in the *Ir25a-T2A-QF2* knock-in

1428 line and compared the sequence to our *wildtype* lab stock. We found no evidence of indels in

1429 the knock-in line. Primers used:

1430 Tsp42Ej_FOR:

1431 GAGAAGTCGTTTCCCATAACACCCT

1432 Tsp42Ej_REV:

1433 GAGGAGCAGTTTTCGGAGTCGCCTTC

1434 ### *HACK Marker Screening*

1435 Adult flies were anaesthetized on a $CO_2$ pad and screened in one of two ways: either with a
1436 Nightsea Stereo Microscope Fluorescence Adapter with the green SFA-GR LED light source
1437 (Nightsea LLC, Lexington, MA) and viewed with a Zeiss Stemi SV6 stereo microscope; or
1438 illuminated with an X-Cite 120Q excitation light source and viewed with a Zeiss SteREO
1439 Discovery V8 microscope equipped with a ds-Red filter.

1440 ### *Whole Animal Imaging*

1441 Whole adults were anaesthetized on ice before imaging. Whole larvae, pupae, or freshly
1442 dissected adult heads were affixed to slides with clear nail polish before imaging. All animals
1443 were imaged on an Olympus SZX7 microscope equipped with GFP and RFP filters. Animals
1444 were illuminated with an X-Cite Series 120Q light source. Images were acquired using a
1445 QImaging QIClick Cooled digital CCD camera and Q-Capture Pro 7 software. Multiple images
1446 were taken at different focal planes and then merged in Photoshop (CS6). Gain was adjusted in
1447 Fiji. Images appear in the following figures/panels: Figure 2B, D, F, H; Figure 2-Figure
1448 Supplement 1D; Figure 2-Figure Supplement 3A; Figure 2-Figure Supplement 4.

1449 ### *Immunohistochemistry*

1450 All flies were used at 3- to 11-days old. Apart from the cryosection protocols and portions of the
1451 antennal whole-mount protocol, all immunostaining steps were done on a nutator. All steps
1452 involving or following the addition of fluorescently conjugated secondary antibodies were done
1453 in the dark.

1454 Brain and ventral nerve cord (VNC) staining was performed as in (Xie et al., 2018).
1455 Tissue was dissected in PBS and then fixed for 20 minutes at room temperature (RT) in 4%
1456 paraformaldehyde in PBT (1XPBS with 0.3% Triton X-100). After fixation, tissue was quickly
1457 rinsed three times with PBT, then put through three longer washes in PBT at RT (at least 15
1458 minutes each). Tissue was blocked in PBT + 5% normal goat serum (NGS) at RT for at least 30

1459 minutes, then transferred to block + primary antibody solution, and incubated at 4°C in primary
1460 antibodies for 1-2 days. Tissue was then washed three times with PBT at RT (at least 15
1461 minutes per wash) and incubated in secondary antibody solution in block at 4°C for 1 day.
1462 Tissue was washed three final times with PBT at RT for 15 minutes each, and then mounted in
1463 SlowFade gold (Thermo Fisher Scientific #S36936). For experiments in which the 10XQUAS-
1464 6XGFP or 20XUAS-6XGFP reporters were used, the endogenous, unstained GFP signal was
1465 visualized, and no secondary green antibodies were used. Primary antibodies used: mouse anti-
1466 nc82 (DSHB, 1:25), rat anti-mCD8 (Thermo Fisher #14-0081-82, 1:100 or 1:200). Secondary
1467 antibodies used: Cy3 goat anti-rat (Jackson ImmunoResearch #112-165-167, 1:200), Cy3 goat
1468 anti-mouse (Jackson ImmunoResearch #115-165-166, 1:200), Alexa 647 goat anti-rat (Jackson
1469 ImmunoResearch #112-605-167, 1:200), Alexa 647 goat anti-mouse (Jackson
1470 ImmunoResearch #115-605-166, 1:200).

1471 Whole-mount staining of maxillary palps was performed according to the brain staining
1472 protocol above, with the exception of a shorter fixation step (15 minutes). Primary antibodies
1473 used: rabbit anti-Ir25a (gift from Richard Benton, University of Lausanne, 1:100), rabbit anti-
1474 Orco (gift from Leslie Vosshall, Rockefeller University, 1:100), rat anti-elav (DSHB, 1:100).
1475 Secondary antibodies used: Cy3 goat anti-rabbit (Jackson ImmunoResearch #111-165-144,
1476 1:200), Alexa 647 goat anti-rabbit (Jackson ImmunoResearch #111-605-144, 1:200), Alexa 647
1477 goat anti-rat (Jackson ImmunoResearch #112-605-167, 1:200). For whole-mount staining of
1478 *Orco*$^{2}$ mutant palps, 3-day-old flies were used to check for Orco expression before neurons
1479 degenerate (Task and Potter, 2021).

1480 The protocol for whole-mount staining of antennae was adapted from (Karim et al., 2014;
1481 Saina and Benton, 2013; Younger et al., 2020). Fly heads were dissected into CCD buffer (50
1482 units chitinase, 1000 units chymotrypsin (25 mg of 40 units/mg), 10 mL HEPES larval buffer
1483 (119 mM NaCl, 48 mM KCl, 2 mM $CaCl_2$, 2 mM $MgCl_2$, 25 mM HEPES), 100 µl DMSO) on ice,
1484 then warmed on a 37°C heat block for 10 min. Heads were incubated in CCD buffer at 37°C

1485 while rotating for 1 hour 20 minutes. Antennae were subsequently dissected off heads into
1486 fixative solution (4% PFA in PBT). All subsequent steps were done without rotation to prevent
1487 antennae from sticking to the walls or lids of the tubes. Antennae were fixed at room
1488 temperature for 40 min, then washed with PBT three times at room temperature, at least 15
1489 minutes each time, and blocked in PBT plus 5% NGS for at least 1 hour at room temperature.
1490 Antennae were incubated in primary antibodies in blocking solution at 4°C for four days, washed
1491 three times for 15 minutes each at room temperature, and incubated in secondary antibody
1492 solution at 4°C for three days. Antennae were then washed three times for 15 minutes each
1493 time at room temperature and mounted in SlowFade Gold. Primary antibody: rabbit anti-Orco
1494 (gift from Leslie Vosshall, 1:100); secondary antibody: Cy3 goat anti-rabbit (Jackson
1495 ImmunoResearch #111-165-144, 1:200). The endogenous GFP signal was visualized.
1496 The cryosection protocol was adapted from (Spletter et al., 2007). Fly heads were
1497 dissected and lined up in cryomolds (Tissue-Tek #4565), covered with OCT compound (Tissue-
1498 Tek #4583), and frozen at -80°C. Samples were sectioned at ~12 μm on a Microm HM 500
1499 cryostat (Microm International GmbH, Walldorf, Germany) and collected on SuperFrost Plus
1500 slides (Fisher #12-550-15). Slides were stored at -80°C until further processing. Slides were
1501 fixed at RT for 15 minutes in 4% paraformaldehyde in PBT (1XPBS with 0.3% Triton X-100),
1502 washed three times in PBT at RT (15 minutes each), blocked at RT for at least 30 minutes in
1503 PBT + 2.5% NGS + 2.5% normal donkey serum (NDS), then incubated overnight at 4°C in
1504 primary antibodies in fresh block solution in a special humidified chamber. On the next day,
1505 slides were washed three times (15 minutes each) with PBT at RT, and then incubated in
1506 secondary antibodies in block at 4°C overnight in the same humidified chamber covered in foil.
1507 Finally, slides were washed three times (15 minutes each) with PBT at RT. DAPI (1:10,000) was
1508 included in the first wash as a nuclear counterstain. After washes, slides were mounted in
1509 SlowFade gold (Thermo Fisher Scientific #S36936). Primary antibody used: guinea pig anti-Ir8a

1510 (gift from Richard Benton, University of Lausanne, 1:1,000). Secondary antibody used: Cy3
1511 donkey anti-guinea pig (Jackson ImmunoResearch #706-165-148, 1:200).
1512 For sacculus staining, 7-10 day old flies were placed in an alignment collar. Their heads
1513 were encased in OCT (Tissue-Plus Fisher) in a silicone mold, frozen on dry ice, and snapped
1514 off. The head blocks were stored in centrifuge tubes at -80°C. A Leica cryostat was used to
1515 collect 20 µm sections of antennae. Immunohistochemical staining was carried out by fixing
1516 tissue in 4% paraformaldehyde for 10 minutes, followed by three 5 minute washes in 1XPBS.
1517 Tissue was washed in 1XPBS containing 0.2% Triton-X (PBST) for 30 minutes to permeabilize
1518 the cuticle. Lastly, tissue was washed in PBST containing 1% Bovine Serum Albumin (BSA) to
1519 block non-specific antibody binding. Primary antibody solution was made in PBST+1%BSA, 200
1520 µl was pipetted onto each slide under bridged coverslips, and slides were placed at 4°C
1521 overnight to incubate. The following day, primary antibody was removed, and slides were
1522 washed three times for 10 minutes each in PBST. Secondary antibody solution was made in
1523 PBST+1%BSA, 200uL was pipetted onto each slide under bridged coverslips, and left at room
1524 temperature in a dark box to incubate for 2 hours. After the 2 hour incubation, slides were
1525 washed three times for 5 minutes each in PBST. After the last wash, the slides were allowed to
1526 dry in the dark staining box for ~30 minutes before being mounted in Vectashield, coverslipped,
1527 and stored at 4°C. Primary antibodies: rabbit anti-Ir25a (gift from Richard Benton, University of
1528 Lausanne, 1:100), guinea pig anti-Ir8a (gift from Richard Benton, University of Lausanne,
1529 1:100), rabbit anti-Ir64a (gift from Greg Suh, NYU/KAIST, 1:100). Secondary antibodies:
1530 Jackson Immuno Cy3 conjugated AffiniPure 568 goat anti-rabbit (111-165-144), 1:500;
1531 AlexaFluor 568 goat anti-guinea pig (A11075), 1:500.

1532 ***In situ HCR***

1533 Cryosectioning for antennal *in situs* was performed as described above. The HCR protocol was
1534 adapted from Molecular Instruments HCR v3.0 protocol for fresh frozen or fixed frozen tissue
1535 sections (Choi et al., 2018). Slides were fixed in ice-cold 4% PFA in PBT for 15 minutes at 4°C,

1536 dehydrated in an ethanol series (50% EtOH, 70% EtOH, 100% EtOH, 100% EtOH, 5 minutes
1537 each step), and air dried for 5 minutes at RT. Slides were then incubated in proteinase K
1538 solution in a humidified chamber for 10 minutes at 37°C, rinsed twice with PBS and dried, then
1539 pre-hybridized for 10 minutes at 37°C in a humidified chamber. Slides were incubated in probe
1540 solution (0.4 pmol Ir76b probe) overnight in the 37°C humidified chamber. On day two, slides
1541 were washed with a probe wash buffer/SSCT series (75% buffer/25% SSCT, 50% buffer/50%
1542 SSCT, 25% buffer/75% SSCT, 100% SSCT, 15 minutes each) at 37°C, then washed for 5 min
1543 at RT with SSCT and dried. Slides were pre-amplified for 30 min at RT in the humidified
1544 chamber while hairpins were snap cooled (6 pmol concentration). Slides were incubated in fresh
1545 amplification buffer with hairpins overnight in a dark humidified chamber at RT. On day three,
1546 slides were rinsed in SSCT at RT (2 x 30 minutes, 1 x 10 minutes with 1:10,000 DAPI, 1 x 5
1547 minutes) and mounted in SlowFade Diamond (Thermo Fisher S36972). For the overnight steps,
1548 slides were covered with HybriSlips (Electron Microscopy Sciences 70329-62) to prevent
1549 solution evaporation.

1550 The whole-mount palp *in situ* protocol was adapted from a combination of (Prieto-Godino
1551 et al., 2020; Saina and Benton, 2013; Younger et al., 2020) and the *Drosophila* whole-mount
1552 embryo protocol from Molecular Instruments (Choi et al., 2016). All steps after dissection were
1553 performed while rotating unless otherwise noted. Fly mouthparts (palps and proboscises) were
1554 dissected into CCD buffer (same as for whole-mount IHC on antennae above), incubated for 20
1555 minutes in CCD at 37°C (5 minutes on heat block, 15 minutes rotating), then pre-fixed in 4%
1556 PFA in PBT for 20 minutes at RT. Tissue was washed with 0.1% PBS-Tween on ice (4 x 5
1557 minutes), incubated for 1 hour at RT in 80% methanol/20% DMSO, and washed for 10 minutes
1558 in PBS-Tween at RT. Tissue was then incubated in Proteinase K solution (1:1,000) in PBS-
1559 Tween at RT for 30 minutes, then washed in PBS-Tween at RT (2 x 10 minutes) and post-fixed
1560 in 4% PFA in PBS-Tween at RT for 20 minutes. After post-fixation, tissue was washed in PBS-
1561 Tween at RT (3 x 15 minutes), then pre-hybridized in pre-heated probe hybridization buffer at

1562 37°C for 30 minutes. Tissue was incubated in probe solution (2 – 4 pmol in hybridization buffer)
1563 at 37°C for two nights. On day three, tissue was washed in pre-heated probe wash buffer at
1564 37°C (5 x 10 minutes), then washed in SSCT (1XSSC plus 1% Tween) at RT (2 x 5 minutes).
1565 Tissue was pre-amplified with RT-equilibrated amplification buffer at RT for 10 minutes, then
1566 incubated in hairpin mixture (6 pmol snap-cooled hairpins in amplification buffer) in the dark at
1567 RT overnight. On day four, tissue was washed at RT with SSCT (2 x 5 minutes, 2 x 30 minutes,
1568 1 x 5 minutes), then mounted in SlowFade Diamond (Thermo Fisher S36972). Sequences for all
1569 *in situ* probes can be found in Figure 6-Source Data 2. Example images for palp *in situs* can be
1570 found in Figure 6-Figure Supplement 2.

1571 ***Confocal Imaging and Analysis***

1572 Brains, ventral nerve cords, maxillary palps, and antennal cryosections were imaged on a Zeiss
1573 LSM 700 confocal microscope equipped with Fluar 10x/0.50 air M27, LCI Plan-Neofluar 25x/0.8
1574 water Korr DIC M27, and C-Apochromat 63x/1.2 water Korr M27 objectives. Images were
1575 acquired at 512 x 512-pixel resolution with 0.58, 2.37 or 6.54 µm z-steps for each objective,
1576 respectively. For illustration purposes, confocal images were processed in Fiji/ImageJ to
1577 collapse Z-stacks into a single image using maximum intensity projection. Where noted, single
1578 slices or partial z projections were used as opposed to full stacks. For co-labeling experiments,
1579 Fiji was used to convert red LUTs to orange for a colorblind-friendly palette. Similarly, in Figure
1580 2-Figure Supplement 1E, Fiji was used to convert magenta LUT to blue for clarity. For Figure
1581 4B, Fiji was used to convert the two-channel maximum intensity projection to a grey LUT, and
1582 the cell-counting plug-in was used in separate channels to identify single- and double-labeled
1583 cells. Fiji was also used to adjust the gain in separate channels in all figures/images; no other
1584 image processing was performed on the confocal data. For Figure 7A, glomeruli were assigned
1585 to the categories strong, intermediate, and weak by visual inspection of the strength of their
1586 innervation compared to the previously reported glomeruli for each respective knock-in line.

1587 Strong glomeruli generally have similar brightness/intensity of GFP signal as most of the
1588 originally reported glomeruli for the given knock-in line.
1589 For sacculus staining (Figure 5C-E), slides were imaged on a Nikon A1R confocal
1590 microscope in the UConn Advanced Light Microscopy Facility with a 40X oil immersion objective
1591 at 1024 x 1024-pixel resolution. Stacks of images (0.5 µm z-step size) were gathered and
1592 analyzed with ImageJ/Fiji software. Image processing was performed as described above.
1593 Magnification used:
1594 10X: Figure 1D (Brain), Figure 2-Figure Supplement 1E
1595 25X: Figure 2-Figure Supplement 1F-G, Figure 3-Figure Supplement 1A-B
1596 40X: Figure 5C-E
1597 63X: Figure 2C, E, G, I; Figure 3A-D, Figure 4B-C, Figure 5A-B, Figure 2-Figure Supplement
1598 3E-H, Figure 3-Figure Supplement 2A-E, Figure 5-Figure Supplement 1, Figure 6-Figure
1599 Supplement 2

1600 ***Basiconic Single Sensillum Recordings***

1601 Flies were immobilized and visualized as previously described (Lin and Potter, 2015). Basiconic
1602 sensilla were identified either using fluorescent-guided SSR (for ab3 sensilla) or using reference
1603 odorants (for ab2 and pb1-3 sensilla) (de Bruyne et al., 1999; Lin and Potter, 2015). The glass
1604 recording electrode was filled with Beadle-Ephrussi Ringer's solution (7.5g of NaCl + 0.35g of
1605 KCl + 0.279g of $CaCl_2$-$2H_2O$ in 1L $H_2O$). Extracellular activity was recorded by inserting the
1606 glass electrode into the shaft or base of the sensillum of 3- to 10-day-old flies (unless otherwise
1607 specified in the young *Orco*$^2$ mutant experiments). A tungsten reference electrode was inserted
1608 into the fly eye. Signals were amplified 100X (USB-IDAC System; Syntech, Hilversum, the
1609 Netherlands), input into a computer via a 16-bit analog-digital converter and analyzed off-line
1610 with AUTOSPIKE software (USB-IDAC System; Syntech). The low cutoff filter setting was 50
1611 Hz, and the high cutoff was 5 kHz. Stimuli consisted of 1000 ms air pulses passed over odorant
1612 sources. The Δ spikes/second was calculated by counting the spikes in a 1000 ms window from

1613 ~500 ms after odorant stimuli were triggered, subtracting the spikes in a 1000 ms window prior
1614 to each stimulation. For ab3 recordings from *wildtype*, *Orco*$^{2}$ mutant, and *Ir25a*$^{2}$ mutant flies,
1615 spikes were counted in a 500 ms window from the start of the response and multiplied by 2.
1616 Then, the spikes in the 1000 ms window prior to stimulation was subtracted from this to
1617 calculate the Δ spikes/second. Stimuli used: mineral oil (Sigma CAS #8042-47-5), ethyl acetate
1618 (Sigma CAS #141-78-6), pentyl acetate (Sigma CAS #628-63-7), benzaldehyde (Sigma CAS
1619 #100-52-7), ethyl butyrate (Sigma CAS #105-54-4), hexanol (Sigma CAS #111-27-3), e2-
1620 hexenal (Sigma CAS #6728-26-3), geranyl acetate (Sigma CAS # 105-87-3), 2-heptanone
1621 (Sigma CAS # 110-43-0), 1-octen-3-ol (Sigma CAS #3391-86-4), 2,3-butanedione (Sigma CAS
1622 #431-03-8), phenylacetaldehyde (Sigma CAS # 122-78-1), phenethylamine (Sigma CAS # 64-
1623 04-0), propionic acid (Sigma CAS #79-09-4), 1,4-diaminobutane (Sigma CAS #110-60-1),
1624 pyrrolidine (Sigma CAS #123-75-1), p-cresol (Sigma CAS #106-44-5), and methyl salicylate
1625 (Sigma CAS #119-36-8). Odorants were dissolved in mineral oil at a concentration of 1%, and
1626 20 µl of solution was pipetted onto filter paper in a glass Pasteur pipette. Stimuli were delivered
1627 by placing the tip of the Pasteur pipette through a hole in a plastic pipette (Denville Scientific
1628 Inc, 10ml pipette) that carried a purified continuous air stream (8.3 ml/s) directed at the antenna
1629 or maxillary palp. A solenoid valve (Syntech) diverted delivery of a 1000 ms pulse of charcoal-
1630 filtered air (5 ml/s) to the Pasteur pipette containing the odorant dissolved on filter paper. Fresh
1631 odorant pipettes were used for no more than 5 odorant presentations. *Ir25a*$^{2}$ and *Orco*$^{2}$ mutant
1632 fly lines were outcrossed into the *w*$^{1118}$ *wildtype* genetic background. Full genotypes for ab3
1633 fgSSR were: *Pin/CyO;Or22a-Gal4,15XUAS-IVS-mcd8GFP/TM6B* (*wildtype*), *Ir25a*$^{2}$;*Or22a-*
1634 *Gal4,15XUAS-IVS-mcd8GFP/TM6B* (*Ir25a*$^{2}$ *mutant*), *Or22a-Gal4/10XUAS-IVS-mcd8GFP*
1635 *(attp40);Orco*$^{2}$ (*Orco*$^{2}$ *mutant*). These stocks were made from the following Bloomington Stocks
1636 (outcrossed to the Potter lab *w*$^{1118}$ genetic background): BDSC# 9951, 9952, 23130, 32186,
1637 32193, 41737.

1638 ### *Coeloconic Single Sensillum Recordings*

1639 Coeloconic SSR was performed similarly as for basiconic sensilla. 3-5-day old female flies were
1640 wedged in the tip of a 200 µl pipette, with the antennae and half the head exposed. A tapered
1641 glass electrode was used to stabilize the antenna against a coverslip. A BX51WI microscope
1642 (Olympus) was used to visualize the prep, which was kept under a 2,000mL/min humidified and
1643 purified air stream. A borosilicate glass electrode was filled with sensillum recording solution
1644 (Kaissling and Thorson, 1980) and inserted into the eye as a reference electrode. An
1645 aluminosilicate glass electrode was filled with the same recording solution and inserted into
1646 individual sensilla. Different classes of coeloconic sensilla were identified by their known
1647 location on the antenna and confirmed with their responses to a small panel of diagnostic odors.
1648 No more than 4 sensilla per fly were recorded. Each sensillum was tested with multiple
1649 odorants, with a rest time of at least 10s between applications. The odorants used were acetic
1650 acid (Fisher, 1%, CAS# 64-19-7), ammonium hydroxide (Fisher, 0.1%, CAS# 7664-41-7),
1651 cadaverine (Sigma-Aldrich, 1%, CAS# 462-94-2), hexanol (ACROS Organics, 0.001%, CAS#
1652 111-27-3), 2,3-butanedione (ACROS Organics, 1%, CAS# 431-03-8), phenethylamine (ACROS
1653 Organics, 1%, CAS# 64-04-0), propanal (ACROS Organics, 1%, CAS# 123-38-6), and 1,4-
1654 diaminobutane (ACROS Organics, 1%, CAS# 110-60-1). Odorants were diluted in water or
1655 paraffin oil. Odorant cartridges were made by placing a 13 mm antibiotic assay disc (Whatman)
1656 into a Pasteur pipette, pipetting 50 µl odorant onto the disc, and closing the end with a 1 mL
1657 plastic pipette tip. Each odorant cartridge was used a maximum of four times. The tip of the
1658 cartridge was inserted into a hole in the main airflow tube, and odorants were applied at
1659 500mL/min for 500ms. Delivery was controlled via LabChart Pro v8 software (ADInstruments),
1660 which directed the opening and closing of a Lee valve (02-21-08i) linked to a ValveBank 4
1661 controller (AutoMate Scientific). Extracellular action potentials were collected with an EXT-02F
1662 amplifier (NPI) with a custom 10X head stage. Data were acquired and AC filtered (300-1,700
1663 Hz) at 10kHz with a PowerLab 4/35 digitizer and LabChart Pro v8 software. Spikes were

1664 summed in coeloconic recordings due to their similar sizes, and they were counted over a 500
1665 ms window, starting at 100 ms after stimulus onset.

1666 ### *Optogenetics*

1667 *Ir25a-T2A-QF2* was crossed to *QUAS-CsChrimson* #11C and double balanced to establish a
1668 stable stock (*Ir25a-T2A-QF2*/*CyO; QUAS-CsChrimson* #11C/*TM6B)*. Newly eclosed flies (age <
1669 1 day old) were transferred to fly vials containing 0.4 mM all trans-retinal in fly food (Sigma-
1670 Aldrich #R2500, dissolved in pure DMSO with stock concentration of 0.4 M). Vials with flies
1671 were kept in the dark for at least 4 days before experiments. 627nm LED light source (1-up LED
1672 Lighting Kit, PART #: ALK-1UP-EH-KIT) powered by an Arduino Uno
1673 (www.arduino.cc/en/Main/ArduinoBoardUno) was used to activate CsChrimson. By setting the
1674 voltage to 2V and the distance of the light source to 20 cm between the LED and the fly
1675 antenna, the light intensity was equivalent to 1.13 $W/m^2$. The antenna was stimulated for 500
1676 ms followed by 5 s of recovery period for the total recording length of 20 s (3 stimulations). The
1677 identity of ab2 and ab3 sensilla were first verified with 1% ethyl acetate (Sigma #270989) and
1678 1% pentyl acetate (Sigma #109584) before optogenetic experiments. Identification of ab9
1679 sensilla was assisted by fluorescence-guided Single Sensillum Recording (fgSSR) (Lin and
1680 Potter, 2015) using *Or67b-Gal4* (BDSC #9995) recombined with *15XUAS-IVS-mCD8::GFP*
1681 (BDSC #32193). The Δ spikes/second was calculated as for other basiconic SSR recordings.

1682 ### *Single-nucleus RNA-sequencing Analyses*

1683 Dataset analyzed in this paper was published in (McLaughlin et al., 2021). The expression
1684 levels for the *Ir co-receptors* across all OSNs were lower than for *Orco*, even for their
1685 corresponding 'canonical' glomeruli. To account for these differences and facilitate
1686 comparisons, we performed within-gene normalization in Figure 4-Source Data 1 and used the
1687 normalized values to generate the AL maps in Figure 4A. The normalization was performed as
1688 follows: first, we determined the fraction of cells within each cluster expressing the given co-

1689 receptor (read Counts Per Million, CPM threshold ≥3). The cluster with the highest fraction value
1690 was taken as the maximum. Then, the fraction for each cluster was divided by this maximum
1691 value. The normalized value shows the relative strength of expression within each cluster for the
1692 given co-receptor gene.

1693 ### *EM Neuron Reconstruction*

1694 VM6 OSNs (Figures 5F-G) were reconstructed in the FAFB EM volume (Zheng et al., 2018)
1695 using FlyWire (https://flywire.ai/) (Dorkenwald et al., 2020). Initial candidates were selected
1696 based on either being upstream of the VM6 (previously called VC5 in Bates et al., 2020)
1697 projection neurons or based on co-fasciculation with already identified VM6 OSNs. Analyses
1698 were performed in Python using the open-source packages *navis*
1699 (https://github.com/schlegelp/navis) and *fafbseq* (https://github.com/flyconnectome/fafbseg-py).
1700 OSNs were clustered using FAFB synapse predictions (Buhmann et al., 2021) for a synapse-
1701 based NBLAST ("syNBLAST", implemented in *navis*). The reconstructions can be viewed at
1702 https://flywire.ai/#links/Task2021a/all.

1703 ## Quantification and Statistical Analysis

1704 ### *Cell Counting*

1705 To quantify knock-in co-expression with the corresponding antibodies (Figure 2), the 3D
1706 reconstruction software Amira (FEI, Oregon, USA) was used to manually mark individual cell
1707 bodies throughout the z-stack in each channel (antibody in far red channel, knock-in in green
1708 channel), and the cell markers between channels were compared.

1709 For sacculus cell counts (Figure 5C-E), cells were counted within ImageJ/Fiji using the
1710 cell counter tool. Counts were done manually by going through each stack within an image and
1711 using different colored markers for each cell type. Cell count data was gathered into an Excel
1712 spreadsheet, and analyzed for percent colocalization with n=9 antennal sections.

1713 ### *Statistics*

1714 Statistical analyses on SSR recordings were done in GraphPad Prism (version 8), except for
1715 optogenetic experiments, which were analyzed in Microsoft Excel. Box plots were made using
1716 GraphPad Prism; bar graphs were made in Excel. For all analyses, significance level $\alpha = 0.05$.
1717 The following analyses were performed on all SSR data (excluding optogenetics): within
1718 genotype, Kruskal-Wallis test with uncorrected Dunn's to determine which odorant responses
1719 were significantly different from mineral oil or paraffin oil control; between genotype, Mann-
1720 Whitney *U* to compare responses of two genotypes to the same odorant (e.g. *wildtype* vs *Ir25a*$^2$
1721 mutant, or *wildtype* versus *Orco-T2A-QF2* knock-in). Summary tables in Figure 6 are filled in
1722 based on the following criteria: no response means neither *wildtype* nor *Ir25a*$^2$ mutant odor-
1723 evoked activity for given odorant was significantly different from its respective mineral oil control,
1724 nor was the difference between the genotypes statistically significant; no difference means that
1725 either *wildtype* or mutant or both had a significantly different odor-evoked response to the
1726 stimulus compared to mineral oil control, but the difference between the two genotypes was not
1727 statistically significant; higher response (in either *wildtype* or mutant) means that there was a
1728 statistically significant difference between genotypes for the given odorant. This could mean
1729 that: a) one genotype did not have a response, while the other did; b) both genotypes had a
1730 response, and one was higher; c) responses are different from each other, but not from their
1731 respective mineral oil controls; or d) neural activity was inhibited by the odorant in one genotype
1732 compared to mineral oil control, and either not inhibited in the other genotype or inhibited to a
1733 lesser degree. Non-parametric tests were chosen due to small sample sizes and/or data that
1734 were not normally distributed.

1735 In Figure 6I, stimulus responses which were statistically significantly different from
1736 mineral oil control were those whose Δ spike values were zero, due to the fact that the mineral
1737 oil control Δ spike value was non-zero (median = 1.2, range = 0 to 2). Because of this, we did

1738 not deem these differences as biologically relevant. Nevertheless, *p* values are reported in the

1739 figure legend of Figure 6, and detailed information can be found in Figure 6-Source Data 1.

1740

# References


Abuin, L., Bargeton, B., Ulbrich, M.H., Isacoff, E.Y., Kellenberger, S., and Benton, R. (2011). Functional architecture of olfactory ionotropic glutamate receptors. Neuron *69*, 44-60.

Abuin, L., Prieto-Godino, L.L., Pan, H., Gutierrez, C., Huang, L., Jin, R., and Benton, R. (2019). In vivo assembly and trafficking of olfactory Ionotropic Receptors. BMC Biol *17*, 34.

Ache, B.W., and Young, J.M. (2005). Olfaction: diverse species, conserved principles. Neuron *48*, 417-430.

Ai, M., Blais, S., Park, J.Y., Min, S., Neubert, T.A., and Suh, G.S. (2013). Ionotropic glutamate receptors IR64a and IR8a form a functional odorant receptor complex in vivo in *Drosophila*. J Neurosci *33*, 10741-10749.

Ai, M., Min, S., Grosjean, Y., Leblanc, C., Bell, R., Benton, R., and Suh, G.S. (2010). Acid sensing by the *Drosophila* olfactory system. Nature *468*, 691-695.

Auer, T.O., Khallaf, M.A., Silbering, A.F., Zappia, G., Ellis, K., Alvarez-Ocana, R., Arguello, J.R., Hansson, B.S., Jefferis, G., Caron, S.J.C*., et al.* (2020). Olfactory receptor and circuit evolution promote host specialization. Nature *579*, 402-408.

Awasaki, T., Huang, Y., O'Connor, M.B., and Lee, T. (2011). Glia instruct developmental neuronal remodeling through TGF-β signaling. Nat Neurosci *14*, 821-823.

Baena-Lopez, L.A., Alexandre, C., Mitchell, A., Pasakarnis, L., and Vincent, J.P. (2013). Accelerated homologous recombination and subsequent genome modification in *Drosophila*. Development *140*, 4818-4825.

Bates, A.S., Schlegel, P., Roberts, R.J.V., Drummond, N., Tamimi, I.F.M., Turnbull, R., Zhao, X., Marin, E.C., Popovici, P.D., Dhawan, S*., et al.* (2020). Complete Connectomic Reconstruction of Olfactory Projection Neurons in the Fly Brain. Curr Biol *30*, 3183-3199.e3186.

Benton, R., Sachse, S., Michnick, S.W., and Vosshall, L.B. (2006). Atypical membrane topology and heteromeric function of *Drosophila* odorant receptors in vivo. PLoS Biol *4*, e20.

Benton, R., Vannice, K.S., Gomez-Diaz, C., and Vosshall, L.B. (2009). Variant ionotropic glutamate receptors as chemosensory receptors in *Drosophila*. Cell *136*, 149-162.

Berck, M.E., Khandelwal, A., Claus, L., Hernandez-Nunez, L., Si, G., Tabone, C.J., Li, F., Truman, J.W., Fetter, R.D., Louis, M*., et al.* (2016). The wiring diagram of a glomerular olfactory system. eLife *5*.

Bhalerao, S., Sen, A., Stocker, R., and Rodrigues, V. (2003). Olfactory neurons expressing identified receptor genes project to subsets of glomeruli within the antennal lobe of *Drosophila melanogaster*. J Neurobiol *54*, 577-592.

Bischof, J., Maeda, R.K., Hediger, M., Karch, F., and Basler, K. (2007). An optimized transgenesis system for *Drosophila* using germ-line-specific *phiC31* integrases. PNAS *104*, 3312-3317.

Bosch, J.A., Knight, S., Kanca, O., Zirin, J., Yang-Zhou, D., Hu, Y., Rodiger, J., Amador, G., Bellen, H.J., Perrimon, N*., et al.* (2020). Use of the CRISPR-Cas9 System in *Drosophila* Cultured Cells to Introduce Fluorescent Tags into Endogenous Genes. Curr Protoc Mol Biol *130*, e112.

Brand, A.H., and Perrimon, N. (1993). Targeted gene expression as a means of altering cell fates and generating dominant phenotypes. Development *118*, 401-415.

Budelli, G., Ni, L., Berciu, C., van Giesen, L., Knecht, Z.A., Chang, E.C., Kaminski, B., Silbering, A.F., Samuel, A., Klein, M*., et al.* (2019). Ionotropic Receptors Specify the Morphogenesis of Phasic Sensors Controlling Rapid Thermal Preference in *Drosophila*. Neuron *101*, 738-747 e733.

1783 Buhmann, J., Sheridan, A., Malin-Mayor, C., Schlegel, P., Gerhard, S., Kazimiers, T., Krause, R., Nguyen,
1784 T.M., Heinrich, L., Lee, W.-C.A.*, et al.* (2021). Automatic detection of synaptic partners in a whole-brain
1785 *Drosophila* electron microscopy data set. Nat Methods *18*, 771-774.

1786 Butterwick, J.A., Del Marmol, J., Kim, K.H., Kahlson, M.A., Rogow, J.A., Walz, T., and Ruta, V. (2018).
1787 Cryo-EM structure of the insect olfactory receptor Orco. Nature *560*, 447-452.

1788 Carey, A.F., and Carlson, J.R. (2011). Insect olfaction from model systems to disease control. PNAS *108*,
1789 12987-12995.

1790 Chai, P.C., Cruchet, S., Wigger, L., and Benton, R. (2019). Sensory neuron lineage mapping and
1791 manipulation in the *Drosophila* olfactory system. Nat Commun *10*, 643.

1792 Chen, C., Buhl, E., Xu, M., Croset, V., Rees, J.S., Lilley, K.S., Benton, R., Hodge, J.J., and Stanewsky, R.
1793 (2015). *Drosophila* Ionotropic Receptor 25a mediates circadian clock resetting by temperature. Nature
1794 *527*, 516-520.

1795 Chen, H.-M., Yao, X., Ren, Q., Chang, C.-C., Liu, L.-Y., Miyares, R.L., and Lee, T. (2020). Enhanced Golic+:
1796 highly effective CRISPR gene targeting and transgene HACKing in *Drosophila*. Development *147*.

1797 Chen, Y., and Amrein, H. (2017). Ionotropic Receptors Mediate *Drosophila* Oviposition Preference
1798 Through Sour Gustatory Receptor Neurons. Curr Biol *27*, 2741-2750 e2744.

1799 Chen, Y.D., and Dahanukar, A. (2017). Molecular and Cellular Organization of Taste Neurons in Adult
1800 *Drosophila* Pharynx. Cell Rep *21*, 2978-2991.

1801 Choi, H.M.T., Calvert, C.R., Husain, N., Huss, D., Barsi, J.C., Deverman, B.E., Hunter, R.C., Kato, M., Lee,
1802 S.M., Abelin, A.C.T.*, et al.* (2016). Mapping a multiplexed zoo of mRNA expression. Development *143*,
1803 3632-3637.

1804 Choi, H.M.T., Schwarzkopf, M., Fornace, M.E., Acharya, A., Artavanis, G., Stegmaier, J., Cunha, A., and
1805 Pierce, N.A. (2018). Third-generation in situ hybridization chain reaction: multiplexed, quantitative,
1806 sensitive, versatile, robust. Development *145*.

1807 Clyne, P.J., Warr, C.G., Freeman, M.R., Lessing, D., Kim, J., and Carlson, J.R. (1999). A novel family of
1808 divergent seven-transmembrane proteins: candidate odorant receptors in Drosophila. Neuron *22*,
1809 327-338.

1810 Couto, A., Alenius, M., and Dickson, B.J. (2005). Molecular, anatomical, and functional organization of
1811 the *Drosophila* olfactory system. Curr Biol *15*, 1535-1547.

1812 Croset, V., Rytz, R., Cummins, S.F., Budd, A., Brawand, D., Kaessmann, H., Gibson, T.J., and Benton, R.
1813 (2010). Ancient protostome origin of chemosensory ionotropic glutamate receptors and the evolution
1814 of insect taste and olfaction. PLoS Genet *6*, e1001064.

1815 de Bruyne, M., Clyne, P.J., and Carlson, J.R. (1999). Odor Coding in a Model Olfactory Organ: The
1816 *Drosophila* Maxillary Palp. J Neurosci *19*, 4520-4532.

1817 de Bruyne, M., Foster, K., and Carlson, J.R. (2001). Odor Coding in the *Drosophila* Antenna. Neuron *30*,
1818 537-552.

1819 DeGennaro, M., McBride, C.S., Seeholzer, L., Nakagawa, T., Dennis, E.J., Goldman, C., Jasinskiene, N.,
1820 James, A.A., and Vosshall, L.B. (2013). orco mutant mosquitoes lose strong preference for humans and
1821 are not repelled by volatile DEET. Nature *498*, 487-491.

1822 Depetris-Chauvin, A., Galagovsky, D., and Grosjean, Y. (2015). Chemicals and chemoreceptors:
1823 ecologically relevant signals driving behavior in *Drosophila*. Front Ecol Evol *3*, 41.

1824 Diao, F., Ironfield, H., Luan, H., Diao, F., Shropshire, W.C., Ewer, J., Marr, E., Potter, C.J., Landgraf, M.,
1825 and White, B.H. (2015). Plug-and-play genetic access to *Drosophila* cell types using exchangeable exon
1826 cassettes. Cell Rep *10*, 1410-1421.

1827 Diao, F., and White, B.H. (2012). A novel approach for directing transgene expression in *Drosophila*: T2A-
1828 Gal4 in-frame fusion. Genetics *190*, 1139-1144.

1829 Dorkenwald, S., McKellar, C., Macrina, T., Kemnitz, N., Lee, K., Lu, R., Wu, J., Popovych, S., Mitchell, E.,
1830 Nehoran, B.*, et al.* (2020). FlyWire: Online community for whole-brain connectomics. bioRxiv,
1831 2020.2008.2030.274225.

1832 Du, L., Zhou, A., Sohr, A., and Roy, S. (2018). An Efficient Strategy for Generating Tissue-specific Binary
1833 Transcription Systems in *Drosophila* by Genome Editing. J Vis Exp.

1834 Dunipace, L., Meister, S., McNealy, C., and Amrein, H. (2001). Spatially restricted expression of candidate
1835 taste receptors in the *Drosophila* gustatory system. Curr Biol *11*, 822-835.

1836 Dweck, H.K.M., Ebrahim, S.A.M., Thoma, M., Mohamed, A.A.M., Keesey, I.W., Trona, F., Lavista-Llanos,
1837 S., Svatoš, A., Sachse, S., Knaden, M.*, et al.* (2015). Pheromones mediating copulation and attraction in
1838 *Drosophila*. PNAS *112*, E2829-E2835.

1839 Endo, K., Aoki, T., Yoda, Y., Kimura, K.-i., and Hama, C. (2007). Notch signal organizes the *Drosophila*
1840 olfactory circuitry by diversifying the sensory neuronal lineages. Nat Neurosci *10*, 153-160.

1841 Enjin, A., Zaharieva, E.E., Frank, D.D., Mansourian, S., Suh, G.S., Gallio, M., and Stensmyr, M.C. (2016).
1842 Humidity Sensing in *Drosophila*. Curr Biol *26*, 1352-1358.

1843 Fandino, R.A., Haverkamp, A., Bisch-Knaden, S., Zhang, J., Bucks, S., Nguyen, T.A.T., Schroder, K.,
1844 Werckenthin, A., Rybak, J., Stengl, M.*, et al.* (2019). Mutagenesis of odorant coreceptor Orco fully
1845 disrupts foraging but not oviposition behaviors in the hawkmoth *Manduca sexta*. PNAS *116*, 15677-
1846 15685.

1847 Fishilevich, E., and Vosshall, L.B. (2005). Genetic and functional subdivision of the *Drosophila* antennal
1848 lobe. Curr Biol *15*, 1548-1553.

1849 Frank, D.D., Enjin, A., Jouandet, G.C., Zaharieva, E.E., Para, A., Stensmyr, M.C., and Gallio, M. (2017).
1850 Early Integration of Temperature and Humidity Stimuli in the *Drosophila* Brain. Curr Biol *27*, 2381-2388
1851 e2384.

1852 Frechter, S., Bates, A.S., Tootoonian, S., Dolan, M.J., Manton, J., Jamasb, A.R., Kohl, J., Bock, D., and
1853 Jefferis, G. (2019). Functional and anatomical specificity in a higher olfactory centre. eLife *8*.

1854 Fujii, S., Yavuz, A., Slone, J., Jagge, C., Song, X., and Amrein, H. (2015). *Drosophila* sugar receptors in
1855 sweet taste perception, olfaction, and internal nutrient sensing. Curr Biol *25*, 621-627.

1856 Ganguly, A., Pang, L., Duong, V.K., Lee, A., Schoniger, H., Varady, E., and Dahanukar, A. (2017). A
1857 Molecular and Cellular Context-Dependent Role for Ir76b in Detection of Amino Acid Taste. Cell Rep
1858 *18*, 737-750.

1859 Gao, Q., and Chess, A. (1999). Identification of candidate *Drosophila* olfactory receptors from genomic
1860 DNA sequence. Genomics *60*, 31-39.

1861 Gao, Q., Yuan, B., and Chess, A. (2000). Convergent projections of *Drosophila* olfactory neurons to
1862 specific glomeruli in the antennal lobe. Nat Neurosci *3*, 780-785.

1863 Gloor, G.B., Nassif, N.A., Johnson-Schlitz, D.M., Preston, C.R., and Engels, W.R. (1991). Targeted gene
1864 replacement in *Drosophila* via P element-induced gap repair. Science *253*, 1110-1117.

1865 Gnerer, J.P., Venken, K.J., and Dierick, H.A. (2015). Gene-specific cell labeling using MiMIC transposons.
1866 Nucleic Acids Res *43*, e56.

1867 Goldman, A.L., Van der Goes van Naters, W., Lessing, D., Warr, C.G., and Carlson, J.R. (2005).
1868 Coexpression of two functional odor receptors in one neuron. Neuron *45*, 661-666.

1869 Gomez-Diaz, C., Martin, F., Garcia-Fernandez, J.M., and Alcorta, E. (2018). The Two Main Olfactory
1870 Receptor Families in *Drosophila*, ORs and IRs: A Comparative Approach. Front Cell Neurosci *12*, 253.

1871 Goulding, S.E., zur Lage, P., and Jarman, A.P. (2000). *amos*, a Proneural Gene for *Drosophila* Olfactory
1872 Sense Organs that Is Regulated by *lozenge*. Neuron *25*, 69-78.

1873 Grabe, V., Baschwitz, A., Dweck, H.K.M., Lavista-Llanos, S., Hansson, B.S., and Sachse, S. (2016).
1874 Elucidating the Neuronal Architecture of Olfactory Glomeruli in the *Drosophila* Antennal Lobe. Cell Rep
1875 *16*, 3401-3413.

1876 Grabe, V., and Sachse, S. (2018). Fundamental principles of the olfactory code. Biosystems *164*, 94-101.

1877 Gratz, S.J., Ukken, F.P., Rubinstein, C.D., Thiede, G., Donohue, L.K., Cummings, A.M., and O'Connor-Giles,
1878 K.M. (2014). Highly specific and efficient CRISPR/Cas9-catalyzed homology-directed repair in
1879 *Drosophila*. Genetics *196*, 961-971.

1880 Groth, A.C., Fish, M., Nusse, R., and Calos, M.P. (2004). Construction of transgenic *Drosophila* by using
1881 the site-specific integrase from phage phiC31. Genetics *166*, 1775-1782.

1882 Gupta, B.P., and Rodrigues, V. (1997). Atonal is a proneural gene for a subset of olfactory sense organs in
1883 *Drosophila*. Genes Cells *2*, 225-233.

1884 Hallem, E.A., and Carlson, J.R. (2006). Coding of odors by a receptor repertoire. Cell *125*, 143-160.

1885 Hallem, E.A., Ho, M.G., and Carlson, J.R. (2004). The molecular basis of odor coding in the *Drosophila*
1886 antenna. Cell *117*, 965-979.

1887 Hansson, B.S., and Stensmyr, M.C. (2011). Evolution of insect olfaction. Neuron *72*, 698-711.

1888 Harris, W.A. (1972). The maxillae of *Drosophila melanogaster* as revealed by scanning electron
1889 microscopy. J Morphol *138*, 451-456.

1890 Haverkamp, A., Hansson, B.S., and Knaden, M. (2018). Combinatorial Codes and Labeled Lines: How
1891 Insects Use Olfactory Cues to Find and Judge Food, Mates, and Oviposition Sites in Complex
1892 Environments. Front Physiol *9*, 49.

1893 Horne, J.A., Langille, C., McLin, S., Wiederman, M., Lu, Z., Xu, C.S., Plaza, S.M., Scheffer, L.K., Hess, H.F.,
1894 and Meinertzhagen, I.A. (2018). A resource for the *Drosophila* antennal lobe provided by the
1895 connectome of glomerulus VA1v. eLife *7*.

1896 Hussain, A., Zhang, M., Ucpunar, H.K., Svensson, T., Quillery, E., Gompel, N., Ignell, R., and Grunwald
1897 Kadow, I.C. (2016). Ionotropic Chemosensory Receptors Mediate the Taste and Smell of Polyamines.
1898 PLoS Biol *14*, e1002454.

1899 Jaeger, A.H., Stanley, M., Weiss, Z.F., Musso, P.Y., Chan, R.C., Zhang, H., Feldman-Kiss, D., and Gordon,
1900 M.D. (2018). A complex peripheral code for salt taste in *Drosophila*. eLife *7*.

1901 Jhaveri, D., Sen, A., Reddy, G.V., and Rodrigues, V. (2000a). Sense organ identity in the *Drosophila*
1902 antenna is specified by the expression of the proneural gene atonal. Mech Dev *99*, 101-111.

1903 Jhaveri, D., Sen, A., and Rodrigues, V. (2000b). Mechanisms underlying olfactory neuronal connectivity in
1904 *Drosophila*-the atonal lineage organizes the periphery while sensory neurons and glia pattern the
1905 olfactory lobe. Dev Biol *226*, 73-87.

1906 Jinek, M., Chylinski, K., Fonfara, I., Hauer, M., Doudna, J.A., and Charpentier, E. (2012). A programmable
1907 dual-RNA-guided DNA endonuclease in adaptive bacterial immunity. Science *337*, 816-821.

1908 Jones, W.D., Cayirlioglu, P., Kadow, I.G., and Vosshall, L.B. (2007). Two chemosensory receptors together
1909 mediate carbon dioxide detection in *Drosophila*. Nature *445*, 86-90.

1910 Kaissling, K.-E., and Thorson, J. (1980). Insect olfactory sensilla: structural, chemical and electrical
1911 aspects of the functional organisation. In Receptors for neurotransmitters, hormones and pheromones
1912 in insects (Elsevier/North-Holland Biomedical Press), pp. 261-282.

1913 Kanca, O., Zirin, J., Garcia-Marques, J., Knight, S.M., Yang-Zhou, D., Amador, G., Chung, H., Zuo, Z., Ma,
1914 L., He, Y.*, et al.* (2019). An efficient CRISPR-based strategy to insert small and large fragments of DNA
1915 using short homology arms. eLife *8*, e51539.

1916 Karim, M.R., Endo, K., Moore, A.W., and Taniguchi, H. (2014). Whole mount immunolabeling of olfactory
1917 receptor neurons in the *Drosophila* antenna. J Vis Exp, 51245.

1918 Klapoetke, N.C., Murata, Y., Kim, S.S., Pulver, S.R., Birdsey-Benson, A., Cho, Y.K., Morimoto, T.K., Chuong,
1919 A.S., Carpenter, E.J., Tian, Z.*, et al.* (2014). Independent optical excitation of distinct neural
1920 populations. Nat Methods *11*, 338-346.

1921 Knecht, Z.A., Silbering, A.F., Cruz, J., Yang, L., Croset, V., Benton, R., and Garrity, P.A. (2017). Ionotropic
1922 Receptor-dependent moist and dry cells control hygrosensation in *Drosophila*. eLife *6*.

1923 Knecht, Z.A., Silbering, A.F., Ni, L., Klein, M., Budelli, G., Bell, R., Abuin, L., Ferrer, A.J., Samuel, A.D.,
1924 Benton, R.*, et al.* (2016). Distinct combinations of variant ionotropic glutamate receptors mediate
1925 thermosensation and hygrosensation in *Drosophila*. eLife *5*.

1926 Koh, T.W., He, Z., Gorur-Shandilya, S., Menuz, K., Larter, N.K., Stewart, S., and Carlson, J.R. (2014). The
1927 *Drosophila* IR20a clade of ionotropic receptors are candidate taste and pheromone receptors. Neuron
1928 *83*, 850-865.

1929 Kondoh, K., Lu, Z., Ye, X., Olson, D.P., Lowell, B.B., and Buck, L.B. (2016). A specific area of olfactory
1930 cortex involved in stress hormone responses to predator odours. Nature *532*, 103-106.

1931 Kurtovic, A., Widmer, A., and Dickson, B.J. (2007). A single class of olfactory neurons mediates
1932 behavioural responses to a *Drosophila* sex pheromone. Nature *446*, 542-546.

1933 Kwon, J.Y., Dahanukar, A., Weiss, L.A., and Carlson, J.R. (2007). The molecular basis of CO2 reception in
1934 *Drosophila*. PNAS *104*, 3574-3578.

1935 Lai, S.-L., and Lee, T. (2006). Genetic mosaic with dual binary transcriptional systems in *Drosophila*. Nat
1936 Neurosci *9*, 703-709.

1937 Laissue, P.P., Reiter, C.H., Hiesinger, P.R., Halter, S., Fischbach, K.F., and Stocker, R.F. (1999). Three-
1938 dimensional reconstruction of the antennal lobe in *Drosophila melanogaster*. J Comp Neurol *405*, 543-
1939 552.

1940 Larsson, M.C., Domingos, A.I., Jones, W.D., Chiappe, M.E., Amrein, H., and Vosshall, L.B. (2004). *Or83b*
1941 encodes a broadly expressed odorant receptor essential for *Drosophila* olfaction. Neuron *43*, 703-714.

1942 Lee, P.-T., Zirin, J., Kanca, O., Lin, W.-W., Schulze, K.L., Li-Kroeger, D., Tao, R., Devereaux, C., Hu, Y.,
1943 Chung, V.*, et al.* (2018). A gene-specific T2A-GAL4 library for *Drosophila*. eLife *7*, e35574.

1944 Lee, T., and Luo, L. (1999). Mosaic Analysis with a Repressible Cell Marker for Studies of Gene Function
1945 in Neuronal Morphogenesis. Neuron *22*, 451-461.

1946 Li-Kroeger, D., Kanca, O., Lee, P.T., Cowan, S., Lee, M.T., Jaiswal, M., Salazar, J.L., He, Y., Zuo, Z., and
1947 Bellen, H.J. (2018). An expanded toolkit for gene tagging based on MiMIC and scarless CRISPR tagging
1948 in *Drosophila*. eLife *7*.

1949 Li, H., Janssens, J., De Waegeneer, M., Kolluru, S.S., Davie, K., Gardeux, V., Sealens, W., David, F., Brbic,
1950 M., Leskovec, J.*, et al.* (2021). Fly Cell Atlas: a single-cell transcriptomic atlas of the adult fruit fly.
1951 bioRxiv, 2021.2007.2004.451050.

1952 Li, Q., Barish, S., Okuwa, S., Maciejewski, A., Brandt, A.T., Reinhold, D., Jones, C.D., and Volkan, P.C.
1953 (2016). A Functionally Conserved Gene Regulatory Network Module Governing Olfactory Neuron
1954 Diversity. In PLoS Genet, pp. e1005780.

1955 Lin, C.-C., and Potter, C.J. (2015). Re-Classification of *Drosophila melanogaster* Trichoid and Intermediate
1956 Sensilla Using Fluorescence-Guided Single Sensillum Recording. PLoS One *10*, e0139675.

1957 Lin, C.-C., and Potter, C.J. (2016a). Editing Transgenic DNA Components by Inducible Gene Replacement
1958 in *Drosophila melanogaster*. Genetics *203*, 1613-1628.

1959 Lin, C.-C., and Potter, C.J. (2016b). Non-mendelian dominant maternal effects caused by CRISPR/Cas9
1960 transgenic components in *Drosophila melanogaster*. G3 (Bethesda) *6*, 3685-3691.

1961 MacWilliam, D., Kowalewski, J., Kumar, A., Pontrello, C., and Ray, A. (2018). Signaling Mode of the
1962 Broad-Spectrum Conserved CO2 Receptor Is One of the Important Determinants of Odor Valence in
1963 *Drosophila*. Neuron *97*, 1153-1167.e1154.

1964 Mansourian, S., Corcoran, J., Enjin, A., Löfstedt, C., Dacke, M., and Stensmyr, M.C. (2016). Fecal-Derived
1965 Phenol Induces Egg-Laying Aversion in *Drosophila*. Curr Biol *26*, 2762-2769.

1966 Marin, E.C., Büld, L., Theiss, M., Sarkissian, T., Roberts, R.J.V., Turnbull, R., Tamimi, I.F.M., Pleijzier, M.W.,
1967 Laursen, W.J., Drummond, N.*, et al.* (2020). Connectomics Analysis Reveals First-, Second-, and Third-
1968 Order Thermosensory and Hygrosensory Neurons in the Adult *Drosophila* Brain. Curr Biol *30*, 3167-
1969 3182.e3164.

1970 McLaughlin, C.N., Brbić, M., Xie, Q., Li, T., Horns, F., Kolluru, S.S., Kebschull, J.M., Vacek, D., Xie, A., Li, J.*,*
1971 *et al.* (2021). Single-cell transcriptomes of developing and adult olfactory receptor neurons in
1972 *Drosophila*. eLife *10*, e63856.

1973 Menuz, K., Larter, N.K., Park, J., and Carlson, J.R. (2014). An RNA-seq screen of the *Drosophila* antenna
1974 identifies a transporter necessary for ammonia detection. PLoS Genet *10*, e1004810.

1975 Min, S., Ai, M., Shin, S.A., and Suh, G.S. (2013). Dedicated olfactory neurons mediating attraction
1976 behavior to ammonia and amines in *Drosophila*. PNAS *110*, E1321-1329.

1977 Papes, F., Logan, D.W., and Stowers, L. (2010). The Vomeronasal Organ Mediates Interspecies Defensive
1978 Behaviors through Detection of Protein Pheromone Homologs. Cell *141*, 692-703.

1979 Park, J.H., and Kwon, J.Y. (2011). A systematic analysis of *Drosophila* gustatory receptor gene expression
1980 in abdominal neurons which project to the central nervous system. Mol Cells *32*, 375-381.

1981 Pask, G.M., and Ray, A. (2016). Insect Olfactory Receptors: An Interface between Chemistry and Biology.
1982 In Chemosensory Transduction (Elsevier), pp. 101-122.

1983 Pinto, L., Stocker, R.F., and Rodrigues, V. (1988). Anatomical and neurochemical classification of the
1984 antennal glomeruli in *Drosophila melanogaster* meigen (Diptera: Drosophilidae). Int J Insect Morphol
1985 Embryol *17*, 335-344.

1986 Port, F., Chen, H.M., Lee, T., and Bullock, S.L. (2014). Optimized CRISPR/Cas tools for efficient germline
1987 and somatic genome engineering in *Drosophila*. PNAS *111*, E2967-2976.

1988 Potter, C.J., Tasic, B., Russler, E.V., Liang, L., and Luo, L. (2010). The Q system: a repressible binary
1989 system for transgene expression, lineage tracing, and mosaic analysis. Cell *141*, 536-548.

1990 Prieto-Godino, L.L., Rytz, R., Cruchet, S., Bargeton, B., Abuin, L., Silbering, A.F., Ruta, V., Dal Peraro, M.,
1991 and Benton, R. (2017). Evolution of Acid-Sensing Olfactory Circuits in Drosophilids. Neuron *93*, 661-
1992 676.e666.

1993 Prieto-Godino, L.L., Silbering, A.F., Khallaf, M.A., Cruchet, S., Bojkowska, K., Pradervand, S., Hansson,
1994 B.S., Knaden, M., and Benton, R. (2020). Functional integration of "undead" neurons in the olfactory
1995 system. Sci Adv *6*, eaaz7238.

1996 Ray, A., Van der Goes van Naters, W., and Carlson, J.R. (2008). A regulatory code for neuron-specific
1997 odor receptor expression. PLoS Biol *6*, e125.

1998 Ray, A., Van der Goes van Naters, W., Shiraiwa, T., and Carlson, J.R. (2007). Mechanisms of odor
1999 receptor gene choice in *Drosophila*. Neuron *53*, 353-369.

2000 Riabinina, O., Luginbuhl, D., Marr, E., Liu, S., Wu, M.N., Luo, L., and Potter, C.J. (2015). Improved and
2001 expanded Q-system reagents for genetic manipulations. Nat Methods *12*, 219-222, 215 p following
2002 222.

2003 Riabinina, O., Task, D., Marr, E., Lin, C.-C., Alford, R., O'Brochta, D.A., and Potter, C.J. (2016).
2004 Organization of olfactory centres in the malaria mosquito *Anopheles gambiae*. Nat Commun *7*, 13010.

2005 Saina, M., and Benton, R. (2013). Visualizing Olfactory Receptor Expression and Localization in
2006 *Drosophila*. In Olfactory Receptors: Methods and Protocols, C.J. Crasto, ed. (Totowa, NJ: Humana
2007 Press), pp. 211-228.

2008 Sanchez-Alcaniz, J.A., Silbering, A.F., Croset, V., Zappia, G., Sivasubramaniam, A.K., Abuin, L., Sahai, S.Y.,
2009 Munch, D., Steck, K., Auer, T.O.*, et al.* (2018). An expression atlas of variant ionotropic glutamate
2010 receptors identifies a molecular basis of carbonation sensing. Nat Commun *9*, 4252.

2011 Sato, K., Pellegrino, M., Nakagawa, T., Nakagawa, T., Vosshall, L.B., and Touhara, K. (2008). Insect
2012 olfactory receptors are heteromeric ligand-gated ion channels. Nature *452*, 1002-1006.

2013 Scheffer, L.K., Xu, C.S., Januszewski, M., Lu, Z., Takemura, S.-y., Hayworth, K.J., Huang, G.B., Shinomiya,
2014 K., Maitlin-Shepard, J., Berg, S.*, et al.* (2020). A connectome and analysis of the adult *Drosophila*
2015 central brain. eLife *9*, e57443.

2016 Schindelin, J., Arganda-Carreras, I., Frise, E., Kaynig, V., Longair, M., Pietzsch, T., Preibisch, S., Rueden, C.,
2017 Saalfeld, S., and Schmid, B. (2012). Fiji: an open-source platform for biological-image analysis. Nat
2018 Methods *9*, 676-682.

2019 Schlegel, P., Bates, A.S., Stürner, T., Jagannathan, S.R., Drummond, N., Hsu, J., Serratosa Capdevila, L.,
2020 Javier, A., Marin, E.C., Barth-Maron, A.*, et al.* (2021). Information flow, cell types and stereotypy in a
2021 full olfactory connectome. eLife *10*, e66018.

2022 Scott, K. (2018). Gustatory Processing in *Drosophila melanogaster*. Annu Rev Entomol *63*, 15-30.

2023 Scott, K., Brady, R., Cravchik, A., Morozov, P., Rzhetsky, A., Zuker, C., and Axel, R. (2001). A
2024 Chemosensory Gene Family Encoding Candidate Gustatory and Olfactory Receptors in *Drosophila*. Cell
2025 *104*, 661-673.

2026 Seki, Y., Dweck, H.K.M., Rybak, J., Wicher, D., Sachse, S., and Hansson, B.S. (2017). Olfactory coding from
2027 the periphery to higher brain centers in the *Drosophila* brain. BMC Biol *15*, 56.

2028 Shearin, H.K., Macdonald, I.S., Spector, L.P., and Stowers, R.S. (2014). Hexameric GFP and mCherry
2029 reporters for the *Drosophila* GAL4, Q, and LexA transcription systems. Genetics *196*, 951-960.

2030 Siddiqi, O. (1987). Neurogenetics of olfaction in *Drosophila melanogaster*. Trends Genet *3*, 137-142.

2031 Siegal, M.L., and Hartl, D.L. (1996). Transgene Coplacement and high efficiency site-specific
2032 recombination with the Cre/loxP system in *Drosophila*. Genetics *144*, 715-726.

2033 Silbering, A.F., Rytz, R., Grosjean, Y., Abuin, L., Ramdya, P., Jefferis, G.S., and Benton, R. (2011).
2034 Complementary function and integrated wiring of the evolutionarily distinct *Drosophila* olfactory
2035 subsystems. J Neurosci *31*, 13357-13375.

2036 Spletter, M.L., Liu, J., Liu, J., Su, H., Giniger, E., Komiyama, T., Quake, S., and Luo, L. (2007). Lola regulates
2037 *Drosophila* olfactory projection neuron identity and targeting specificity. Neural Dev *2*, 14.

2038 Stengl, M. (2010). Pheromone transduction in moths. Front Cell Neurosci *4*, 133-133.

2039 Stensmyr, M.C., Dweck, H.K., Farhan, A., Ibba, I., Strutz, A., Mukunda, L., Linz, J., Grabe, V., Steck, K.,
2040 Lavista-Llanos, S*., et al.* (2012). A Conserved Dedicated Olfactory Circuit for Detecting Harmful
2041 Microbes in *Drosophila*. Cell *151*, 1345-1357.

2042 Stocker, R.F. (1994). The organization of the chemosensory system in *Drosophila melanogaster*: a
2043 review. Cell Tissue Res *275*, 3-26.

2044 Stocker, R.F. (2001). *Drosophila* as a focus in olfactory research: mapping of olfactory sensilla by fine
2045 structure, odor specificity, odorant receptor expression, and central connectivity. Microsc Res Tech *55*,
2046 284-296.

2047 Su, C.Y., Menuz, K., and Carlson, J.R. (2009). Olfactory perception: receptors, cells, and circuits. Cell *139*,
2048 45-59.

2049 Suh, G.S.B., Wong, A.M., Hergarden, A.C., Wang, J.W., Simon, A.F., Benzer, S., Axel, R., and Anderson,
2050 D.J. (2004). A single population of olfactory sensory neurons mediates an innate avoidance behaviour
2051 in *Drosophila*. Nature *431*, 854-859.

2052 Task, D., Lin, C.-C., Afify, A., Li, H., Vulpe, A., Menuz, K., and Potter, C.J. (2020). Widespread Polymodal
2053 Chemosensory Receptor Expression in *Drosophila* Olfactory Neurons. bioRxiv,
2054 2020.2011.2007.355651.

2055 Task, D., and Potter, C.J. (2021). Rapid degeneration of *Drosophila* olfactory neurons in Orco mutant
2056 maxillary palps. microPublication Biology.

2057 Thurmond, J., Goodman, J.L., Strelets, V.B., Attrill, H., Gramates, L.S., Marygold, S.J., Matthews, B.B.,
2058 Millburn, G., Antonazzo, G., and Trovisco, V. (2019). FlyBase 2.0: the next generation. Nucleic Acids
2059 Res *47*, D759-D765.

2060 Trible, W., Olivos-Cisneros, L., McKenzie, S.K., Saragosti, J., Chang, N.-C., Matthews, B.J., Oxley, P.R., and
2061 Kronauer, D.J.C. (2017). Orco mutagenesis causes loss of antennal lobe glomeruli and impaired social
2062 behavior in ants. Cell *170*, 727-735. e710.

2063 van Breugel, F., Huda, A., and Dickinson, M.H. (2018). Distinct activity-gated pathways mediate
2064 attraction and aversion to CO2 in *Drosophila*. Nature *564*, 420-424.

2065 Van der Maaten, L., and Hinton, G. (2008). Visualizing data using t-SNE. J Mach Learn Res *9*.

2066 Venkatesh, S., and Singh, R.N. (1984). Sensilla on the third antennal segment of *Drosophila*
2067 *melanogaster* meigen (Diptera : Drosophilidae). Int J Insect Morphol Embryol *13*, 51-63.

2068 Vilain, S., Vanhauwaert, R., Maes, I., Schoovaerts, N., Zhou, L., Soukup, S., da Cunha, R., Lauwers, E.,
2069 Fiers, M., and Verstreken, P. (2014). Fast and efficient *Drosophila melanogaster* gene knock-ins using
2070 MiMIC transposons. G3 (Bethesda) *4*, 2381-2387.

2071 Vosshall, L.B., Amrein, H., Morozov, P.S., Rzhetsky, A., and Axel, R. (1999). A Spatial Map of Olfactory
2072 Receptor Expression in the *Drosophila* Antenna. Cell *96*, 725-736.

2073 Vosshall, L.B., and Hansson, B.S. (2011). A unified nomenclature system for the insect olfactory
2074 coreceptor. Chem Senses *36*, 497-498.

2075 Vosshall, L.B., and Stocker, R.F. (2007). Molecular architecture of smell and taste in *Drosophila*. Annu
2076 Rev Neurosci *30*, 505-533.

2077 Vosshall, L.B., Wong, A.M., and Axel, R. (2000). An Olfactory Sensory Map in the Fly Brain. Cell *102*, 147-
2078 159.

2079 Vulpe, A., Kim, H.S., Ballou, S., Wu, S.-T., Grabe, V., Nava Gonzales, C., Liang, T., Sachse, S., Jeanne, J.M.,
2080 Su, C.-Y.*, et al.* (2021a). An ammonium transporter is a non-canonical olfactory receptor for ammonia.
2081 Curr Biol.

2082 Vulpe, A., Mohapatra, P., and Menuz, K. (2021b). Functional characterization of odor responses and
2083 gene expression changes in olfactory co-receptor mutants in *Drosophila*. bioRxiv,
2084 2021.2006.2018.449017.

2085 Wilson, R.I. (2013). Early olfactory processing in *Drosophila*: mechanisms and principles. Annu Rev
2086 Neurosci *36*, 217-241.

2087 Xie, T., Ho, M.C.W., Liu, Q., Horiuchi, W., Lin, C.-C., Task, D., Luan, H., White, B.H., Potter, C.J., and Wu,
2088 M.N. (2018). A genetic toolkit for dissecting dopamine circuit function in *Drosophila*. Cell Rep *23*, 652-
2089 665.

2090 Xue, Z., Ren, M., Wu, M., Dai, J., Rong, Y.S., and Gao, G. (2014). Efficient gene knock-out and knock-in
2091 with transgenic Cas9 in *Drosophila*. G3 (Bethesda) *4*, 925-929.

2092 Yan, H., Jafari, S., Pask, G., Zhou, X., Reinberg, D., and Desplan, C. (2020). Evolution, developmental
2093 expression and function of odorant receptors in insects. J Exp Biol *223*.

2094 Yan, H., Opachaloemphan, C., Mancini, G., Yang, H., Gallitto, M., Mlejnek, J., Leibholz, A., Haight, K.,
2095 Ghaninia, M., Huo, L.*, et al.* (2017). An Engineered *orco* Mutation Produces Aberrant Social Behavior
2096 and Defective Neural Development in Ants. Cell *170*, 736-747.e739.

2097 Yao, C.A., Ignell, R., and Carlson, J.R. (2005). Chemosensory Coding by Neurons in the Coeloconic Sensilla
2098 of the *Drosophila* Antenna. J Neurosci *25*, 8359-8367.

2099 Younger, M.A., Herre, M., Ehrlich, A.R., Gong, Z., Gilbert, Z.N., Rahiel, S., Matthews, B.J., and Vosshall,
2100 L.B. (2020). Non-canonical odor coding ensures unbreakable mosquito attraction to humans. bioRxiv,
2101 2020.2011.2007.368720.

2102 Zhang, Y.V., Ni, J., and Montell, C. (2013). The molecular basis for attractive salt-taste coding in
2103 *Drosophila*. Science *340*, 1334-1338.

2104 Zheng, Z., Lauritzen, J.S., Perlman, E., Robinson, C.G., Nichols, M., Milkie, D., Torrens, O., Price, J., Fisher,
2105 C.B., and Sharifi, N. (2018). A complete electron microscopy volume of the brain of adult *Drosophila*
2106 *melanogaster*. Cell *174*, 730-743. e722.

2107